NUMERICAL SIMULATION OF NON-REACTING TURBULENT FLOWS OVER A CONSTANT TEMPERATURE SOLID SURFACE IN REGRESSION

A THESIS SUBMITTED TO
THE GRADUATE SCHOOL OF NATURAL AND APPLIED SCIENCES
OF
MIDDLE EAST TECHNICAL UNIVERSITY

BY

CENKER KARAEREN

IN PARTIAL FULFILLMENT OF THE REQUIREMENTS
FOR
THE DEGREE OF MASTER OF SCIENCE
IN
MECHANICAL ENGINEERING

DECEMBER 2007

Approval of the thesis:

NUMERICAL SIMULATION OF

NON-REACTING TURBULENT FLOWS OVER A

CONSTANT TEMPERATURE SOLID SURFACE IN REGRESSION

submitted by **CENKER KARAEREN** in partial fulfillment of the requirements for the degree of **Master of Science in Mechanical Engineering Department**, **Middle East Technical University** by,

Prof. Dr. Canan ÖZGEN
Dean, Graduate School of Natural and Applied Sciences _____

Prof. Dr. Sıtkı Kemal İDER
Head of Department, Mechanical Engineering _____

Prof. Dr. Kahraman ALBAYRAK
Supervisor, Mechanical Engineering Dept., METU _____

Prof. Dr. Kazım AKYÜZLÜ
Co-Supervisor, Mechanical Engineering Dept.,
University of New Orleans. _____

Examining Committee Members:

Prof. Dr. Haluk AKSEL
Mechanical Engineering Dept., METU _____

Prof. Dr. Kahraman ALBAYRAK
Mechanical Engineering Dept., METU _____

Prof. Dr. Nafiz ALEMDAROĞLU
Aerospace Engineering Dept., METU _____

Assoc. Prof. Abdullah ULAŞ
Mechanical Engineering Dept., METU _____

Asst. Prof. Cüneyt SERT
Mechanical Engineering Dept., METU _____

Date: December 7, 2007

I hereby declare that all information in this document has been obtained and presented in accordance with academic rules and ethical conduct. I also declare that, as required by these rules and conduct, I have fully cited and referenced all material and results that are not original to this work.

Cenker KARAEREN

ABSTRACT

NUMERICAL SIMULATION OF NON-REACTING TURBULENT FLOWS OVER A CONSTANT TEMPERATURE SOLID SURFACE IN REGRESSION

KARAEREN, Cenker
M. Sc., Department of Mechanical Engineering
Supervisor: Prof. Dr. Kahraman ALBAYRAK
Co. Supervisor: Prof. Dr. Kazım AKYÜZLÜ

December 2007, 116 pages

In this study, an attempt is made to obtain convergent and stable solutions of the *K*-ε turbulence model equations for non-reacting turbulent flows over an isothermal solid surface in regression. A physics based mathematical model is used to describe the flow and temperature field over the moving surface. The flow is assumed to be two-dimensional, unsteady, incompressible with boundary layer approximations. Parabolized form of the standard *K*-ε equations is adopted to simulate turbulence in the flow.

Regression of the solid surface causes the bounds of the solution domain to change with time, therefore a coordinate transformation is used in the vertical direction. The computational domain with fixed boundaries is discretized using an orthogonal grid system where a coordinate stretching is used in the vertical direction. A second order accurate, explicit finite difference technique is used for discretization of the governing equations. The final set of discretized equations is then solved using a solution algorithm specifically developed for this study. The verification of the

solution algorithm includes a grid independence study, time increment study, and a comparison of the steady state results for the laminar and the turbulent flow cases. Finally, a parametric study is conducted using the proposed solution algorithm to test the stability of the numerical results for different Reynolds numbers, regression rates, and surface temperatures. It is concluded that the proposed numerical solution algorithm is capable of providing convergent and stable solutions of the two-equation turbulence model.

Keywords: Turbulent flow, regression, moving boundary

ÖZ

SABİT SICAKLIKLI GERİLEMELİ YÜZEYLERİN ÜZERİNDEN TÜRBÜLANSLI REAKSİYONSUZ AKIŞLARIN SAYISAL SİMÜLASYONU

Karaeren, Cenker
Yüksek Lisans, Makina Mühendisliği Bölümü
Tez Yöneticisi: Prof. Dr. Kahraman ALBAYRAK
Tez Yardımcı Yöneticisi: Prof. Dr. Kazım AKYÜZLÜ

Aralık 2007, 116 sayfa

Bu çalışmada sabit sıcaklıktaki, gerilemeli düz bir plaka üzerindeki yanmasız, türbülanslı akışlarda K-ε denklemleri için yakınsayan ve kararlı çözümle elde edilmesi amaçlanmıştır. Hareketli yüzey üzerindeki akış ve sıcaklık alanlarını tanımlamak için fizik tabanlı bir matematiksel model kullanılmıştır. Akış iki boyutlu, sıkıştırılamaz ve türbülanslı olarak kabul edilmiştir, sınır tabakası tahminleri geçerlidir. Türbülans modellemesi için standart K-ε denklemlerinin parabolik formu kullanılmıştır.

Katı yüzeyin gerilemesinden dolayı gaz tabakasının sınırları değişmektedir; bunun için dikey yönde bir koordinat dönüşümü gerçekleştirilmiştir. Sabit sınırları olan bu sayısal alan dikey yönde esnetilmiş, sınır tabakasına yakın bölgede daha ince bir ağ elde edilmiştir. Denklemler matematiksel olarak ikinci derecede kesin, açık bir yöntemle bilgisayar çözümü için cebirsel hale getirilmiştir. Bu denklemlerin çözümde özel olarak geliştirilmiş bir çözüm algoritması kullanılmıştır.

Çözüm algoritmasının doğrulanması için ağ boyutundan bağımsızlık ve zaman ilerlemesinden bağımsızlık çalışmaları yapılmış, laminar ve türbülanslı durumlar için sürekli çözümler literatürdeki diğer çalışmalarla karşılaştırılmıştır.

Son olarak parametrik bir çalışma yapılmış, çözüm algoritmasının kararlılığı farklı Reynolds sayıları, gerileme hızları ve yüzey sıcaklıklarında test edilmiştir. Sayısal çözüm algoritmasının türbülans modeli için kararlı ve yakınsayan sonuçlar verdiği sonucuna varılmıştır.

Anahtar Kelimeler: Türbülanslı akış, gerileme, hareketli sınır tabakası

ACKNOWLEDGEMENTS

I would like to express my deepest gratitude to my supervisor, Prof. Dr. Kahraman Albayrak, and my co. supervisor Prof. Dr. Kazım Akyüzlü for their continuous guidance, encouragement and both academic and personal support throughout my thesis study.

I would like to express my appreciation to my colleagues, Gökhan Tekin, Emir Kutluay, Anıl Koçkar, Ali Özgü Nursal and Özgür Emrah Koçak for numerous fruitful discussions and wise comments during the development of my thesis.

I also thank my friends, especially my colleague Ali Aktaş for making the thesis period enjoyable and colorful and Başar Aykut for his invaluable support during the programming stage.

Finally, for and beyond this thesis study, I am indebted to my parents for their never-ending love, belief and patience throughout my academic life. Without their encouragement, completion of this thesis would not have been possible.

TABLE OF CONTENTS

PLAGIARISM iii
ABSTRACT iv
ÖZ vi
ACKNOWLEDGEMENTS viii
TABLE OF CONTENTS ix
LIST OF TABLES xiii
LIST OF FIGURES xiv
NOMENCLATURE xvii
CHAPTER
1. INTRODUCTION 1
1.1 Motivation and Scope 1
1.2 Outline 3
2. LITERATURE SURVEY 4
2.1 Turbulence models 4
2.1.1 Statistical Models 5
2.1.2 Algebraic Models 5
2.1.3 One-Equation Models 6
2.1.4 Two-Equation Models 6
2.1.4.1 k-ε Model 7
2.1.4.2 k-ω Model 8
2.2 Numerical Methods for Solution 9
2.2.1 Explicit MacCormack Method 10
2.2.2 Hopscotch Method 12
2.2.3 Brailovskaya Method 12
2.2.4 Allen-Cheng Method 13
2.2.5 Lax-Wendroff Method 13
2.2.6 Implicit Methods 13

2.3 Comparison of the Finite-Differencing Methods 14
2.3.1 Backward Differencing 14
2.3.2 Central Differencing 15
2.3.3 Forward Differencing 15
3. DESCRIPTION OF THE PHYSICAL MODEL 16
3.1 Physical Model 16
4. MODELING OF THE GAS FLOW 18
4.1 Modeling of the Gas Flow 18
4.1.1 Continuity Equation 18
4.1.2 Momentum Equation 19
4.1.3 Energy Equation 20
4.1.4 K-ε Equations 20
4.1.5 Boundary and Initial Conditions 21
4.2 Final Form of the Mathematical Model 23
5. MOVING BOUNDARY TRANSFORMATION AND STRETCHING 24
5.1 Introduction 24
5.2 Transformation of the Equations 24
5.2.1 Transformation of the Gas Domain 25
5.2.2 Changes in Mathematical Domain After Transformation 27
5.3 Stretching of the Equations 28
5.4 Final Form of the Transformed and Stretched Governing Differential Equations 30
6. NUMERICAL SOLUTION TECHNIQUE 32
6.1 Introduction 32
6.2 Final Numerical Domain 32
6.3 Numerical Technique and Differencing Scheme Used in the Previous Study 34
6.4 Numerical Technique and Differencing Scheme Used in the Present Study 35
6.5 Final Form of the Linearized and Discretized Equations 36

6.6 Remarks on the Initial Conditions 41
6.7 Time Delay 41
6.8 Numerical Solution Procedure 42
6.9 Computer Code 44
7. VERIFICATION OF THE COMPUTER CODE 45
7.1 Introduction 45
7.2 Comparison of the Numerical Solution with Blasius solution 45
7.3 Comparison of the Turbulent Boundary Layer Velocity Profile with Various Studies 50
7.4 Grid Independence Study 52
7.4.1 Horizontal Velocity Profiles 53
7.4.2 Temperature Profiles 55
7.5 Time Increment and Convergence Study 56
7.5.1 Horizontal Velocity 57
7.5.2 Temperature 61
7.6 Singular Points in Histogram Plots 62
8. COMPARISON OF THE RESULTS OF THE PRESENT AND PREVIOUS PROGRAMS 63
8.1 Introduction 63
8.1.1 Horizontal Velocity Profiles 64
8.1.2 Velocity Vectors and Contours 67
8.1.3 Temperature Contours 69
8.1.4 Turbulent Viscosity Contours 71
8.1.5 Histogram Plots of Selected Variables 73
9. PARAMETRIC STUDY 75
9.1 Study with Different Regression Rates 75
9.1.1 Horizontal Velocity Profiles 75
9.1.2 Temperature Contours 76
9.2 Study with Different Reynolds Numbers 81
9.2.1 Horizontal Velocity Profiles and Contours 81
9.2.2 Temperature Contours 84

9.3 Study with Different Surface Temperatures 86
9.3.1 Temperature Contours..... 87
10. CONCLUSIONS..... 89
11. RECOMMENDATIONS 91
REFERENCES..... 93
APPENDIX A 97
TRANSFORMATION, STRETCHING AND LINEARIZATION OF PARABOLIC TURBULENT KINETIC ENERGY EQUATION 97
APPENDIX B 103
FLOWCHART OF THE COMPUTER CODE 103
APPENDIX C 115
LAMINAR BOUNDARY LAYER 115

LIST OF TABLES

TABLES

Table 2.1 Differencing Sequence for MacCormack Scheme 11
Table 7.1 List of Input Parameters used in Runs with Number 1, 2 45
Table 7.2 List of Runs for Blasius Profile Comparison 46
Table 7.3 List of Input Parameters used in Runs with Number 3-13 52
Table 7.4 List of Runs for Grid Independence Study 53
Table 7.5 List of Runs for Time Increment Independency Study 57
Table 8.1 List of Runs for Comparison of Present and Previous Studies 63
Table 9.1 List of Runs for Different Regression Rate Study 75
Table 9.2 List of Runs for Different Reynolds Number Study 81
Table 9.3 List of Runs for Different Surface Temperatures 86
Table B.1 List of Subroutines Used in the Computer Code 112
Table B.2 List of Variables Used in the Computer Code 114
Table C.1 Comparison of the Results of the Present Solution and Blasius Solution for Laminar Case at $x = 3.24x10^{-2}\,m$ 116

LIST OF FIGURES

FIGURES

Figure 3.1 Definition of the Physical Model 16
Figure 4.1 Boundary Conditions 21
Figure 5.1 Schematic of the Moving Boundary 25
Figure 5.2 Sketch of the Mathematical Domain Before Transformation 27
Figure 5.3 Sketch of the Mathematical Domain After Transformation 28
Figure 5.4 Sketch of the Mathematical Domain After Stretching 29
Figure 6.1 Numerical Domain for 21x61 Mesh Size at the Beginning of Simulation 33
Figure 6.2 Numerical Domain for 21x61 Mesh Size at the End of Simulation 33
Figure 7.1 Comparison of the Results of the Previous Program, Present Program an the Blasius Solution at $x = 3.81x10^{-3} m$ 47
Figure 7.2 Comparison of the Results of the Previous Program, Present Program an the Blasius Solution at $x = 1.905x10^{-2} m$ 48
Figure 7.3 Comparison of the Results of the Previous Program, Present Program an the Blasius Solution at $x = 3.24x10^{-2} m$ 49
Figure 7.4 Comparison of the Turbulent and Laminar Boundary Layer Velocity Profiles 50
Figure 7.5 Comparison of the Turbulent Boundary Layer Velocity Profiles Measured by Schetz, predicted by Antoniou and Present Program 51
Figure 7.6 Horizontal Velocity Profiles at $x = 1.905x10^{-2} m$ for 3 Different Mesh Sizes 54
Figure 7.7 Temperature Profiles at $x = 1.905x10^{-2} m$ for 3 Different Mesh Sizes .. 55

Figure 7.8 Histogram of Horizontal Velocities at Node (3,59), Initially at $x = 3.81x10^{-3} m$, $y = 3.95x10^{-3} m$, for 3 Different Time Increments 58
Figure 7.9 Histogram of Horizontal Velocities at Node (3,59), Initially at $x = 3.81x10^{-3} m$, $y = 3.95x10^{-3} m$, in Logarithmic Scale for 3 Different Time Increments 59
Figure 7.10 Horizontal Velocity Profiles at $x = 1.905x10^{-2} m$ for 3 Different Time Increments 60
Figure 7.11 Histogram of Temperatures at Node (3,59), Initially at $x = 3.81x10^{-3} m$, $y = 3.95x10^{-3} m$, for 3 Different Time Increments 61
Figure 7.12 Close-look to the Histogram of Horizontal Velocity at Node (3,59), Initially at $x = 3.81x10^{-3} m$, $y = 3.95x10^{-3} m$ 62
Figure 8.1 Velocity Profiles of the Previous and Present Programs at $x = 3.81x10^{-3} m$ 64
Figure 8.2 Velocity Profiles of the Previous and Present Programs at $x = 1.905x10^{-2} m$ 65
Figure 8.3 Velocity Profiles of the Previous and Present Programs at $x = 3.24x10^{-2} m$ 66
Figure 8.4 Velocity Vectors of Previous Program 67
Figure 8.5 Velocity Vectors of Present Program 68
Figure 8.6 Temperature Contours of Previous Program 69
Figure 8.7 Temperature Contours of Present Program 70
Figure 8.8 Turbulent Viscosity Contours of Previous Program 71
Figure 8.9 Turbulent Viscosity Contours of Present Program 72
Figure 8.10 Variation of the Horizontal Velocities with Time at Node (11,59), Initially at $x = 3.81x10^{-3} m$, $y = 3.95x10^{-3} m$ 73
Figure 8.11 Variation of the Temperatures with Time at Node (11,59), Initially at $x = 3.81x10^{-3} m$, $y = 3.95x10^{-3} m$ 74
Figure 9.1 Horizontal Velocity Profiles at $x = 1.905x10^{-2} m$ for 3 Different Regression Rates 76

Figure 9.2 Temperature Contours of the Present Study 77
Figure 9.3 Temperature Contours of the Present Study 77
Figure 9.4 Temperature Contours of the Present Study 78
Figure 9.5 Temperature Contours of the Present Study 78
Figure 9.6 Horizontal Velocity Profiles at $x = 1.905x10^{-2} m$ for 3 Different Reynolds Numbers 82
Figure 9.7 Horizontal Velocity Contours of Present Study 83
Figure 9.8 Horizontal Velocity Contours of Present Study 83
Figure 9.9 Horizontal Velocity Contours of Present Study 84
Figure 9.10 Temperature Contours of Present Study 85
Figure 9.11 Temperature Contours of Present Study 85
Figure 9.12 Temperature Contours of Present Study 86
Figure 9.13 Temperature Contours of Present Study 87
Figure 9.14 Temperature Contours of Present Study 88
Figure B.1 Flowchart of the Computer Code 104

NOMENCLATURE

Symbols

$C_{\varepsilon 1}$	coefficient for turbulent dissipation energy
$C_{\varepsilon 2}$	coefficient for turbulent dissipation energy
C_{μ}	coefficient for eddy viscosity
c_p	specific heat at constant pressure
c_v	specific heat at constant volume
h	initial thickness of the gas
H	total height of the gas
i	node number in horizontal direction
IN	total number of nodes in horizontal direction
j	node number in vertical direction
JN	total number of nodes in vertical direction
k	thermal conductivity
K	turbulent kinetic energy
L	length of the plate
r	regression
$\dot{r}$	regression rate
Pr	Prandtl number
$\mathrm{Pr}_{\varepsilon}$	turbulent Prandtl number for dissipation energy
Pr_{K}	turbulent Prandtl number for kinetic energy
Pr_{t}	turbulent Prandtl number
R	gas constant
Re	Reynolds number

t	time
T	temperature
u	horizontal velocity
v	vertical velocity
x	horizontal coordinate
y	vertical coordinate

Greek symbols

$\Delta\eta$	space increment in stretched vertical direction
$\Delta\sigma$	space increment in transformed vertical direction
Δt	time increment
Δx	space increment in x-direction
Δy	space increment in y-direction
ε	turbulent dissipation energy
η	stretched vertical coordinate, non-dimensional vertical coordinate for Blasius solution
μ	absolute viscosity
ρ	density
σ	transformed vertical coordinate

Subscripts

eff	effective
s	surface
t	turbulent
∞	free stream

Superscripts

n	iteration number

CHAPTER 1

INTRODUCTION

Hybrid rockets combine advantages of both solid rockets and liquid-fuel rockets, therefore becoming more attractive. In hybrid rockets, the solid fuel is hollowed out to produce a combustion port very similar to that of a solid rocket motor type system. The fuel must be initially ignited in order to vaporize some of the fuel into a region just above the solid surface. Then, by injecting the oxidizer at a high mass flow rate and pressure into the chamber the oxidizer and fuel are allowed to react in a thin boundary layer just above the surface of the fuel. The combustion gases pass through the remainder of the combustion port and expanded via a nozzle.

Those rockets also have start, stop and restart capabilities. Hybrid rocket systems are safer to produce and store, ecologically safer with proper propellant choice.

When modeling such a system, it must be considered that the location of the solid-gas interface changes with time, as the solid fuel burns out. This moving boundary must be modeled with proper mathematical transformation to deal with regression of the surface.

1.1 Motivation and Scope

In this study, a previous computer code, which is written for predicting flow field for “turbulent flow over a solid surface in non-uniform regression”, is developed to be more stable under higher regression rates. The same numerical differencing scheme of the previous code is used to develop the present code, but a two-step time averaging method is used for the linearization of equations. A detailed explanation of the solution procedure and differencing scheme can be found in Chapter 6.

The mathematical model is physics based. Momentum equation, continuity equation, energy equation and K-ε turbulence equations are used to construct the mathematical model. The flow is assumed to be incompressible and turbulent; flow field is two-dimensional.

The equations for the cartesian (x-y) coordinates are transformed into a fixed coordinate system (x-σ) because of the moving boundary condition. The regression of the solid surface causes the bounds of the numerical domain to change; therefore vertical coordinates are normalized based on the total height of the gas domain.

Then, the transformed equations are stretched in the vertical direction using a logarithmic transformation to provide mesh refinement at the boundaries where the gradients of the flow parameters are very high. After stretching, the numerical domain is changed to the (x-η) coordinates.

The transformed and stretched form of the energy, x-momentum, continuity, and turbulence equations are solved with an appropriate numerical technique that is second order accurate in time.

A two-step time averaging method is used for the solution of the transformed and stretched equations. The developed computer code first reads the boundary and initial conditions that are specified within input files, and then predicts the flow field at the next time step, $n+1$. Then using those predicted values, flow field at next time step, $n+2$ is predicted. By averaging the flow field variables at time n and $n+2$, flow field at time $n+1$ is obtained.

Throughout the study, present program is run for uniform regression at the boundary, constant regression rate and constant interface temperature.

1.2 Outline

Chapter 2 consists of a literature survey on different type of turbulence models, numerical methods, and finite differencing methods.

In Chapter 3 the description of the physical model is given.

Chapter 4 involves the modeling of the gas flow.

In Chapter 5, transformation and stretching procedure for moving boundary is explained.

In Chapter 6, numerical solution technique is given in detail.

In Chapter 7, results of the developed computer code are compared with the Blasius solution for laminar flow over a flat plate, and turbulent flow over a flat plate investigated by other researchers. Then it is verified that the developed program works independent of time increment and mesh size.

The results of the present computer code and the previous code are compared in Chapter 8.

Program is run for three different Reynolds numbers, three different regression rates and two interface temperatures and results are presented in Chapter 9.

Concluding remarks are presented in Chapter 10.

Recommendations for possible future works are given in Chapter 11.

CHAPTER 2

LITERATURE SURVEY

2.1 Turbulence Models

Turbulence is the state of fluid motion, which is characterized by apparently random and chaotic vorticity. When turbulence is present, it usually dominates all other flow phenomena and results in increased energy dissipation, mixing, heat transfer, and drag. Almost all fluid flows that is the subject of science and engineering are turbulent.

Turbulent flows can often be observed to arise from laminar flows as the Reynolds number is increased. This happens because small disturbances to the flow are no longer damped by the flow, but begin to grow by taking energy from the original laminar flow.

The manner in which the instabilities grow naturally in a flow can be examined using the equations governing the flow. They are derived by decomposing the motion into a mean and fluctuating part.

$$x = X + x' \tag{2.1}$$

One reason of decomposing variables is that it is usually more important to know the mean values instead of time histories. There are many models developed for predicting the effects of turbulence.

2.1.1 Statistical Models

Some of the study of turbulence is focused on statistics and stochastic processes, simply because the instantaneous motions are complicated to understand. This should does not mean that the governing equations are stochastic. In other words, even though the solutions for a given set of initial and boundary conditions can be perfectly repeatable and predictable at a given time and point in space, it may be impossible to guess from the information at one point or time what will it be at another. Moreover, a slight change in the initial or boundary conditions may cause large changes in the solution at a given time and location.

In order to predict the flow field, many experimental results must be present. Moreover, it is intended to develop a physics based model so statistical methods are out of the scope of this work. Works in the literature can be seen for further details [17],[18],[19].

2.1.2 Algebraic Models

An algebraic equation can be used to compute turbulence. The Reynolds stress tensor is then computed using an assumption which relates the Reynolds stress tensor to the velocity gradients and the turbulent viscosity. This assumption is called the Boussinesq assumption. Algebraic models are also called as zero-equation models.

Both eddy viscosity and mixing length models require the unknown functions to be related to the local values of the boundary layer, such as the boundary layer thickness δ and the displacement thickness δ_1. There are several models developed for that purpose such as the models by T. Cebeci and A.M.O Smith [20], R. Michel et al. [21], M.P Escudier [22].

The algebraic turbulence models are only an approximation for all other boundary layers. One or more equation models are more precise.

2.1.3 One Equation Models

All non-algebraic models use the equation for the kinetic energy of the turbulent fluctuations (K-equation) in the form:

$$\rho\left(\bar{u}\frac{\partial K}{\partial x}+\bar{v}\frac{\partial K}{\partial y}\right)=\mu\frac{\partial^2 K}{\partial y^2}-\frac{\partial}{\partial y}\left[\overline{v'(p'+\frac{\rho}{2}q^2)}\right]+\tau_t\frac{\partial \bar{u}}{\partial y}-\rho(\overline{u'^2}-\overline{v'^2})\frac{\partial \bar{u}}{\partial x}-\rho\varepsilon$$

(2.2)

which is based on the work of L. Prandtl. The terms on the right hand side are as follows: viscous diffusion, turbulent diffusion, production (two terms) and (pseudo) dissipation.

Following references can be seen for different one-equation models developed by Bradshaw et al. [23], Rubesin M. W. [24], Goldberg U.C. [25], Baldwin B.S. and Barth T.J.[26] .

2.1.4 Two Equation Models

If the equation developed by Prandtl is defined for the turbulent shear stress, by replacing ν_t with τ_t, two further equations for the unknown functions *K(x,y)* and $\varepsilon(x,y)$ are then required to close the system of equations. This will lead to two or more equation models.

K-ε and k-ω have become standard models for turbulence prediction and commonly used for most engineering problems. Most often one of the transported variable is K, turbulent kinetic energy. The second transported variable depends on the model chosen. Turbulent dissipation energy ε or the specific dissipation ω used

for the following methods. Summaries of two-equation models have been given by W.C. Reynolds[27] and C.G. Speziale et al.[28].

2.1.4.1 K-ε Model

The standard K-ε model is in the form [14]:

K-equation:

$$\frac{\partial}{\partial t}(\rho K)+\frac{\partial}{\partial x_i}(\rho K u_i)=\frac{\partial}{\partial x_j}\left((\mu+\frac{\mu_t}{\sigma_k})\frac{\partial K}{\partial x_j}\right)-\rho\overline{u_i' u_j'}\frac{\partial u_j}{\partial x_i}+\beta g_i\frac{\mu_t}{\mathrm{Pr}_t}\frac{\partial T}{\partial x_i} \\ -\rho\varepsilon-Y_M+S_k \tag{2.3}$$

ε-equation:

$$\frac{\partial}{\partial t}(\rho\varepsilon)+\frac{\partial}{\partial x_i}(\rho\varepsilon u_i)=\frac{\partial}{\partial x_j}\left((\mu+\frac{\mu_t}{\sigma_\varepsilon})\frac{\partial \varepsilon}{\partial x_j}\right)-C_{1\varepsilon}\frac{\varepsilon}{K}(\rho\overline{u_i' u_j'}+C_{3\varepsilon}\beta g_i\frac{\mu_t}{\mathrm{Pr}_t}\frac{\partial T}{\partial x_i}) \\ -C_{2\varepsilon}\rho\frac{\varepsilon^2}{K}+S_\varepsilon \tag{2.4}$$

As well as the standard K-ε model, there are also modified K-ε models in the literature some of which are claimed to be more precise.

The RNG model was developed using Re-Normalization Group (RNG) methods by Yakhot et al to renormalize the Navier-Stokes equations, to account for the effects of smaller scales of motion. In the standard K-ε model the eddy viscosity is determined from a single turbulence length scale, so the calculated turbulent diffusion is that which occurs only at the specified scale, whereas in reality all scales of motion will contribute to the turbulent diffusion. The RNG approach, which is a mathematical technique that can be used to derive a turbulence model similar to the K-ε, results in a modified form of the ε-equation which attempts to account for the different scales of motion through changes to the production term.

There are number of ways to write transport equations for K and ε, a simple interpretation where buoyancy is neglected is:

$$\frac{\partial}{\partial t}(\rho K)+\frac{\partial}{\partial x_i}(\rho K u_i)=\frac{\partial}{\partial x_j}\left((\mu+\frac{\mu_t}{\sigma_k})\frac{\partial K}{\partial x_j}\right)+P_k-\rho\varepsilon \tag{2.5}$$

$$\frac{\partial}{\partial t}(\rho \varepsilon)+\frac{\partial}{\partial x_i}(\rho \varepsilon u_i)=\frac{\partial}{\partial x_j}\left((\mu+\frac{\mu_t}{\sigma_\varepsilon})\frac{\partial \varepsilon}{\partial x_j}\right)-C_{1\varepsilon}\frac{\varepsilon}{K}P_k-C_{2\varepsilon}\rho\frac{\varepsilon^2}{K} \tag{2.6}$$

K-ε model does not give very accurate results near the boundaries. This model is not suitable for drag or lift calculations of airfoils.

2.1.4.2 K-ω Model

In k-ω model, instead of turbulent dissipation energy, specific dissipation ω is used as the second variable of turbulence. It is the variable that determines the scale of turbulence, whereas the first variable K, determines the energy in the turbulence. ω is defined as:

$$\omega=\frac{1}{C_\mu}\frac{\varepsilon}{K} \quad \text{where} \quad C_\mu \approx 0.09 \tag{2.7}$$

and the equations defining the model are:

K-equation

$$\frac{\partial K}{\partial t}+U_j\frac{\partial K}{\partial x_j}=\tau_{ij}\frac{\partial U_i}{\partial x_j}-\beta^* K\omega+\frac{\partial}{\partial x_j}\left[(\nu+\sigma^*\nu_T)\frac{\partial K}{\partial x_j}\right] \tag{2.8}$$

ω-equation

$$\frac{\partial \omega}{\partial t} + U_j \frac{\partial \omega}{\partial x_j} = \alpha \frac{\omega}{k} \tau_{ij} \frac{\partial U_i}{\partial x_j} - \beta^* \omega^2 + \frac{\partial}{\partial x_j}\left[(\nu + \sigma \nu_T) \frac{\partial \omega}{\partial x_j} \right] \tag{2.9}$$

There are some modifications made to the standard K-ω model. Wilcox's modified K-ω model, SST K-ω model are examples to those modified models.

2.2 Numerical Methods for Solution

Numerical differentiation is a technique of numerical analysis to produce an estimate of the derivative of a mathematical function using values from the function and other knowledge about the function. It is widely used for solution of engineering problems, especially for fluid flow. The idea is based on evaluating the derivative of a function with the knowledge of its value on some points.

The method selected depends on the nature of the equation that is going to be solved. There are various methods with different accuracy levels, convergence rates and computational times required to find the solution.

Several methods are used for the solution of Navier-Stokes equations, energy equation, turbulence equations, and continuity equation.

The unsteady, incompressible, Navier-Stokes equations are a mixed set of hyperbolic-elliptic equations, which are difficult to solve because of the differences in numerical techniques required to solve for hyperbolic and elliptic type equations. Nearly all successful solutions of the incompressible Navier-Stokes equations have employed the unsteady form of the equations. The steady-state solution is obtained by marching the solution in time until convergence is achieved. The procedure is called time-dependent approach and is used for the solution of momentum equations.

Both explicit and implicit finite-difference schemes have been used with the time-dependent approach to solve the incompressible Navier-Stokes equations. Nearly all of these methods are second order accurate in space and either first or second order accurate in time. If only the steady-state solution is required, it is often advantageous to employ a scheme, which is not time accurate since the steady-state solution may be achieved with fewer time steps.

Because of the added complexity, only a handful of third-order or higher methods have appeared in the literature to solve the incompressible Navier-Stokes equations. A second-order accurate scheme is thought to be the optimum choice in the sense of computing time and accuracy.

2.2.1 Explicit MacCormack Method

When the original MacCormack scheme [29] is applied to the incompressible Navier-Stokes equations the following algorithm results: The explicit scheme is second-order accurate in both space and time. General forms of the equations are given in forward differencing for the predictor step, and backward differencing is used in the corrector step.

The terms in Navier Stokes equations are grouped such as:

$$\frac{\partial U}{\partial t}+\frac{\partial E}{\partial x}+\frac{\partial F}{\partial y}=0 \tag{2.10}$$

The property U, can be predicted in the first step as:

$$\overline{U}_{i,j}^{n+1}=U_{i,j}^{n}-\frac{\Delta t}{\Delta x}(E_{i+1,j}^{n}-E_{i,j}^{n})-\frac{\Delta t}{\Delta y}(F_{i,j+1}^{n}-F_{i,j}^{n}) \tag{2.11}$$

and corrected in the second step as:

$$U_{i,j}^{n+1} = \frac{1}{2}\left[U_{i,j}^{n} + \overline{U_{i,j}^{n+1}} - \frac{\Delta t}{\Delta x}(\overline{E_{i,j}^{n+1}} - \overline{E_{i-1,j}^{n+1}}) - \frac{\Delta t}{\Delta y}(\overline{F_{i,j}^{n+1}} - \overline{F_{i,j-1}^{n+1}}) \right] \tag{2.12}$$

The forward and backward differencing can be alternated between predictor and corrector steps as well as between the two spatial derivatives in a sequential fashion. This eliminates the bias due to one-sided differencing. An example is given in the table below:

Table 2.1 Differencing Sequence for MacCormack Scheme

	PREDICTOR		CORRECTOR	
STEP	x-derivative	y-derivative	x-derivative	y-derivative
1	F	F	B	B
2	B	B	F	F
3	F	F	B	B
4	B	F	F	B
5	F	B	B	F
6	B	F	F	B
7	F	B	B	F
8	B	B	F	F

F, forward difference; B, backward difference

The derivatives appearing in the viscous terms of E and F must be differenced correctly in order to maintain the second order accuracy. This is accomplished in the following manner. The x derivative terms appearing in E are differenced in the opposite direction to that used for $\partial E/\partial x$ while the y-derivatives are approximated with central differences.

Explicit MacCormack algorithm is a suitable method for solving both steady and unsteady flows at moderate to low Reynolds numbers. However, it is not a satisfactory method for solving high Reynolds number flows where the viscous regions become very thin. For these flows mesh must be highly refined in order to accurately solve the viscous regions. This leads to small time steps and

subsequently long computational times if an explicit scheme such as MacCormack method is used.

There are certain modifications made to MacCormack method to provide higher convergence rate and stability. There are also works on using different time increments in x and y directions, therefore decreasing the computational time [30].

A time averaging method similar to MacCormack method is used for the developed code [31]. Mesh is refined near the solid surface.

2.2.2 Hopscotch Method

In Hopscotch algorithm, there are two sweeps of the solution domain carried out. In the first sweep, the properties are approximated at the nodes where $i+j+n$ is even; then in the second sweep, the properties at the nodes where $i+j+n$ is odd are calculated.

The mixed derivative terms appearing in the Navier-Stokes equations create a problem in Hopscotch scheme. If those terms are differenced in the usual manner, the Hopscotch method is no longer explicit and requires a matrix inversion. This problem can be circumvented by lagging the mixed derivative term.

2.2.3 Brailovskaya Method

Brailovskaya method is a two-step scheme, second order accurate in space and first order accurate in time. It does not give acceptable results except the steady-state solutions. If the solution requires second-order accuracy, MacCormack or Lax-Wendroff method must be used.

2.2.4 Allen-Cheng Method

Allen-Cheng method is an improvement to the Brailovskaya method. The viscous term is differenced in a different way providing that it is more stable. Stability condition for the Allen-Cheng method is independent of viscosity giving it a distinct advantage over the other methods except the Hopscotch method. But it is first order accurate in time, thus it can not be used for the solution of a transient problem.

2.2.5 Lax-Wendroff Method

Lax-Wendroff scheme is similar to MacCormack scheme. It is a two-step predictor-corrector type scheme using the flow parameters between the nodes, instead of at the nodes.

It is first-order accurate in time and second-order accurate in space, but it is required to compute the variables at the half nodes thus the computational time increases. There are some works in the literature to increase the time accuracy of this method to second-order, using $n+1$ time levels in the predictor step instead of $n+1/2$.

2.2.6 Implicit Methods

Implicit methods are widely used for the solution of the Navier-Stokes equations. Solution procedure is generally more complicated for this type of methods. The term implicit means that the dependent variable and the independent variables can not be separated on opposite sides of the equations. Therefore, the set of equations form a matrix, that is generally upper or lower bi-diagonal or triangular. Matrix inversion or decomposition techniques should be used for the solution of those methods.

Implicit methods generally require more computational time, but they are convergent also for coarser mesh sizes. The stability restrictions of the explicit methods do not exist in implicit methods.

2.3 Comparison of the Finite-Differencing Methods

For the numerical solution of the partial differential equations, finite-differencing must be carried out based on the solution domain as a grid of discrete points are substituted for the partial derivatives in the equations of interest.

The equations that are obtained after transformation and stretching must be finite differenced in order to be solved. Finite-differencing must be made according to the nature of the problem.

The continuity, momentum, energy, turbulence and conservation of species equations contain the first and second partial derivatives of the flow properties with respect to the coordinates and time.

The direction of differencing depends on the nature of the problem. There are three options for first order differencing; backward, central and forward differencing.

2.3.1 Backward Differencing

Backward differencing of any partial derivative uses the information of the present node and the previous node with respect to the flow direction to approximate the derivative. If the flow properties of the present node are mainly affected by the previous node, this is the ideal differencing scheme. It is also called “upwind differencing”. It is given by the formula:

$$\left(\frac{\partial u}{\partial x}\right)_{i,j} = \frac{u_{i,j} - u_{i-1,j}}{\Delta x} \tag{2.13}$$

Here the index i represents the node number in x-direction and j represents the node number in η-direction. Δx is the distance of the nodes in x-direction.

2.3.2 Central Differencing

Central differencing of any partial derivative uses the information of both the next node and the previous node to approximate the derivative. If the flow properties of the present node are affected by both nodes equally, this is the ideal differencing scheme. It is given by the formula:

$$\left(\frac{\partial u}{\partial x}\right)_{i,j} = \frac{u_{i+1,j} - u_{i-1,j}}{2\ \Delta x} \tag{2.14}$$

2.3.3 Forward Differencing

Forward differencing of any partial derivative uses the information of both the next node and the current node to approximate the derivative. This scheme can be used to capture backflow. It is given by the formula:

$$\left(\frac{\partial u}{\partial x}\right)_{i,j} = \frac{u_{i+1,j} - u_{i,j}}{\Delta x} \tag{2.15}$$

The scheme used for the computer code is described in detail in section 6.1.

CHAPTER 3

DESCRIPTON OF THE PHYSICAL MODEL

3.1 Physical Model

The physical model is a “flow over a flat plate” with constant regression rate and constant surface temperature. Figure 3.1 shows the schematic of the model. Boundary conditions are given in Chapter 4.

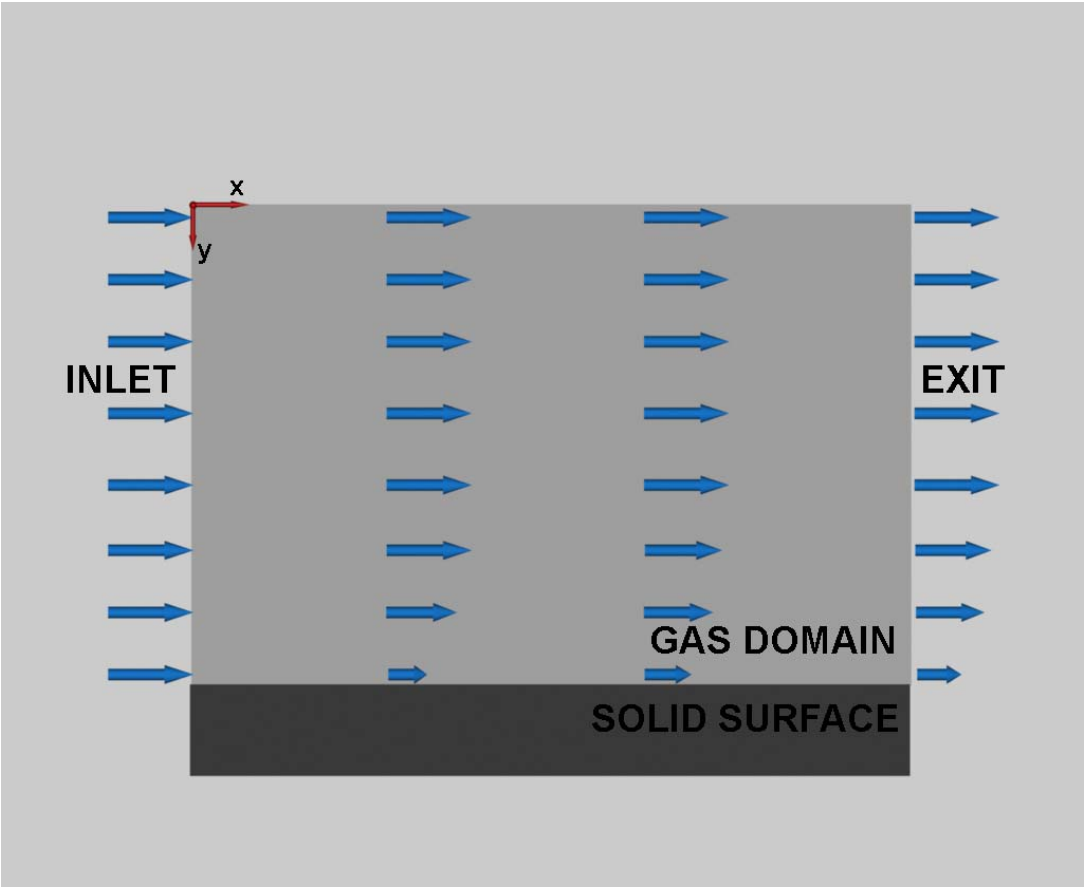

Figure 3.1 Definition of the Physical Model

The main objective of this study is to develop a computer code to calculate the velocity and temperature distribution, taking the effect of turbulence into consideration for the given problem. The gas domain is assumed turbulent, incompressible with boundary layer approximations.

It is assumed that:

- the flow is near-parallel
- the inlet velocity is uniform
- regression is uniform throughout the boundary and constant
- physical properties are constant
- gas is ideal
- solid surface is isothermal

The mathematical model, which describes the physical model given above, is presented in next chapter.

CHAPTER 4

MODELING OF THE GAS FLOW

4.1 Modeling of the Gas Flow

The gas flow over a solid surface is assumed to be two-dimensional, turbulent, incompressible and subsonic with boundary layer approximations. The conservation equations based on boundary layer approximations for an unsteady flow of a gas are given as follows:

4.1.1 Continuity Equation

The general form of the continuity equation in two-dimensional cartesian coordinates is [1]:

$$\frac{\partial \rho}{\partial t} + \frac{\partial (\rho u)}{\partial x} + \frac{\partial (\rho v)}{\partial y} = 0 \tag{4.1}$$

For the incompressible flow case, the continuity equation reduces to:

$$\frac{\partial u}{\partial x} + \frac{\partial v}{\partial y} = 0 \tag{4.2}$$

The continuity equation (4.2) is used in the code to calculate the vertical velocity(v).

4.1.2 Momentum Equation

The x-momentum equation is used in the code to predict the horizontal velocity(u). General form of the momentum equation in x-direction is [1]:

$$\frac{\partial(\rho u)}{\partial t}+\frac{\partial(\rho u^2)}{\partial x}+\frac{\partial(\rho uv)}{\partial y}+\frac{\partial p}{\partial x}-\frac{\partial}{\partial x}\left[\frac{2}{3}\mu_{eff}\left(2\frac{\partial u}{\partial x}-\frac{\partial v}{\partial y}\right)\right]-\frac{\partial}{\partial y}\left[\mu_{eff}\left(\frac{\partial u}{\partial y}-\frac{\partial v}{\partial x}\right)\right]=0 \tag{4.3}$$

The effective viscosity in this equation is defined as:

$$\mu_{eff}=\mu+\mu_t \tag{4.4}$$

where the eddy (turbulent) viscosity is given by:

$$\mu_t=\rho C_\mu \frac{K^2}{\varepsilon} \tag{4.5}$$

For the incompressible case, where u_∞ is assumed constant, the pressure term $\frac{\partial p}{\partial x}$ drops out. If the kinetic and potential energy changes of the fluid and viscous dissipation are neglected, parabolic form of the x-momentum equation (4.3) reduces to [2]:

$$\rho\frac{\partial u}{\partial t}+\rho u\frac{\partial u}{\partial x}+\rho v\frac{\partial u}{\partial y}-\frac{\partial}{\partial y}\left[\mu_{eff}\frac{\partial u}{\partial y}\right]=0 \tag{4.6}$$

This parabolic form of the momentum equation assumes that the viscous dissipation in x-direction is negligible therefore drops out.

4.1.3 Energy Equation

General form of the energy equation is [1]:

$$\frac{\partial}{\partial t}\left[(c_v)\rho T\right]+\frac{\partial}{\partial x}(c_p\rho u T)+\frac{\partial}{\partial y}(c_p\rho v T)-\frac{\partial}{\partial x}(k_{eff}\frac{\partial T}{\partial x})-\frac{\partial}{\partial y}(k_{eff}\frac{\partial T}{\partial y})-$$
$$\mu_{eff}\left[2\left(\frac{\partial u}{\partial x}\right)^2+2\left(\frac{\partial v}{\partial y}\right)^2+\left(\frac{\partial u}{\partial y}+\frac{\partial v}{\partial x}\right)^2\right]=0 \tag{4.7}$$

The flow is incompressible, subsonic and assumed near-parallel therefore conduction in x-direction and viscous dissipation terms are neglected. Fluid properties are assumed constant. Therefore, equation (4.7) becomes:

$$\rho c_p(\frac{\partial T}{\partial t}+u\frac{\partial T}{\partial x}+v\frac{\partial T}{\partial y})=\frac{\partial}{\partial y}(k_{eff}\frac{\partial T}{\partial y}) \tag{4.8}$$

where the effective thermal conductivity is given by:

$$k_{eff}=k+k_t \tag{4.9}$$

the turbulent thermal conductivity is:

$$k_t=\frac{c_p\mu_t}{\mathrm{Pr}_t} \tag{4.10}$$

Energy equation is used in the code to predict temperature (T) of the gas.

4.1.4 K-ε Equations

K and ε are, turbulent kinetic energy and turbulent dissipation energy respectively. These variables are determined from the equations 2.5 and 2.6. For this study, these equations are parabolized and the following equations are obtained:

turbulent kinetic energy (K-equation)

$$\frac{\partial K}{\partial t}+u\frac{\partial K}{\partial x}+v\frac{\partial K}{\partial y}=\left(\frac{\mu}{\rho}+\frac{\mu_t}{\rho\,\mathrm{Pr}_K}\right)\frac{\partial^2 K}{\partial y^2}+\frac{\mu_t}{\rho}\left(\frac{\partial u}{\partial y}\right)^2-\varepsilon \tag{4.11}$$

turbulent dissipation energy (ε-equation)

$$\frac{\partial \varepsilon}{\partial t}+u\frac{\partial \varepsilon}{\partial x}+v\frac{\partial \varepsilon}{\partial y}=\left(\frac{\mu}{\rho}+\frac{\mu_t}{\rho\,\mathrm{Pr}_\varepsilon}\right)\frac{\partial^2 \varepsilon}{\partial y^2}+C_{\varepsilon 1}\frac{\mu_t}{\rho}\frac{\varepsilon}{K}\left(\frac{\partial u}{\partial y}\right)^2-C_{\varepsilon 2}\frac{\varepsilon^2}{K} \tag{4.12}$$

the constants of the K-ε model adopted for this study are given as [4]:

$$C_\mu=0.09 \quad C_{\varepsilon 1}=1.45 \quad C_{\varepsilon 2}=2.0 \quad \mathrm{Pr}_K=1.0 \quad \mathrm{Pr}_\varepsilon=1.3 \tag{4.13}$$

4.1.5 Boundary and Initial Conditions

To close the mathematical formulation, the following boundary and initial conditions are necessary for the gas domain:

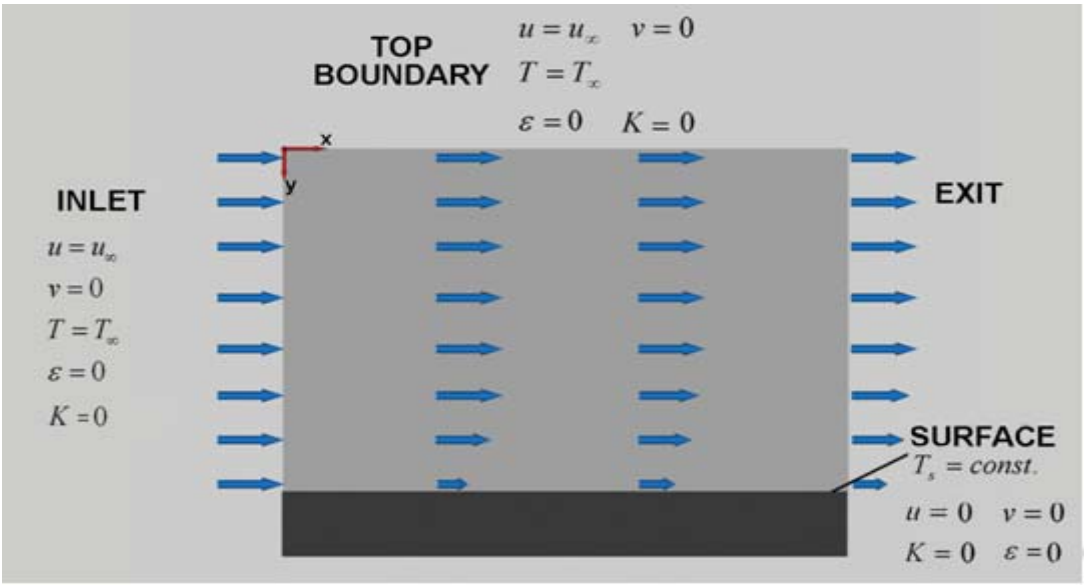

Figure 4.1 Boundary conditions

at the solid surface, $y = h + r(x,t)$

$$u = 0 \tag{4.14}$$

$$v = \dot{r} \text{ (}\textit{regression rate=constant}\text{)} \tag{4.15}$$

$$T_s = const. \tag{4.16}$$

$$K = 0 \tag{4.17}$$

$$\varepsilon = 0 \tag{4.18}$$

at the top boundary, $y = 0$

$$u = u_\infty \tag{4.19}$$

$$v = 0 \tag{4.20}$$

$$T = T_\infty \tag{4.21}$$

$$K = 0 \tag{4.22}$$

$$\varepsilon = 0 \tag{4.23}$$

at the inlet, x=0

$$u = u_\infty \tag{4.24}$$

$$v = 0 \tag{4.25}$$

$$T = T_\infty \tag{4.26}$$

$$K = 0 \tag{4.27}$$

$$\varepsilon = 0 \tag{4.28}$$

initially, at $t = 0$, for the whole domain except the bottom, top and inlet boundaries:

$$u = u_\infty \tag{4.29}$$

$$v = 0 \tag{4.30}$$

$$T = T_\infty \tag{4.31}$$

$$K = 0 \tag{4.32}$$

$$\varepsilon = 0 \tag{4.33}$$

4.2 Final Form of the Mathematical Model

Based on the above assumptions, equations used in the mathematical model are (4.2) (4.6) (4.8) (4.11) and (4.12). These governing differential equations for the present study are solved under the boundary and initial conditions given in section 4.1.5.

CHAPTER 5

MOVING BOUNDARY TRANSFORMATION AND STRETCHING

5.1 Introduction

The governing equations given in Chapter 4 for this study cannot be solved for moving boundary without mathematical transformation. An appropriate transformation as described below, is used to create a fixed boundary, orthogonal domain where these governing equations can be solved. Furthermore, the equations are stretched in vertical direction to increase the accuracy of the numerical solution near the wall where high velocity and temperature gradients exist. Details of the proposed transformation and stretching used in this study are given below.

5.2 Transformation of the equations

The boundary of the solid surface and the gas is a moving boundary, because of the regression of the solid surface. The boundary between the solid and the gas is moving as a function of x and t, therefore all the equations must be transformed into a fixed, orthogonal coordinate system. There is no need to normalize the equations in x-direction since x-coordinates are not affected by the regression. The model of the domain can be seen in Figure 7.1, where the original position of the surface before regression is shown with dashed line and the height of the gas before regression is given as h.

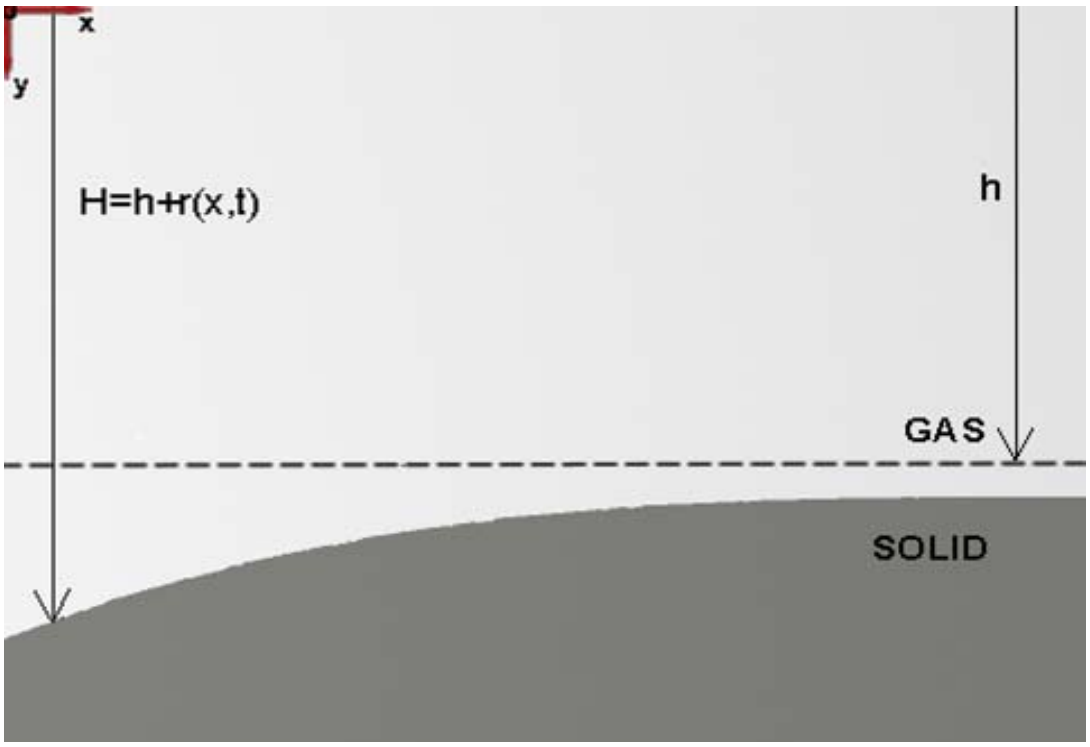

Figure 5.1 Schematic of the Moving Boundary

In order to deal with the moving boundary condition, the coordinate system is changed from x-y to x-σ. The transformation is given in the following sections.

It is shown in Figure 5.1 that regression rate is non-uniform, but throughout this study it is set as constant and uniform.

5.2.1 Transformation of the gas domain

Gas domain is transformed from x-y coordinates into x-σ coordinate system by the given formulas:

$$\sigma = \frac{y}{H} \tag{5.1}$$

where H is the time dependent total height of the gas. It is defined as:

$$H(x,t) = h + r(x,t) \tag{5.2}$$

Based on the transformation given above, the first order time derivative of any variable in the gas domain is calculated from:

$$\frac{\partial}{\partial t}(\,) = \frac{\partial}{\partial t}(\,) + \frac{\partial \sigma}{\partial t}\frac{\partial}{\partial \sigma}(\,) \tag{5.3}$$

where $$\frac{\partial \sigma}{\partial t} = -\frac{\sigma}{H}\frac{\partial r(x,t)}{\partial t} = -\frac{\sigma}{H} r_t = -\frac{\sigma}{H}\dot{r} \tag{5.4}$$

The first order derivative with respect to horizontal coordinate x is defined as:

$$\frac{\partial}{\partial x}(\,) = \frac{\partial}{\partial x}(\,) + \frac{\partial \sigma}{\partial x}\frac{\partial}{\partial \sigma}(\,) \tag{5.5}$$

where $$\frac{\partial \sigma}{\partial x} = -\frac{\sigma}{H}\frac{\partial r(x,t)}{\partial x} = -\frac{\sigma}{H} r_x \tag{5.6}$$

The first order derivative with respect to vertical coordinate y is defined as:

$$\frac{\partial}{\partial y}(\,) = \frac{\partial \sigma}{\partial y}\frac{\partial}{\partial \sigma}(\,) \tag{5.7}$$

where $$\frac{\partial \sigma}{\partial y} = \frac{1}{H} \tag{5.8}$$

The second-order partial derivative with respect to vertical coordinate y is defined as:

$$\frac{\partial}{\partial y}\left(\frac{\partial}{\partial y}(\,)\,\right) = \frac{\partial \sigma}{\partial y}\frac{\partial}{\partial \sigma}\left(\frac{\partial \sigma}{\partial y}\frac{\partial}{\partial \sigma}(\,)\right) \tag{5.9}$$

The transformation of a sample equation, turbulent kinetic energy equation, can be seen in Appendix A.

5.2.2 Changes in Mathematical Domain After Transformation

Mathematical domain before the transformation is given in Figure 5.2.

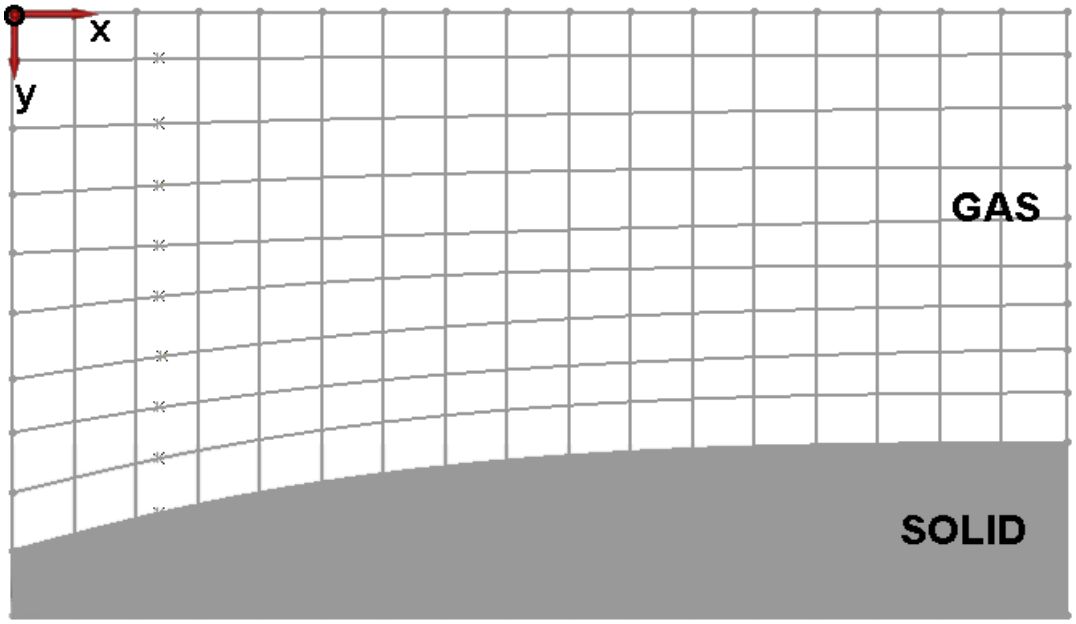

Figure 5.2 Sketch of the Mathematical Domain Before Transformation (x-y domain)

After the transformation, the mathematical domain is normalized in vertical direction. Therefore, the cells became identical.

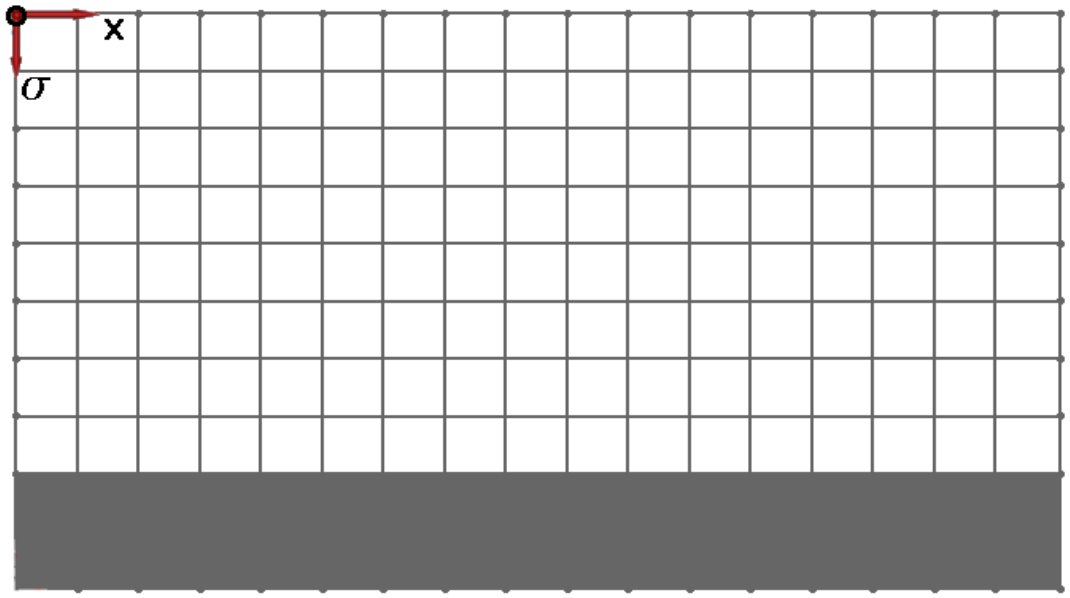

Figure 5.3 Sketch of the Mathematical Domain After Transformation (x-σ domain)

5.3 Stretching of the equations

The transformed governing differential equations in the gas domain must be stretched to generate a finer mesh at the boundaries. The gradients of the flow parameters are very high in the boundary layer; therefore, it is essential to have finer mesh close to the boundary.

Stretching is carried out in vertical direction using a logarithmic transformation. The coordinate system is changed from x-σ to x-η after stretching. The formula used during stretching is given as [15]:

$$\eta = \alpha + (1+\alpha) \times \frac{\ln\left(\{\beta + [\sigma(1+2\alpha)/h] - 2\alpha\}/\{\beta - [\sigma(1+2\alpha)/h] + 2\alpha\}\right)}{\ln[(\beta+1)/(\beta-1)]} \qquad (5.10)$$

In this transformation if α is selected as $\alpha = 0$, therefore the mesh is refined only at $\sigma = h$, at the solid-gas boundary. If α was selected as $\alpha = 0.5$ the mesh will be refined equally at the bottom and top boundaries of the gas domain. The other

parameter β has values such that $1.0 \le \beta \le \infty$. In this study it is selected as [1] $\beta = 1.15$.

To transform the governing differential equations to the new x-η coordinate system, the chain rule of the derivatives is used as:

$$\frac{\partial}{\partial \sigma}() = \frac{\partial \eta}{\partial \sigma}\frac{\partial}{\partial \eta}() \tag{5.11}$$

where

$$\eta_\sigma = \frac{\partial \eta}{\partial \sigma} = \frac{2\beta(1-\alpha)(2\alpha+1)}{h\{\beta^2 - [\sigma(2\alpha+1)/h - 2\alpha]\}\{\ln[(\beta+1)/(\beta-1)]\}} \tag{5.12}$$

After stretching, the computational domain becomes as shown in Figure 5.4. Mesh is highly refined near the solid-gas boundary, where there is high energy interaction, high velocity and temperature gradients.

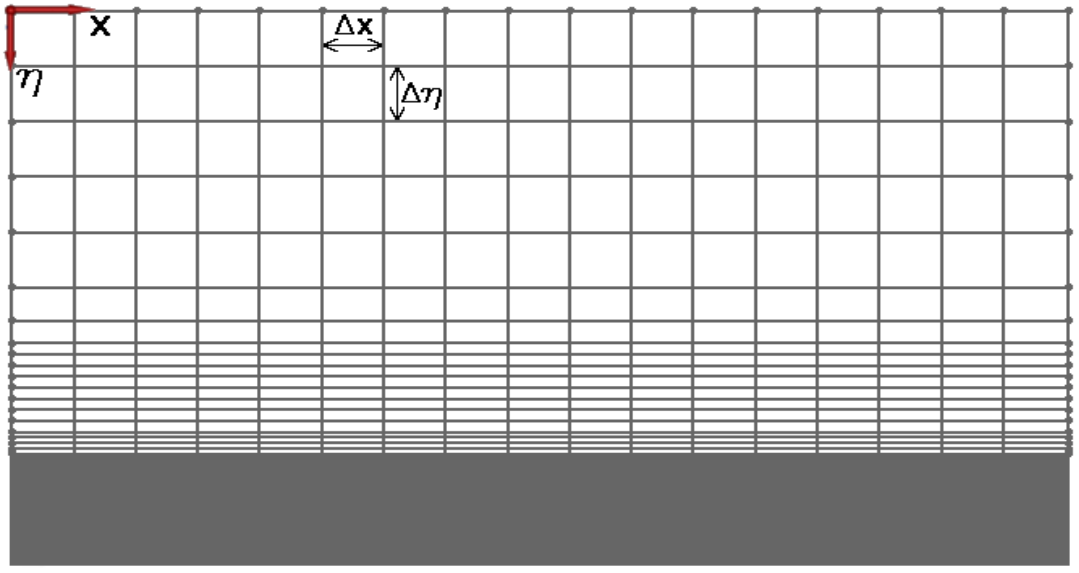

Figure 5.4 Sketch of the Mathematical Domain After Stretching (x-η domain)

After the flow field is predicted in the stretched computational domain, the following inverse transformation is used to go back to the physical domain.

$$\sigma = h\frac{(\beta+2\alpha)[(\beta+1)/(\beta-1)]^{\eta-\alpha/1-\alpha}-\beta+2\alpha}{(2\alpha+1)\left[1+[(\beta+1)/(\beta-1)]^{\eta-\alpha/1-\alpha}\right]} \tag{5.13}$$

The stretching of a sample equation, turbulent kinetic energy equation, is provided in Appendix A.

5.4 Final Form of the Transformed and Stretched Governing Differential Equations

After transformation and stretching, the governing differential equations become:

Continuity:

$$\frac{\partial u}{\partial x}-\frac{\sigma}{H}\eta_\sigma\frac{\partial u}{\partial \eta}r_x+\frac{1}{H}\eta_\sigma\frac{\partial v}{\partial \eta}=0 \tag{5.14}$$

Momentum:

$$\rho\frac{\partial u}{\partial t}-\rho\frac{\sigma}{H}r_t\eta_\sigma\frac{\partial u}{\partial \eta}+\rho u\frac{\partial u}{\partial x}-\rho u\frac{\sigma}{H}r_x\eta_\sigma\frac{\partial u}{\partial \eta}+\rho v\frac{1}{H}\eta_\sigma\frac{\partial u}{\partial \eta}-\mu_{eff}\frac{1}{H^2}\eta_\sigma{}^2\frac{\partial^2 u}{\partial \eta^2}=0 \tag{5.15}$$

Energy:

$$\rho c_p\frac{\partial T}{\partial t}-\rho c_p\frac{\sigma}{H}r_t\eta_\sigma\frac{\partial T}{\partial \eta}+\rho c_p u\frac{\partial T}{\partial x}-\rho c_p\frac{\sigma}{H}r_x u\eta_\sigma\frac{\partial T}{\partial \eta}+\rho c_p\frac{1}{H}v\eta_\sigma\frac{\partial T}{\partial \eta}-k_{eff}\frac{1}{H^2}\eta_\sigma{}^2\frac{\partial^2 T}{\partial \eta^2}=0 \tag{5.16}$$

Turbulent Kinetic Energy:

$$\frac{\partial K}{\partial t}-\frac{\sigma}{H}r_t\eta_\sigma\frac{\partial K}{\partial \eta}+u\frac{\partial K}{\partial x}-\frac{\sigma}{H}r_x u\eta_\sigma\frac{\partial K}{\partial \eta}+\frac{1}{H}v\eta_\sigma\frac{\partial K}{\partial \eta}= \frac{1}{H^2}\left(\frac{\mu}{\rho}+\frac{\mu_t}{\rho\,\mathrm{Pr}_K}\right)\eta_\sigma{}^2\frac{\partial^2 K}{\partial \eta^2}+\frac{\mu_t}{\rho}\frac{1}{H^2}\eta_\sigma{}^2\left(\frac{\partial u}{\partial \eta}\right)^2-\varepsilon \tag{5.17}$$

Turbulent Dissipation Energy:

$$\frac{\partial \varepsilon}{\partial t}-\frac{\sigma}{H}r_t\eta_\sigma\frac{\partial \varepsilon}{\partial \eta}+u\frac{\partial \varepsilon}{\partial x}-\frac{\sigma}{H}r_x u\eta_\sigma\frac{\partial \varepsilon}{\partial \eta}+\frac{1}{H}v\eta_\sigma\frac{\partial \varepsilon}{\partial \eta}= \frac{1}{H^2}\left(\frac{\mu}{\rho}+\frac{\mu_t}{\rho\,\mathrm{Pr}_\varepsilon}\right)\eta_\sigma{}^2\frac{\partial^2 \varepsilon}{\partial \eta^2}+C_{\varepsilon 1}\frac{\varepsilon}{K}\frac{\mu_t}{\rho}\frac{1}{H^2}\eta_\sigma{}^2\left(\frac{\partial u}{\partial \eta}\right)^2-C_{\varepsilon 2}\frac{\varepsilon^2}{K} \tag{5.18}$$

CHAPTER 6

NUMERICAL SOLUTION TECHNIQUE

6.1 Introduction

The governing differential equations are non-linear although parabolic in nature. For solution an explicit, segregated, second order accurate finite difference technique will be adapted. The transformed and stretched governing differential equations (5.14), (5.15), (5.16), (5.17) and (5.18) will be linearized for the computational domain given in Figure 6.1 and Figure 6.2.

6.2 Final Numerical Domain

Sample meshes of the instantaneous computational domain relative to fixed reference of frame are given in the following figures. Mesh is given for two different times, at the beginning and end of simulation, at $t = 0s$ and $t = 0.08s$. i-j indicates the nodal coordinates.

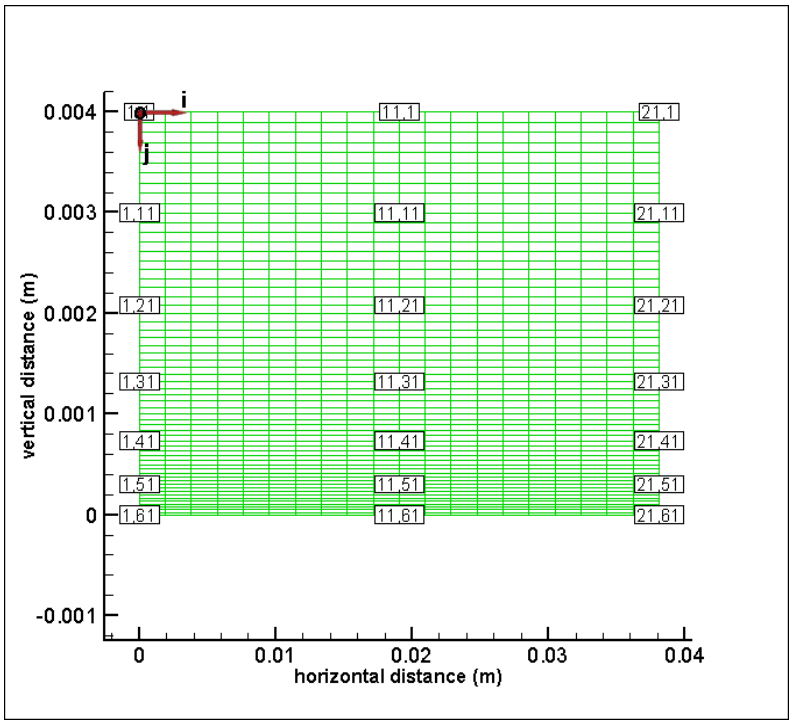

Figure 6.1 Numerical Domain for 21x61 Mesh Size at the Beginning of Simulation ($t = 0s$, Solid Surface at *Vertical Distance* $= 0m$)

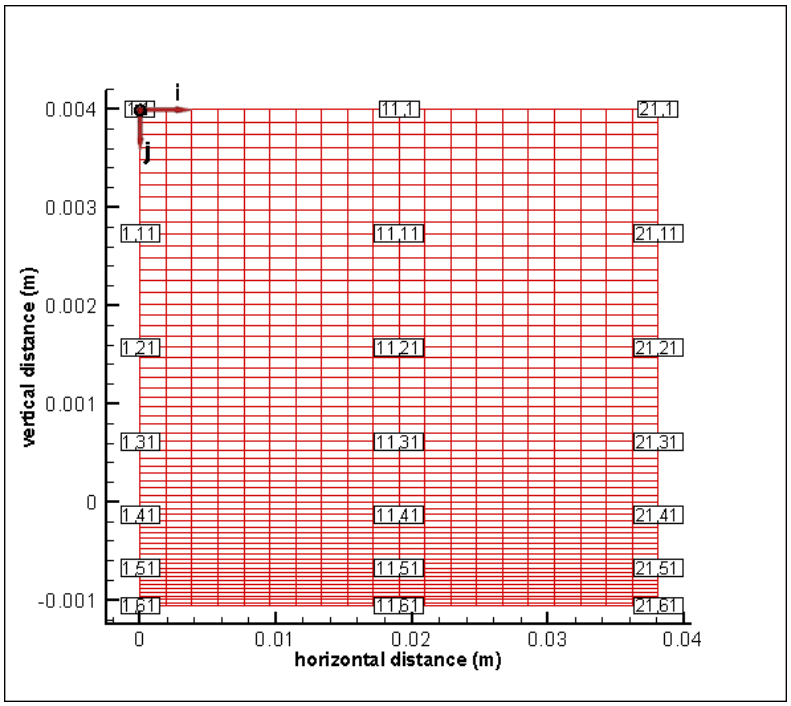

Figure 6.2 Numerical Domain for 21x61 Mesh Size at the End of Simulation, ($t = 0.08s$, $\dot{r} = 0.015m/s$, Solid Surface at *Vertical Distance* $= -1.05x10^{-3}m$)

6.3 Numerical Technique and Differencing Scheme Used in the Previous Study

The transformed and stretched equations are finite-differenced in order to be solved by computer. A single-step explicit scheme was used in the previous study [2].

Momentum, energy and turbulence equations are in the form similar to the form given in [15]:

$$\rho\frac{\partial\phi}{\partial t}+\rho u\frac{\partial\phi}{\partial x}+\rho v\frac{\partial\phi}{\partial y}=\frac{\partial}{\partial y}\left(\lambda\frac{\partial\phi}{\partial y}\right)+S \tag{6.1}$$

where the first term is "inertia of ϕ", second term is "convection of ϕ in x-direction", third term is "convection of ϕ in y-direction", fourth term is "diffusion of ϕ in y-direction" and the last term is "source term". In this equation lambda -diffusion coefficient- is constant. Turbulent $K-\varepsilon$ equations contain additional terms, which are called viscous dissipation terms in y-direction.

The viscous dissipation terms in the turbulent kinetic energy and turbulent energy dissipation equations are:

$$\frac{\mu_t}{\rho}\left(\frac{\partial u}{\partial y}\right)^2 \quad \text{and} \tag{6.2}$$

$$C_{\varepsilon 1}\frac{\mu_t}{\rho}\frac{\varepsilon}{K}\left(\frac{\partial u}{\partial y}\right)^2 \tag{6.3}$$

After transformation and stretching of the equations, while chain differentiation of derivatives with respect to x and t, additional terms appear because $\frac{\partial\sigma}{\partial t}$ and $\frac{\partial\sigma}{\partial x}$ are not zero.

In the previous computer code:

i. backward differencing is used during linearization of convective terms which has derivatives with respect to x, and inertia terms which have derivatives with respect to t

ii. central differencing is used during linearization of convective and inertia terms which have derivatives with respect to η, dissipation terms and diffusive terms

iii. source term does not contain any derivative, so it is not differenced

In Appendix A, linearization of a sample equation, turbulent kinetic energy equation is given for the present computer code. The differencing at the predictor step of the present computer code is exactly the same as the whole differencing of the previous computer code. Finite differencing of each term can be found in A.3.

The following equations are used to predict the following flow properties:

i. continuity equation - vertical velocity (v)
ii. x-momentum equation - horizontal velocity (u)
iii. energy equation - temperature (T)
iv. K-equation - turbulent kinetic energy (K)
v. ε-equation - turbulent dissipation energy (ε)

6.4 Numerical Technique and Differencing Scheme Used in the Present Study

The single-step explicit scheme used in the original program is replaced by a two-step, time averaging method that is second order accurate in time. The same equations are used for the prediction of the flow field.

In the present computer code:

i. in both predictor and corrector stages, backward differencing is used during linearization of convective terms which has derivatives with respect to x, and inertia terms which have derivatives with respect to t

ii. in both predictor and corrector stages, central differencing is used during linearization of convective and inertia terms which have derivatives with respect to η, dissipation terms and diffusive terms

iii. in both predictor and corrector stages, source term does not contain any derivative, so it is not differenced

In Appendix A, differencing of each term of a sample equation, turbulent kinetic energy equation, is given in detail.

6.5 Final Form of the Linearized and Discretized Equations

A similar differencing given in Appendix A is applied to the equations (5.14), (5.15), (5.16), (5.18) and the following linearized and discretized equations given below are obtained. During the discretization, properties and the coefficients of transformation and stretching are assumed constant.

Continuity equation:

First time step (n+1)

$$v_{i,j}^{\overline{n+1}} = v_{i,j+1}^{\overline{n+1}} + \Delta\eta\left(\frac{H}{\eta_\sigma}\right)_{i,j}^{n}\left(\frac{u_{i,j}^{\overline{n+1}} - u_{i-1,j}^{\overline{n+1}}}{\Delta x} - \left(\frac{\sigma}{H} r_x \eta_\sigma\right)_{i,j}^{n} \frac{u_{i,j+1}^{\overline{n+1}} - u_{i,j-1}^{\overline{n+1}}}{2\Delta\eta}\right) \tag{6.4}$$

Second time step (n+2)

$$v_{i,j}^{\overline{n+2}} = v_{i,j+1}^{\overline{n+2}} + \Delta\eta\left(\frac{H}{\eta_\sigma}\right)_{i,j}^{n}\left(\frac{u_{i,j}^{\overline{n+2}} - u_{i-1,j}^{\overline{n+2}}}{\Delta x} - \left(\frac{\sigma}{H} r_x \eta_\sigma\right)_{i,j}^{n} \frac{u_{i,j+1}^{\overline{n+2}} - u_{i,j-1}^{\overline{n+2}}}{2\Delta\eta}\right) \tag{6.5}$$

Time averaging at (n+1)

$$v_{i,j}^{n+1} = \frac{v_{i,j}^{n} + v_{i,j}^{\overline{n+2}}}{2} \tag{6.6}$$

Momentum equation:

First time step (n+1)

$$u_{i,j}^{\overline{n+1}} = u_{i,j}^{n} + \frac{\Delta t}{\rho}\begin{pmatrix} -\rho\left(\frac{\sigma}{H} r_t \eta_\sigma\right)_{i,j}^{n} \frac{u_{i,j+1}^{n} - u_{i,j-1}^{n}}{2\Delta\eta} + \rho u_{i,j}^{n} \frac{u_{i,j}^{n} - u_{i-1,j}^{n}}{\Delta x} \\ -\rho\left(\frac{\sigma}{H} r_x \eta_\sigma u\right)_{i,j}^{n} \frac{u_{i,j+1}^{n} - u_{i,j-1}^{n}}{2\Delta\eta} + \rho\left(\frac{1}{H} v \eta_\sigma\right)_{i,j}^{n} \frac{u_{i,j+1}^{n} - u_{i,j-1}^{n}}{2\Delta\eta} \\ -\left[\frac{1}{H^2} \mu_{eff} \eta_\sigma{}^2\right]_{i,j}^{n} \frac{\left(u_{i,j+1}^{n} - 2u_{i,j}^{n} + u_{i,j-1}^{n}\right)}{(\Delta\eta)^2} \end{pmatrix} \tag{6.7}$$

Second time step (n+2)

$$u_{i,j}^{\overline{n+2}} = u_{i,j}^{\overline{n+1}} + \frac{\Delta t}{\rho}\begin{pmatrix} -\rho\left(\frac{\sigma}{H} r_t \eta_\sigma\right)_{i,j}^{n} \frac{u_{i,j+1}^{\overline{n+1}} - u_{i,j-1}^{\overline{n+1}}}{2\Delta\eta} + \rho u_{i,j}^{\overline{n+1}} \frac{u_{i,j}^{\overline{n+1}} - u_{i-1,j}^{\overline{n+1}}}{\Delta x} \\ -\rho\left(\frac{\sigma}{H} r_x \eta_\sigma\right)_{i,j}^{n} u_{i,j}^{\overline{n+1}} \frac{u_{i,j+1}^{\overline{n+1}} - u_{i,j-1}^{\overline{n+1}}}{2\Delta\eta} + \rho\left(\frac{1}{H} \eta_\sigma\right)_{i,j}^{n} v_{i,j}^{\overline{n+1}} \frac{u_{i,j+1}^{\overline{n+1}} - u_{i,j-1}^{\overline{n+1}}}{2\Delta\eta} \\ -\left[\frac{1}{H^2} \eta_\sigma{}^2\right]_{i,j}^{n} \mu_{eff}{}_{i,j}^{\overline{n+1}} \frac{\left(u_{i,j+1}^{\overline{n+1}} - 2u_{i,j}^{\overline{n+1}} + u_{i,j-1}^{\overline{n+1}}\right)}{(\Delta\eta)^2} \end{pmatrix} \tag{6.8}$$

Time averaging at (n+1)

$$u_{i,j}^{n+1} = \frac{u_{i,j}^{n} + u_{i,j}^{\overline{n+2}}}{2} \tag{6.9}$$

Energy equation:

First time step (n+1)

$$\overline{T_{i,j}^{n+1}} = T_{i,j}^{n} + \frac{\Delta t}{\rho c_p}\begin{pmatrix} -\rho c_p (\frac{\sigma}{H} r_t \eta_\sigma)_{i,j}^{n} \frac{T_{i,j+1}^{n} - T_{i,j-1}^{n}}{2\Delta\eta} + \rho c_p u_{i,j}^{n} \frac{T_{i,j}^{n} - T_{i-1,j}^{n}}{\Delta x} \\ -\rho c_p (\frac{\sigma}{H} r_x \eta_\sigma u)_{i,j}^{n} \frac{T_{i,j+1}^{n} - T_{i,j-1}^{n}}{2\Delta\eta} + \rho c_p (\frac{1}{H} v \eta_\sigma)_{i,j}^{n} \frac{T_{i,j+1}^{n} - T_{i,j-1}^{n}}{2\Delta\eta} \\ -\left[\frac{1}{H^2} k_{eff} \eta_\sigma{}^2\right]_{i,j}^{n} \frac{\left(T_{i,j+1}^{n} - 2T_{i,j}^{n} + T_{i,j-1}^{n}\right)}{(\Delta\eta)^2} \end{pmatrix} \quad (6.10)$$

Second time step (n+2)

$$\overline{T_{i,j}^{n+2}} = \overline{T_{i,j}^{n+1}} + \frac{\Delta t}{\rho c_p}\begin{pmatrix} -\rho c_p (\frac{\sigma}{H} r_t \eta_\sigma)_{i,j}^{n} \frac{\overline{T_{i,j+1}^{n+1}} - \overline{T_{i,j-1}^{n+1}}}{2\Delta\eta} + \rho c_p \overline{u_{i,j}^{n+1}} \frac{\overline{T_{i,j}^{n+1}} - \overline{T_{i-1,j}^{n+1}}}{\Delta x} \\ -\rho c_p (\frac{\sigma}{H} r_x \eta_\sigma)_{i,j}^{n} \overline{u_{i,j}^{n+1}} \frac{\overline{T_{i,j+1}^{n+1}} - \overline{T_{i,j-1}^{n+1}}}{2\Delta\eta} \\ +\rho c_p (\frac{1}{H} \eta_\sigma)_{i,j}^{n} \overline{v_{i,j}^{n+1}} \frac{\overline{T_{i,j+1}^{n+1}} - \overline{T_{i,j-1}^{n+1}}}{2\Delta\eta} \\ -\left[\frac{1}{H^2} \eta_\sigma{}^2\right]_{i,j}^{n} \overline{k_{eff}{}_{i,j}^{n+1}} \frac{\left(\overline{T_{i,j+1}^{n+1}} - 2\overline{T_{i,j}^{n+1}} + \overline{T_{i,j-1}^{n+1}}\right)}{(\Delta\eta)^2} \end{pmatrix} \quad (6.11)$$

Time averaging at (n+1)

$$T_{i,j}^{n+1} = \frac{T_{i,j}^{n} + \overline{T_{i,j}^{n+2}}}{2} \quad (6.12)$$

Turbulent Kinetic Energy Equation:

First time step (n+1)

$$K_{i,j}^{\overline{n+1}} = K_{i,j}^{n} + \Delta t \left(\begin{array}{l} -(\frac{\sigma}{H} r_t \eta_\sigma)_{i,j}^{n} \frac{K_{i,j+1}^{n} - K_{i,j-1}^{n}}{2\Delta\eta} + u_{i,j}^{n} \frac{K_{i,j}^{n} - K_{i-1,j}^{n}}{\Delta x} \\ -(\frac{\sigma}{H} r_x \eta_\sigma u)_{i,j}^{n} \frac{K_{i,j+1}^{n} - K_{i,j-1}^{n}}{2\Delta\eta} + (\frac{1}{H} v \eta_\sigma)_{i,j}^{n} \frac{K_{i,j+1}^{n} - K_{i,j-1}^{n}}{2\Delta\eta} \\ -\left[\frac{1}{H^2} \left(\frac{\mu}{\rho} + \frac{\mu_t}{\rho \mathrm{Pr}_K} \right) \eta_\sigma{}^2 \right]_{i,j}^{n} \frac{\left(K_{i,j+1}^{n} - 2K_{i,j}^{n} + K_{i,j-1}^{n} \right)}{(\Delta\eta)^2} \\ -\left(\frac{\mu_t}{\rho} \frac{1}{H^2} \eta_\sigma{}^2 \right)_{i,j}^{n} \left(\frac{u_{i,j+1}^{n} - u_{i,j-1}^{n}}{2\Delta\eta} \right)^2 + \varepsilon_{i,j}^{n} \end{array} \right) \tag{6.13}$$

Second time step (n+2)

$$K_{i,j}^{\overline{n+2}} = K_{i,j}^{\overline{n+1}} + \Delta t \left(\begin{array}{l} -(\frac{\sigma}{H} r_t \eta_\sigma)_{i,j}^{n} \frac{K_{i,j+1}^{\overline{n+1}} - K_{i,j-1}^{\overline{n+1}}}{2\Delta\eta} + u_{i,j}^{\overline{n+1}} \frac{K_{i,j}^{\overline{n+1}} - K_{i-1,j}^{\overline{n+1}}}{\Delta x} \\ -(\frac{\sigma}{H} r_x \eta_\sigma)_{i,j}^{n} u_{i,j}^{\overline{n+1}} \frac{K_{i,j+1}^{\overline{n+1}} - K_{i,j-1}^{\overline{n+1}}}{2\Delta\eta} + (\frac{1}{H} \eta_\sigma)_{i,j}^{n} v_{i,j}^{\overline{n+1}} \frac{K_{i,j+1}^{\overline{n+1}} - K_{i,j-1}^{\overline{n+1}}}{2\Delta\eta} \\ -\left[\frac{1}{H^2} \left(\frac{\mu}{\rho} + \frac{\mu_t}{\rho \mathrm{Pr}_K} \right) \eta_\sigma{}^2 \right]_{i,j}^{n} \frac{\left(K_{i,j+1}^{\overline{n+1}} - 2K_{i,j}^{\overline{n+1}} + K_{i,j-1}^{\overline{n+1}} \right)}{(\Delta\eta)^2} \\ -\left(\frac{1}{\rho H^2} \eta_\sigma{}^2 \right)_{i,j}^{n} \mu_{t_{i,j}}^{\overline{n+1}} \left(\frac{u_{i,j+1}^{\overline{n+1}} - u_{i,j-1}^{\overline{n+1}}}{2\Delta\eta} \right)^2 + \varepsilon_{i,j}^{\overline{n+1}} \end{array} \right) \tag{6.14}$$

Time averaging at (n+1)

$$K_{i,j}^{n+1} = \frac{K_{i,j}^{n} + K_{i,j}^{\overline{n+2}}}{2} \tag{6.15}$$

Turbulent Dissipation Energy Equation:

First time step (n+1)

$$\overline{\varepsilon_{i,j}^{n+1}} = \varepsilon_{i,j}^{n} + \Delta t \left(\begin{array}{l} -(\frac{\sigma}{H} r_t \eta_\sigma)_{i,j}^{n} \frac{\varepsilon_{i,j+1}^{n} - \varepsilon_{i,j-1}^{n}}{2\Delta\eta} + u_{i,j}^{n} \frac{\varepsilon_{i,j}^{n} - \varepsilon_{i-1,j}^{n}}{\Delta x} \\ -(\frac{\sigma}{H} r_x \eta_\sigma u)_{i,j}^{n} \frac{\varepsilon_{i,j+1}^{n} - \varepsilon_{i,j-1}^{n}}{2\Delta\eta} + (\frac{1}{H} v \eta_\sigma)_{i,j}^{n} \frac{\varepsilon_{i,j+1}^{n} - \varepsilon_{i,j-1}^{n}}{2\Delta\eta} \\ -\left[\frac{1}{H^2} \left(\frac{\mu}{\rho} + \frac{\mu_t}{\rho \mathrm{Pr}_\varepsilon} \right) \eta_\sigma{}^2 \right]_{i,j}^{n} \frac{\left(\varepsilon_{i,j+1}^{n} - 2\varepsilon_{i,j}^{n} + \varepsilon_{i,j-1}^{n} \right)}{(\Delta\eta)^2} \\ -C_{\varepsilon 1} \left(\frac{\mu_t}{\rho} \frac{1}{H^2} \eta_\sigma{}^2 \right)_{i,j}^{n} \left(\frac{\varepsilon}{K} \right)_{i,j}^{n} \left(\frac{u_{i,j+1}^{n} - u_{i,j-1}^{n}}{2\Delta\eta} \right)^2 + C_{\varepsilon 2} \frac{\left(\varepsilon_{i,j}^{n} \right)^2}{K_{i,j}^{n}} \end{array} \right) \tag{6.16}$$

Second time step (n+2)

$$\overline{\varepsilon_{i,j}^{n+2}} = \overline{\varepsilon_{i,j}^{n+1}} + \Delta t \left(\begin{array}{l} -(\frac{\sigma}{H} r_t \eta_\sigma)_{i,j}^{n} \frac{\overline{\varepsilon_{i,j+1}^{n+1}} - \overline{\varepsilon_{i,j-1}^{n+1}}}{2\Delta\eta} + \overline{u_{i,j}^{n+1}} \frac{\overline{\varepsilon_{i,j}^{n+1}} - \overline{\varepsilon_{i-1,j}^{n+1}}}{\Delta x} \\ -(\frac{\sigma}{H} r_x \eta_\sigma)_{i,j}^{n} \overline{u_{i,j}^{n+1}} \frac{\overline{\varepsilon_{i,j+1}^{n+1}} - \overline{\varepsilon_{i,j-1}^{n+1}}}{2\Delta\eta} + (\frac{1}{H} \eta_\sigma)_{i,j}^{n} \overline{v_{i,j}^{n+1}} \frac{\overline{\varepsilon_{i,j+1}^{n+1}} - \overline{\varepsilon_{i,j-1}^{n+1}}}{2\Delta\eta} \\ -\left[\frac{1}{H^2} \left(\frac{\mu}{\rho} + \frac{\mu_t}{\rho \mathrm{Pr}_\varepsilon} \right) \eta_\sigma{}^2 \right]_{i,j}^{\overline{n+1}} \frac{\left(\overline{\varepsilon_{i,j+1}^{n+1}} - 2\overline{\varepsilon_{i,j}^{n+1}} + \overline{\varepsilon_{i,j-1}^{n+1}} \right)}{(\Delta\eta)^2} \\ -C_{\varepsilon 1} \left(\frac{1}{\rho H^2} \eta_\sigma{}^2 \right)_{i,j}^{n} \overline{\mu_{t\,i,j}^{n+1}} \left(\frac{\varepsilon}{K} \right)_{i,j}^{\overline{n+1}} \left(\frac{\overline{u_{i,j+1}^{n+1}} - \overline{u_{i,j-1}^{n+1}}}{2\Delta\eta} \right)^2 + C_{\varepsilon 2} \frac{\left(\overline{\varepsilon_{i,j}^{n+1}} \right)^2}{K_{i,j}^{\overline{n+1}}} \end{array} \right) \tag{6.17}$$

Time averaging at (n+1)

$$\varepsilon_{i,j}^{n+1} = \frac{\varepsilon_{i,j}^{n} + \overline{\varepsilon_{i,j}^{n+2}}}{2} \tag{6.18}$$

6.6 Remarks on the Initial Conditions

Because of computational necessity, initial values of turbulent kinetic energy and turbulent dissipation energy are taken as small values near zero, instead of setting them equal to zero.

at the solid surface, $y = h + r(x,t)$

$$K = 1.0x10^{-2} \tag{6.19}$$

$$\varepsilon = 1.0x10^{-4} \tag{6.20}$$

at the top boundary, $y = 0$

$$K = 1.0x10^{-11} \tag{6.21}$$

$$\varepsilon = 2.1523x10^{-2} \tag{6.22}$$

at the inlet, x=0

$$K = 1.0x10^{-7} \tag{6.23}$$

$$\varepsilon = 0 \tag{6.24}$$

initially, at $t = 0$, for the whole domain except the bottom, top and inlet boundaries:

$$K = 1.1x10^{-7} \tag{6.25}$$

$$\varepsilon = 2.1523x10^{-2} \tag{6.26}$$

6.7 Time Delay

Both the computer codes of the previous and current studies employ a time delay algorithm. At the beginning, both programs start with the given initial conditions except the surface temperature and regression rate and waited until time $t = 0.0098s$. Then both the regression and the solid surface temperature is set to the prescribed value. At the beginning, until $t = 0.0098s$, regression rate $\dot{r} = 0m/s$ and temperature of the solid surface is $T_s = T_\infty$.

6.8 Numerical Solution Procedure

Numerical solution procedure of the present computer code is as follows:

1. Read input operational parameters: $u_\infty, T_\infty, T_s, p_\infty, t_{delay}, \dot{r}(=r_t)$
2. Read input geometrical parameters: H, L
3. Read input turbulence parameters: $(K,\varepsilon)_{initial}, \mathrm{Pr}_K, \mathrm{Pr}_\varepsilon, C_{\varepsilon 1}, C_{\varepsilon 2}$
4. Read input computational parameters: IN, JN, t_{final}
5. Read properties of the gas: c_p, c_v, k, μ, R
6. Calculate the density from ideal gas relation as a function of p,T : ρ
7. Assign the initial conditions to flow field: $(u,v,T,K,\varepsilon)_{i,j}^{n}$
8. Assign $\dot{r}=0, T_s = T_\infty$
9. Predict $T_{i,j}^{\overline{n+1}}$, from the energy equation (6.10)
10. Predict $u_{i,j}^{\overline{n+1}}$, from the momentum equation (6.7)
11. $DO\ \ i = 2, IN-1$

    $DO\ \ j = JN-1, 2$

    Predict $v_{i,j}^{\overline{n+1}}$, from the continuity equation (6.4)

    END DO

    END DO
12. Extrapolate $u_{IN,j}^{\overline{n+1}}$ and $v_{IN,j}^{\overline{n+1}}$, at the exit boundary
13. Predict $K_{i,j}^{\overline{n+1}}$, from the turbulent kinetic energy equation (6.13)
14. Predict $\varepsilon_{i,j}^{\overline{n+1}}$, from the turbulent dissipation energy equation (6.16)
15. Predict $(\mu_t)_{i,j}^{\overline{n+1}}$, from (4.5)
16. Predict $T_{i,j}^{\overline{n+2}}$, from the energy equation (6.11)
17. Predict $u_{i,j}^{\overline{n+2}}$, from the momentum equation (6.8)

18. $DO\ \ i = 2, IN-1$

    $DO\ \ j = JN-1, 2$

    Predict $\overline{v_{i,j}^{n+2}}$, from the continuity equation (6.5)

    END DO

  END DO

19. Predict $\overline{K_{i,j}^{n+2}}$, from the turbulent kinetic energy equation (6.14)

20. Predict $\overline{\varepsilon_{i,j}^{n+2}}$, from the turbulent dissipation energy equation (6.17)

21. Predict $\overline{u_{i,j}^{n+1}}, \overline{v_{i,j}^{n+1}}, \overline{T_{i,j}^{n+1}}, \overline{K_{i,j}^{n+1}}, \overline{\varepsilon_{i,j}^{n+1}}$ using the time averaging equations (6.6), (6.9), (6.12), (6.15), (6.18)

22. Predict $\left(\mu_t\right)_{i,j}^{n+1}$, from (4.5)

23. Extrapolate $u_{IN,j}^{n+1}$ and $v_{IN,j}^{n+1}$, at the exit boundary

24. Update the vertical physical position of the solid surface according to the regression rate

25. Update the vertical physical coordinates of the gas domain according to the regression rate

26. Write the variables to output file: $(u, v, T, K, \varepsilon, \mu_t)_{i,j}^{n+1}$

27. Check if time $t < t_{delay}$

    $YES \rightarrow$ return step 9,

    $ELSE \rightarrow$ continue

28. Assign the prescribed values of the regression rate and surface temperature: $\dot{r}, T_s$

29. Check if time $t < t_{final}$

    $YES \rightarrow$ return step 9,

    $ELSE \rightarrow$ continue

30. Write the variables to output file: $(u, v, T, K, \varepsilon, \mu_t)_{i,j}^{n+1}$

31. END of program

6.9 Computer Code

A Fortran code (program) has been developed which implements the solution procedure given in section 6.8. In Chapter 7, it is verified that the computer program works independent of time increment and mesh size, and the results of the program is compared to Blasius velocity profile and turbulent velocity profiles given by other studies. Flowchart of the computer code is given in Appendix B.

Computer program is run under various conditions and all the results presented in following chapters are obtained from those runs.

CHAPTER 7

VERIFICATION OF THE COMPUTER CODE

7.1 Introduction

This chapter starts with a comparison of the results of the present program with Blasius solution for laminar flow over a flat plate. Then, for the turbulent case, the results of the present program are compared to experimental and numerical results by other researchers. Finally, it is proven that the results of the program are independent of both the mesh size and time increment.

7.2 Comparison of the Numerical Solution with Blasius Solution

The computer code of the present study is verified by comparing to Blasius solution for flow over a flat plate. Blasius solution is valid only for laminar flows, with Reynolds number less than 1.0×10^5. All the presented results in this section are for lower Reynolds numbers. Both the previous computer code and the computer code of the present study are run for zero regression rate. Effect of turbulence is set to zero, since the analysis is for laminar case. The program is allowed to run 0.08s and stopped since steady-state values are reached. List of the input parameters are given in Table 7.1.

Table 7.1 List of Input Parameters Used in Runs with Number 1, 2

PARAMETER	DESCRIPTION	VALUE
u_∞	free stream horizontal velocity	20 *m/s*
T_∞	free stream gas temperature	293 *K*
T_s	temperature of the solid surface	293 *K*

INxJN	number of nodes in x and y directions	21x61
Δt	time increment at each iteration	$1.0x10^{-7}\,s$
L	plate length	$0.0381\,m$
H	total height of the gas domain	$0.004\,m$
$\dot{r}$	regression rate of the solid surface	$0\,m/s$
ρ	density of the gas	$1.3137\,kg/m^3$
μ	absolute viscosity of the gas	$1.5x10^{-5}\,N.s/m^2$
c_p	specific heat of the gas	$922.00\,kJ/kg.K$
μ_t	turbulent viscosity	$0\,N.s/m^2$

Two runs are made in this section. Run number 1 is done with the computer code of the previous study, while the run number 2 is done with the code of the present study.

Table 7.2 List of Runs for Blasius Profile Comparison

RUN NUMBER	DESCRIPTION	Re
1	Laminar flow, computer code of the previous study, for comparison with the Blasius solution, run parameters given in Table 7.1	5.33x10^4
2	Laminar flow, computer code of the present study, for comparison with the Blasius solution, run parameters given in Table 7.1	5.33x10^4

During the analysis, data of velocity profiles are stored for 3 different horizontal distances. The Blasius profile given for non-dimensional variables η and u/u_∞ are found in [14] and η is transformed into y coordinate according to the following equation:

$$\eta = y\sqrt{\frac{\rho u_\infty}{2\mu x}} \tag{7.1}$$

Values of horizontal velocity predicted by the previous and present computer codes and the Blasius solution are tabulated for the 18th node, where $x = 3.24x10^{-2}\,m$. It can be found in Appendix C. It is seen from the table that the maximum deviation from the Blasius solution is around 38.6% close to the boundary, whereas it is 0.21% at $y = 2.81x10^{-3}\,m$. Velocity profiles at three different positions are given as follows:

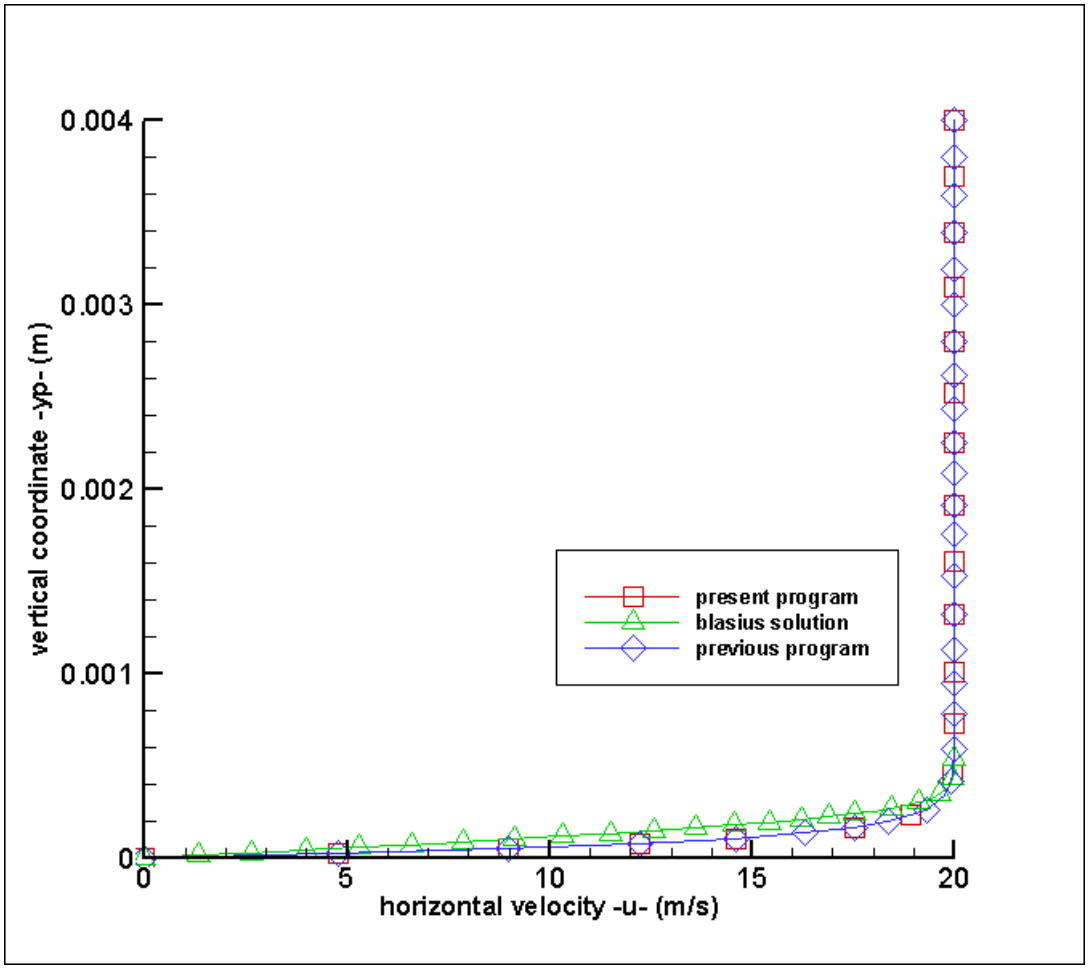

Figure 7.1 Comparison of the Results of the Previous Program, Present Program and the Blasius Solution at $x = 3.81x10^{-3}\,m$ ($u_\infty = 20m/s$, $\mathrm{Re} = 6.67x10^3$, $t = 0.08s$)

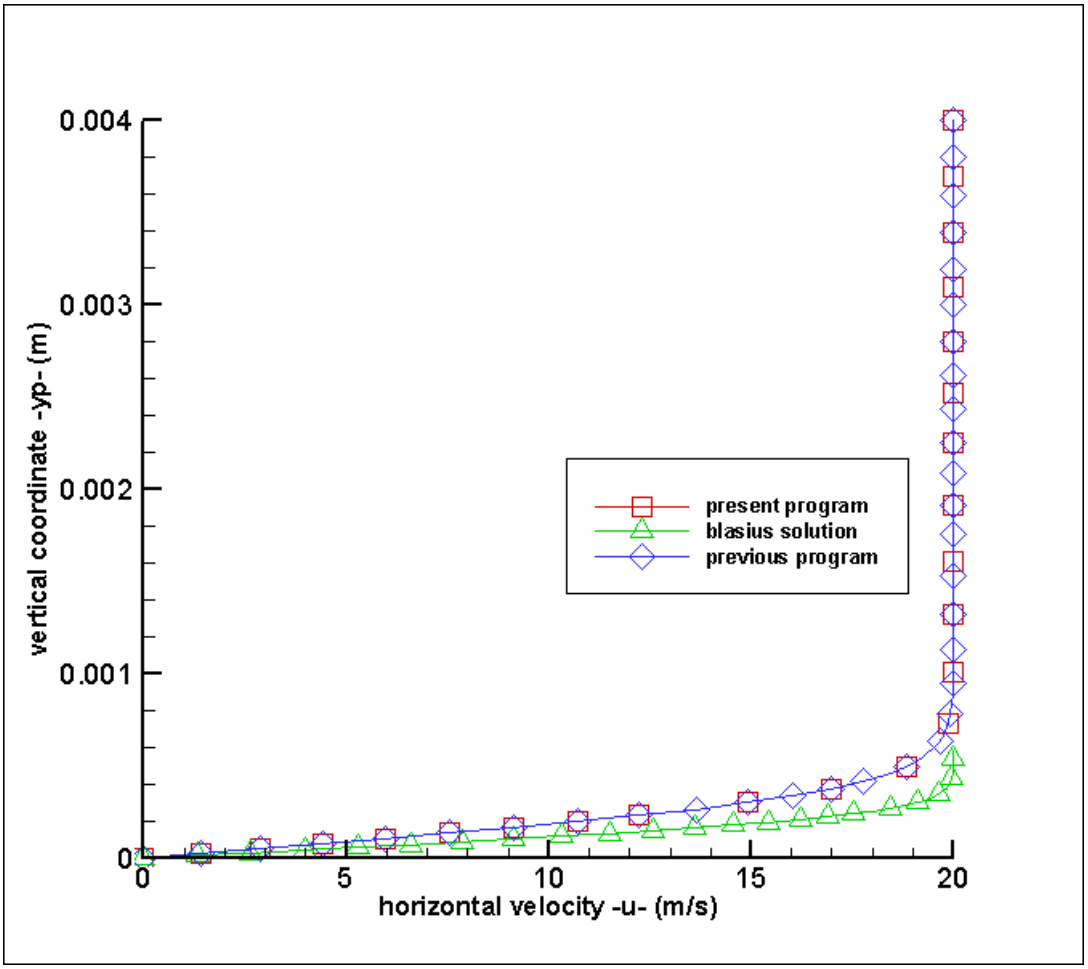

Figure 7.2 Comparison of the Results of the Previous Program, Present Program and the Blasius Solution at $x = 1.905x10^{-2} m$ ($u_\infty = 20 m/s$, $\mathrm{Re} = 3.34x10^4$, $t = 0.08s$)

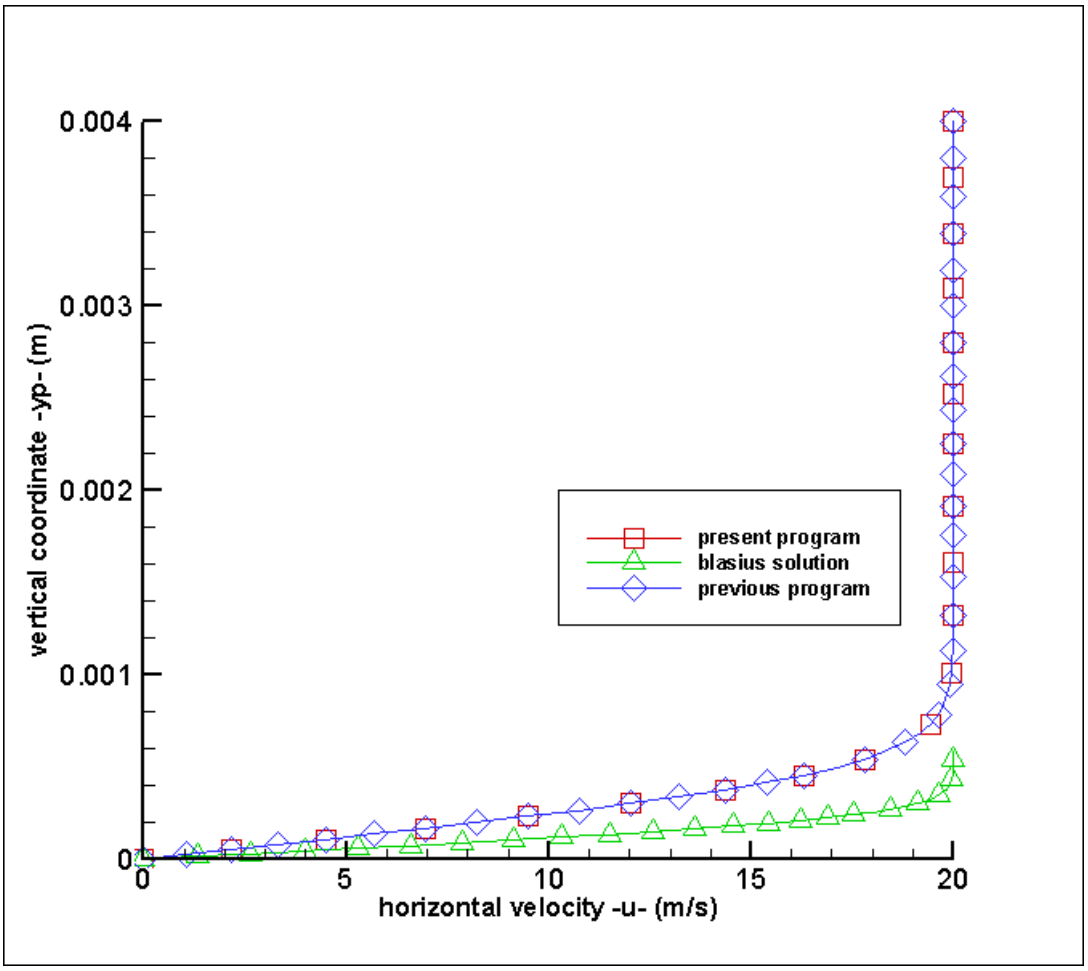

Figure 7.3 Comparison of the Results of the Previous Program, Present Program and the Blasius Solution at $x = 3.24x10^{-2} m$ ($u_\infty = 20 m/s$, $\mathrm{Re} = 5.68x10^4$, $t = 0.08s$)

7.3 Comparison of the Turbulent Boundary Layer Velocity Profile with Various Studies

The turbulence model used for this study is standard $K-\varepsilon$ model, and it is given in Chapter 4 in detail. To validate the application of this turbulence model in the present study, a couple of cases are studied.

The laminar and turbulent boundary layer profiles given by Schetz [32] are:

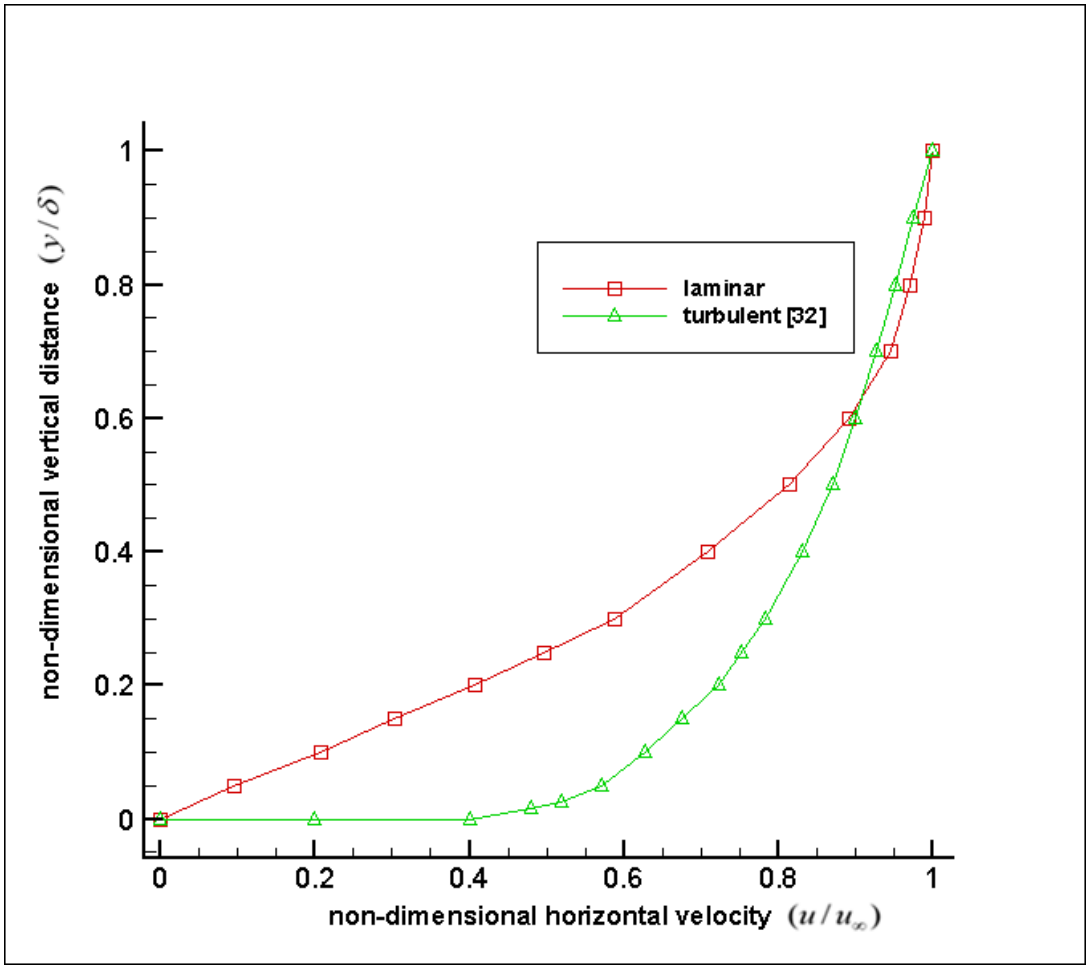

Figure 7.4 Comparison of the Turbulent and Laminar Boundary Layer Velocity Profiles [32]

Turbulent velocity profiles measured by Schetz [32], predicted by Antoniou [9] and present study are as follows.

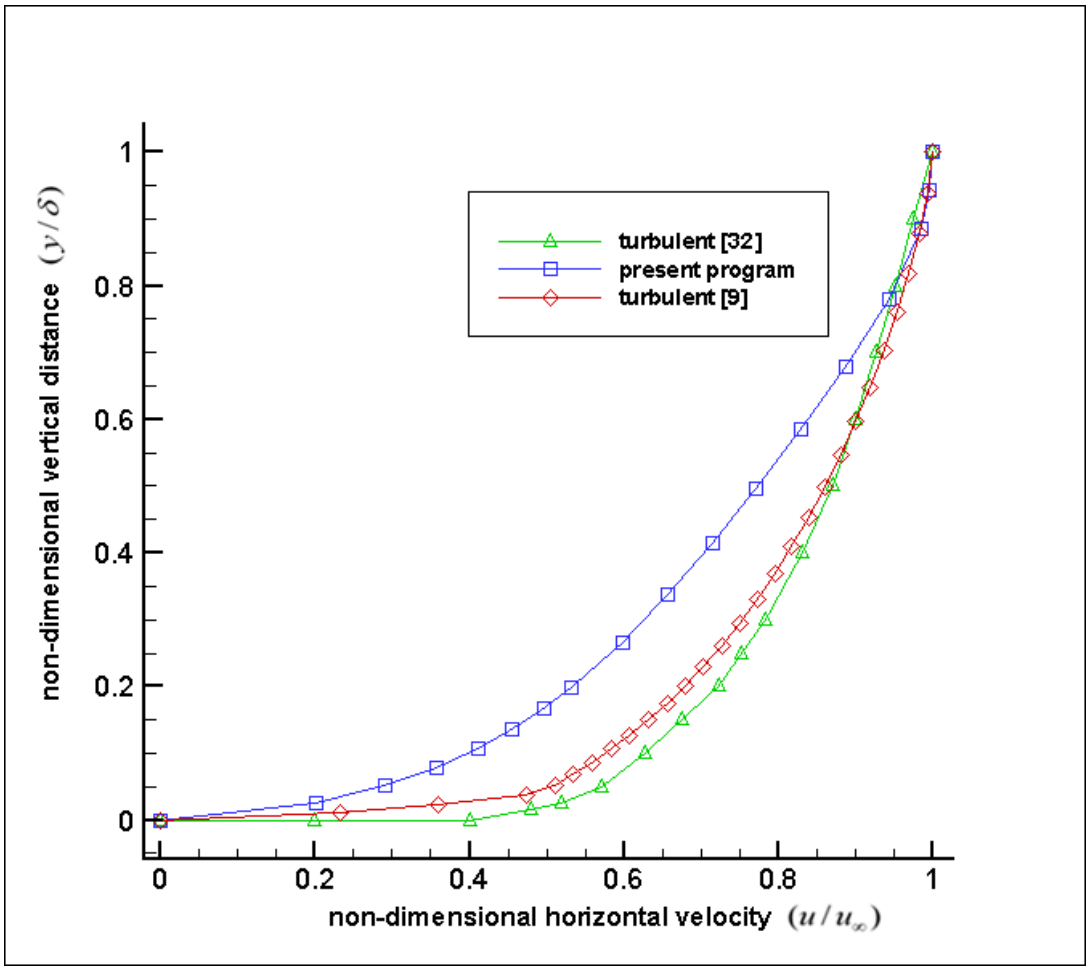

Figure 7.5 Comparison of the Turbulent Boundary Layer Velocity Profiles Measured by Schetz [32], Predicted by Antoniou [9] and Present Program

Antoniou [9] used an implicit scheme for the solution of the compressible, hyperbolic finite-difference equations. For the present study, an explicit scheme is adopted which is given in Chapter 6.

As it can be observed from Figure 7.5, the velocity predicted by the present program is underestimated near the wall with respect to other two studies, because it is parabolic.

7.4 Grid Independence Study

The computer code of the previous study used a mesh size of 21x61. In order to verify that the solution is independent of mesh size, several runs are made with three different mesh sizes, 21x41, 21x61, 31x61, where the first number indicates the mesh size in x-direction and second number indicates the mesh size in y-direction.

Results are found slightly dependent on the mesh size, with maximum difference of 5% for horizontal velocity between 21x41 and 31x61 mesh sizes. Properties vary less than 1% between 21x61 and 31x61. Therefore, for the parametric study, 21x61 mesh size is used.

Following variables are plotted: horizontal velocity, temperature. Velocity and temperature distribution is given at $x = 1.905 x 10^{-2} m$.

Input parameters in Table 7.3 are used for the runs 4,6,7.

Table 7.3 List of Input Parameters Used in Runs with Number 3-13

PARAMETER	DESCRIPTION	VALUE
T_∞	free stream gas temperature	293 *K*
T_s	temperature of the solid surface	600 *K*
t_{delay}	delay time after which regression starts	0.0098*s*
L	plate length	0.0381 *m*
H	total height of the gas domain	0.004 *m*
$\dot{r}$	regression rate of the solid surface	0.015 *m/s*
ρ	density of the gas	$1.3137\, kg/m^3$
μ	absolute viscosity of the gas	$1.5x10^{-5}\ N.s/m^2$

c_p	specific heat of the gas	$922.00\,kJ/kg.K$

Table 7.4 List of Runs for Grid Independence Study

RUN NUMBER	DESCRIPTION	MESH SIZE
4	Turbulent flow, computer code of the present study, Re=$5.33x10^4$, $\dot{r} = 0.015m/s$, $\Delta t = 1.0x10^{-7}s$, run parameters given in Table 7.3	21x61
6	Turbulent flow, computer code of the present study, Re=$5.33x10^4$, $\dot{r} = 0.015m/s$, $\Delta t = 1.0x10^{-7}s$, run parameters given in Table 7.3	21x41
7	Turbulent flow, computer code of the present study, Re=$5.33x10^4$, $\dot{r} = 0.015m/s$, $\Delta t = 1.0x10^{-7}s$, run parameters given in Table 7.3	31x61

7.4.1 Horizontal Velocity Profiles

Horizontal velocity profiles for 3 different mesh size are plotted at horizontal distance $x = 1.905x10^{-2}\,m$. Maximum variation of u is less than 5% between mesh sizes 21x41 and 31x61.

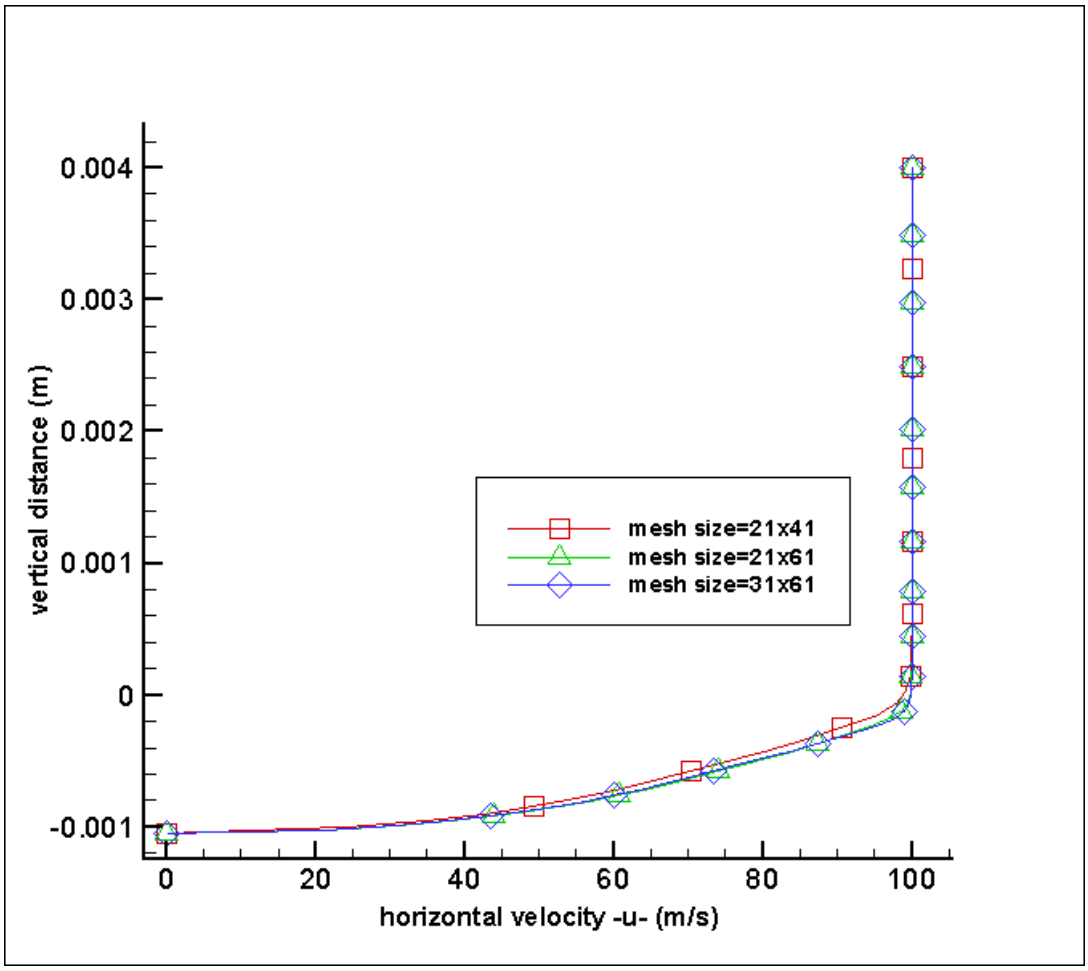

Figure 7.6 Horizontal Velocity Profiles at $x = 1.905x10^{-2} m$, for 3 Different Mesh Sizes ($u_\infty = 100 m/s$, Re $= 1.67x10^5$, $\dot{r} = 0.015 m/s$)

7.4.2 Temperature Profiles

Temperature profiles for 3 different mesh size are plotted at horizontal distance $x = 1.905x10^{-2} m$. Maximum variation of T is less than 2% between mesh sizes 21x41 and 31x61.

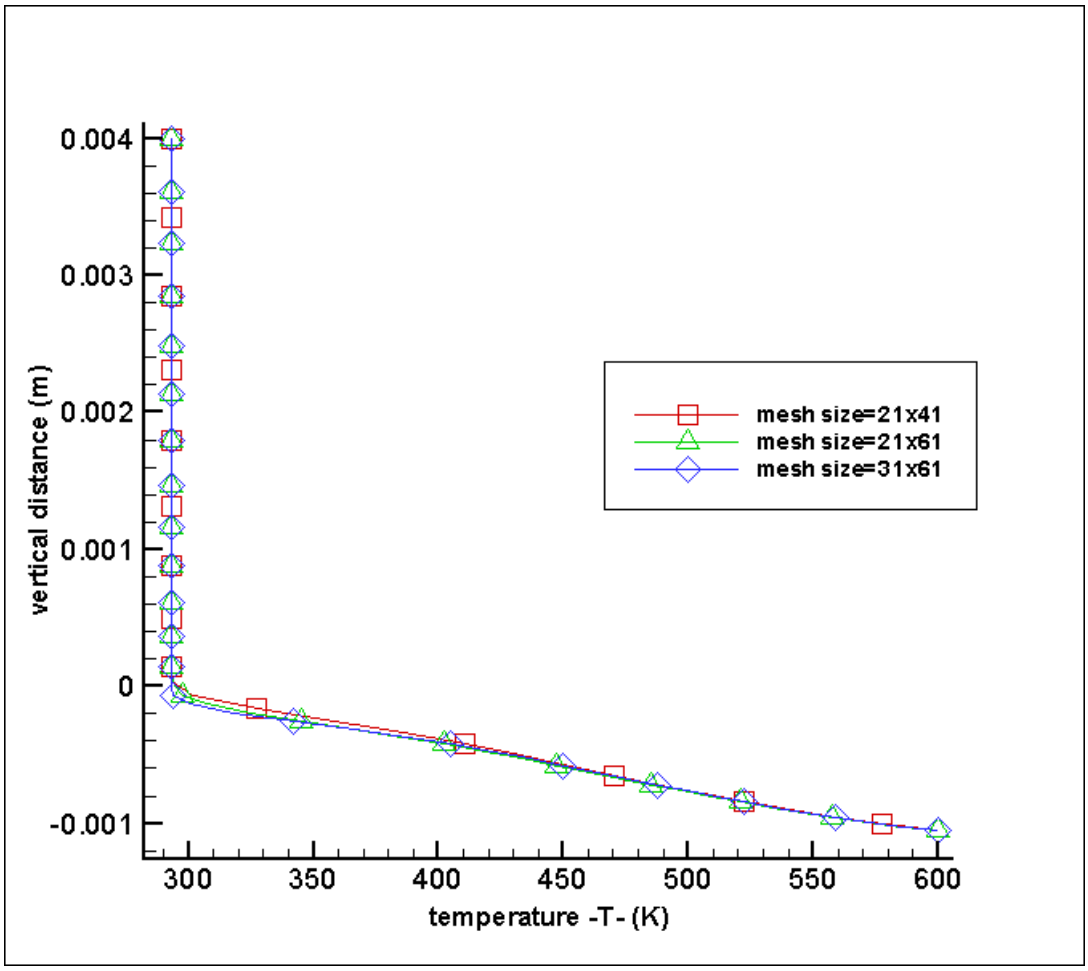

Figure 7.7 Temperature Profiles at $x = 1.905x10^{-2} m$, for 3 Different Mesh Sizes ($u_\infty = 100 m/s$, $\mathrm{Re} = 1.67x10^5$, $\dot{r} = 0.015 m/s$, $T_s = 600K$)

7.5 Time Increment and Convergence Study

In order to verify that the solution is independent of time increment, several runs are made with three different time increments, $\Delta t = 0.5x10^{-7} s$, $\Delta t = 1.0x10^{-7} s$, $\Delta t = 1.5x10^{-7} s$. It is found out that the results are independent of time increment. Therefore, $\Delta t = 1.0x10^{-7} s$ is during the parametric study. Following variables are plotted: horizontal velocity, temperature.

Values of horizontal velocity, vertical velocity, temperature and turbulent viscosity are stored at every 1000 iterations, for 9 nodes. Then this data is used to create histogram plots at those nodes. Nodes are selected such that 3 of them are close to the inlet, 3 of them are in the middle of the plate and three of them are close to the exit of the control volume. Histogram plots at node (3,59) where $x = 3.81x10^{-3} m$ and initially $y = 3.95x10^{-3} m$, are given.

In the histogram of temperature at node (3,59), Figure 7.6 , the temperature remains constant for 0.0098s and then rapidly increases. This is because of the delay time concept given in section 6.5. At $t = 0.0098 s$, temperature at the lower boundary (at the surface of the solid surface) is set to 600K as well as the regression rate is set to a constant value other than 0. Starting from $t = 0.0098 s$, the lower boundary moves downward because of the regression of the solid surface.

Values of the input parameters for all runs in Chapter 7 and 8 are given in the following table. Some of the runs in Chapter 9 also use the same input parameters.

Table 7.5 List of Runs for Time Increment Independency Study

RUN NUMBER	DESCRIPTION	TIME INCREMENT
3	Turbulent flow, computer code of the present study, Re= $5.33x10^4$, $u_\infty = 100m/s$, $\dot{r} = 0.015m/s$, mesh size 21x61, run parameters given in Table 7.3	$0.5x10^{-7}s$
4	Turbulent flow, computer code of the present study, Re= $5.33x10^4$, $u_\infty = 100m/s$, $\dot{r} = 0.015m/s$, mesh size 21x61, run parameters given in Table 7.3	$1.0x10^{-7}s$
5	Turbulent flow, computer code of the present study, Re= $5.33x10^4$, $u_\infty = 100m/s$, $\dot{r} = 0.015m/s$, mesh size 21x61, run parameters given in Table 7.3	$1.5x10^{-7}s$

7.5.1 Horizontal Velocity

The values of horizontal velocities (u) are stored in data files for every 1000 iterations. These files are used to create the histogram plots, which shows the variation of horizontal velocities with time, at node (3,59). Position of that node initially corresponds to $x = 3.81x10^{-3}m$, $y = 3.95x10^{-3}m$ and changes because of regression of the solid surface. The horizontal velocity tends to increase as the position of the node moves away from the boundary.

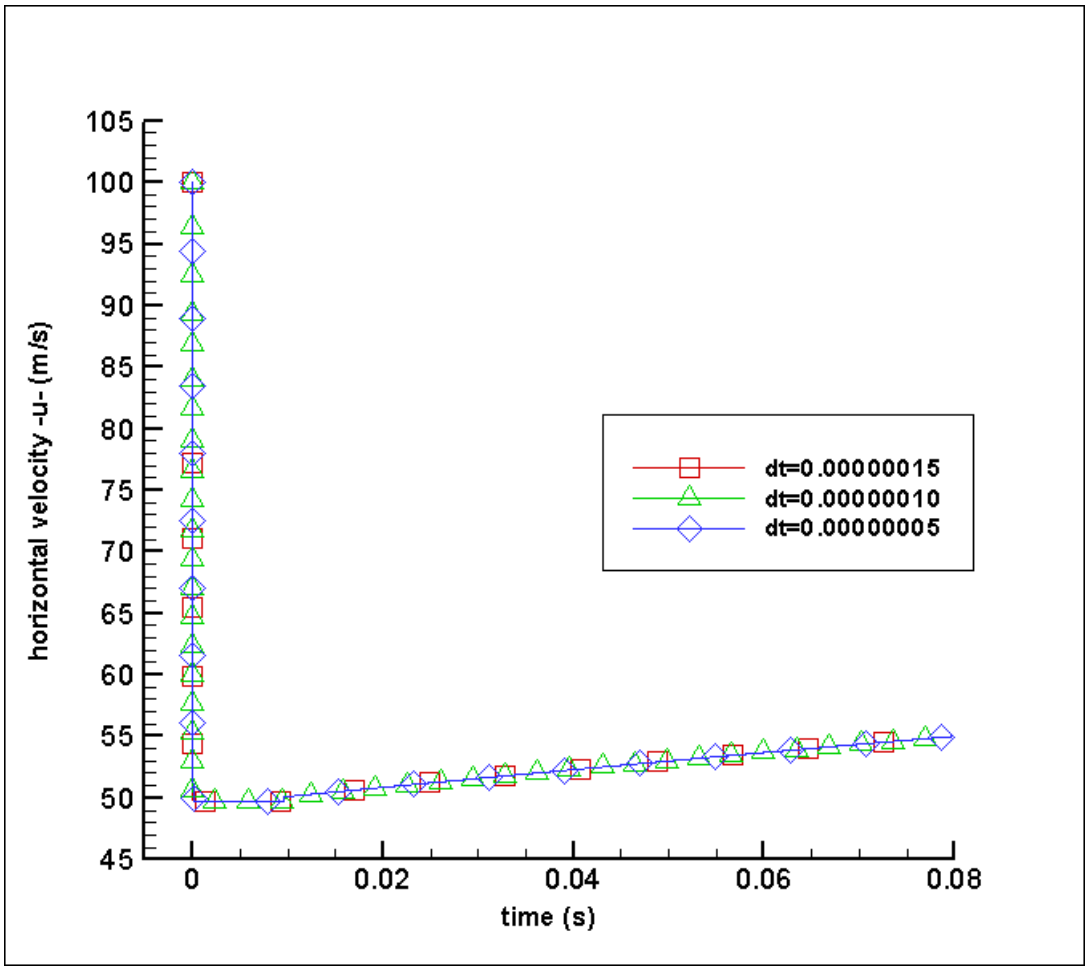

Figure 7.8 Histogram of Horizontal Velocities at Node (3,59), Initially at $x = 3.81x10^{-3} m$, $y = 3.95x10^{-3} m$, for 3 Different Time Increments ($u_\infty = 100 m/s$, $\mathrm{Re} = 3.37x10^4, \dot{r} = 0.015 m/s$)

The following figure shows the development of the boundary layer. Program starts with the initial conditions given in data files and converges to a steady-state value. This value is independent of time increment. As already explained before, regression rate is 0 until $t = t_{delay} = 0.0098s$ and regression starts with the steady state values.

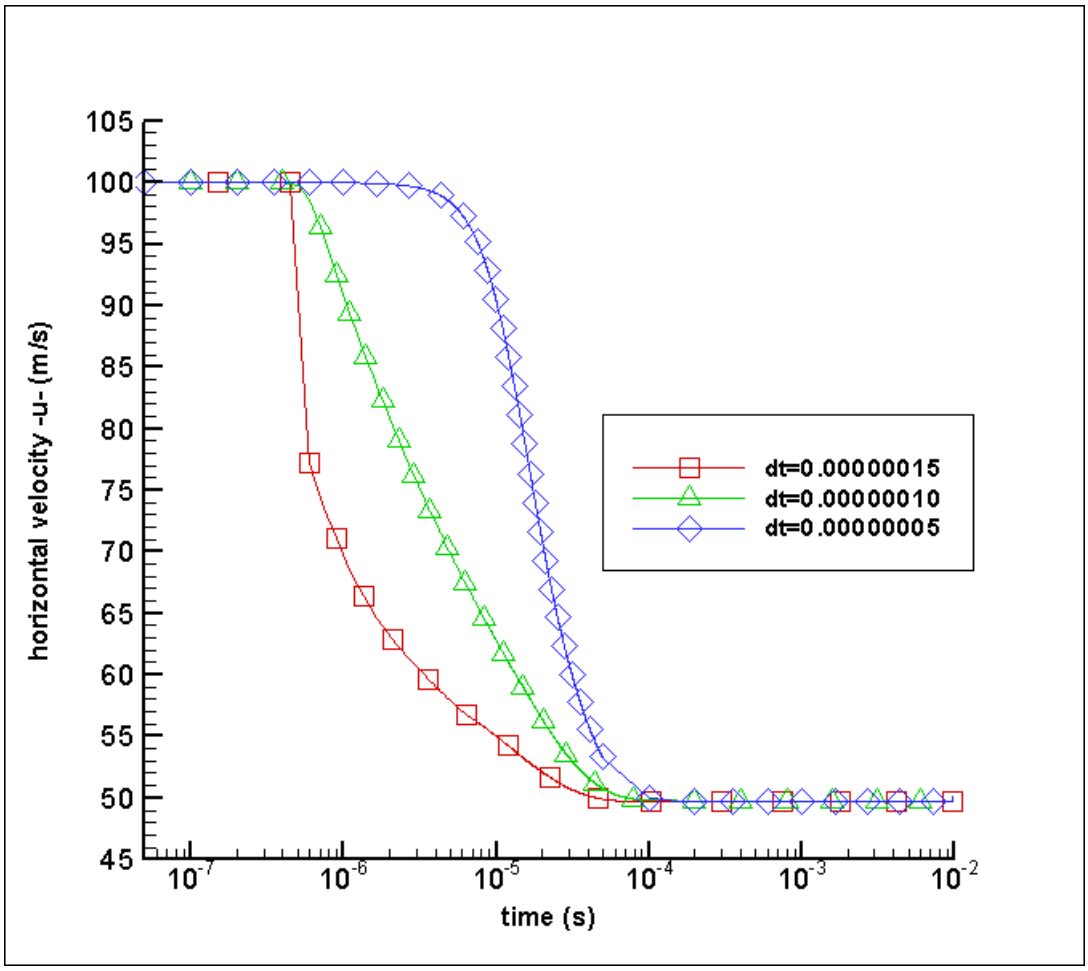

Figure 7.9 Histogram of Horizontal Velocities at Node (3,59) in Logarithmic Time Scale, Initially at $x = 3.81x10^{-3}m$, $y = 3.95x10^{-3}m$, for 3 Different Time Increments ($u_\infty = 100m/s$, $\mathrm{Re} = 3.37x10^4$, $\dot{r} = 0.015m/s$)

Horizontal velocity distribution is plotted at horizontal distance $x = 1.905x10^{-2} m$.

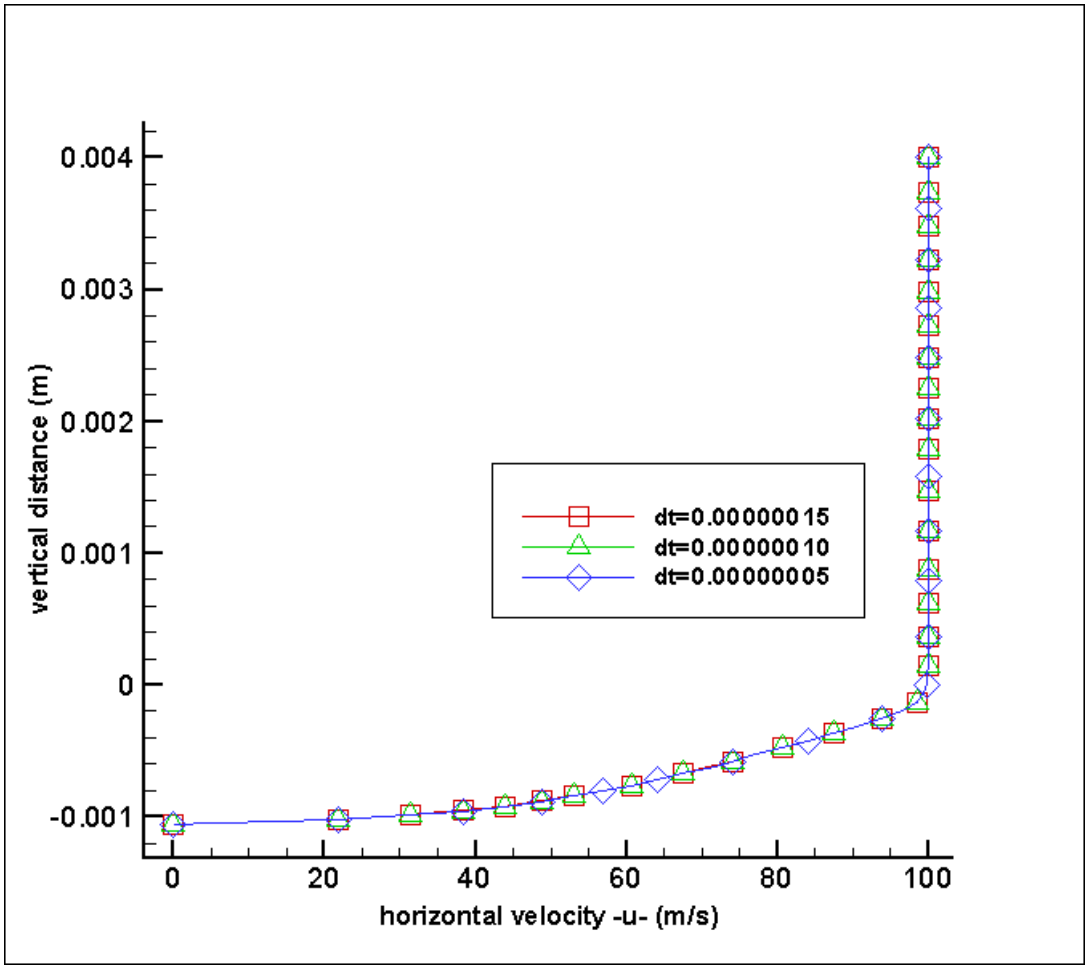

Figure 7.10 Horizontal Velocity Profiles at $x = 1.905x10^{-2} m$, for 3 Different Time Increments ($u_\infty = 100 m/s$, $\mathrm{Re} = 1.67x10^5$, $\dot{r} = 0.015 m/s$)

7.5.2 Temperature

The values of temperatures (T) are stored in data files for every 1000 iterations. These files are used to create the histogram plots, which shows the variation of temperatures with time, at node (3,59). Position of that node initially corresponds to $x = 3.81x10^{-3} m$, $y = 3.95x10^{-3} m$ and changes because of regression of the solid surface. The gas temperature tends to decrease as the position of the node moves away from the boundary.

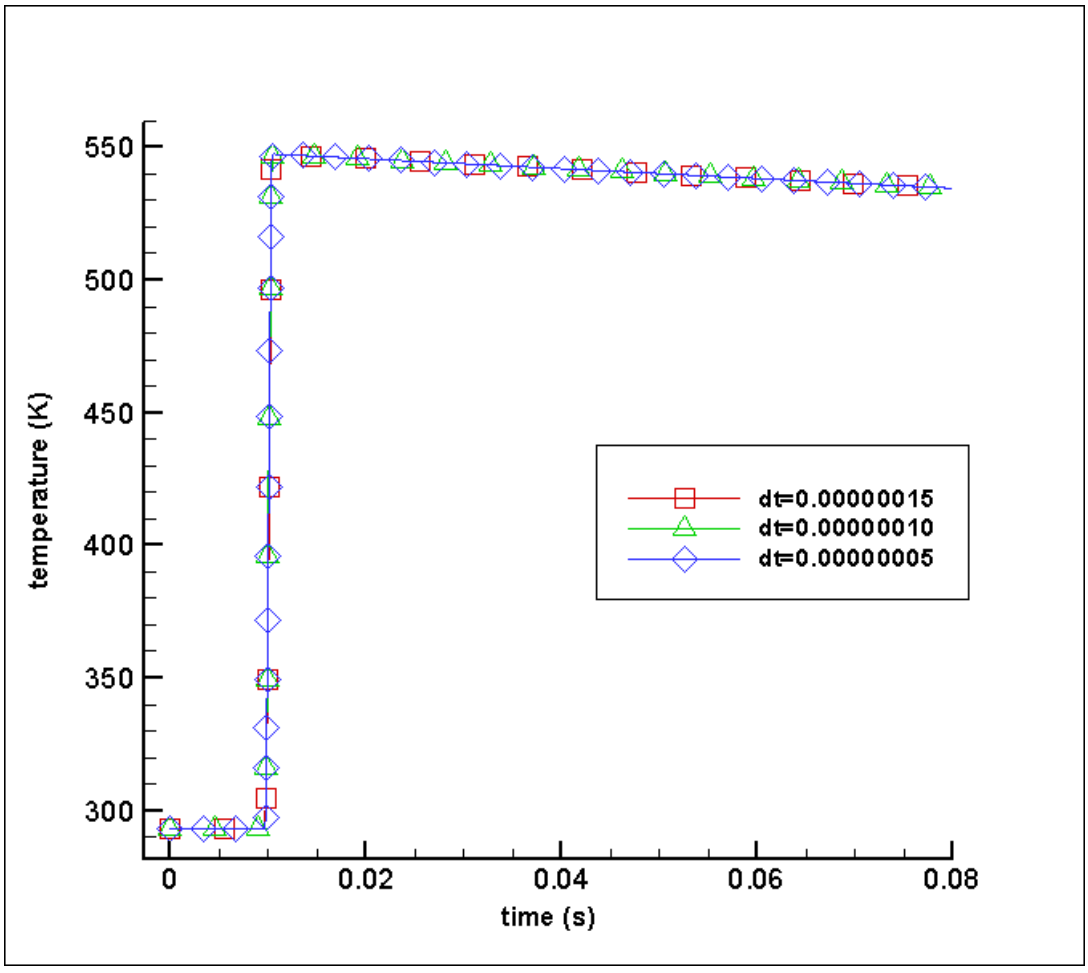

Figure 7.11 Histogram of Temperatures at Node (3,59), Iinitially at $x = 3.81x10^{-3} m$, $y = 3.95x10^{-3} m$, for 3 Different Time Increments ($u_\infty = 100 m/s$, $\mathrm{Re} = 3.37x10^4$, $\dot{r} = 0.015 m/s$)

7.6 Singular Points in Histogram Plots

There are singular points in histogram plots of horizontal velocity, vertical velocity, temperature and turbulent viscosity. Singular points in the plots are originated from the low resolution of the graphs or insufficient number of points are stored during simulation.

Singular points in temperature histograms are caused by the time delay, while surface temperature suddenly increases to 600K at time 0.0098s.

Figure 7.13 shows the close-look to the singular point of the histogram plot of horizontal velocity, Figure 7.4. It can be seen that there is a curve instead of a singular point. Similar results are obtained for other plots.

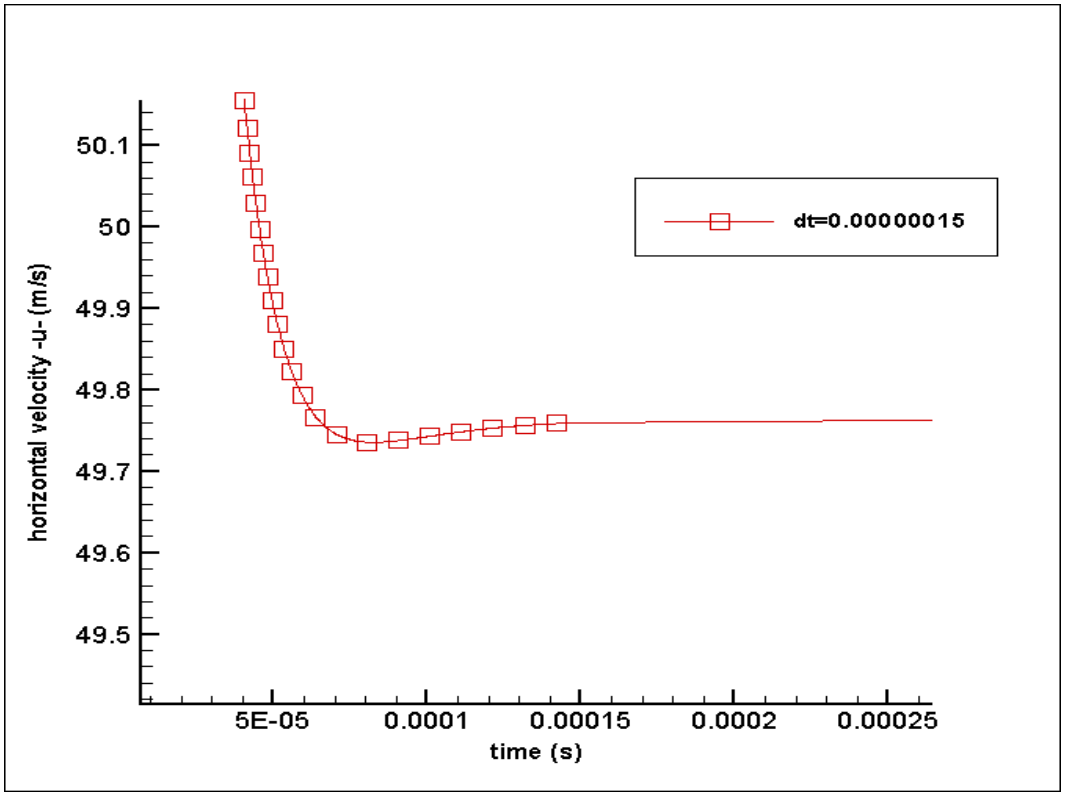

Figure 7.12 Close-look to the Histogram of Horizontal Velocity at Node (3,59), Initially at $x = 3.81x10^{-3}\,m$, $y = 3.95x10^{-3}\,m$

CHAPTER 8

COMPARISON OF THE RESULTS OF THE PRESENT AND PREVIOUS PROGRAMS

8.1 Introduction

Both the previous and present computer codes are run with same input parameters. The obtained results are plotted in the following sections.

Velocity profiles, vector plots of velocity, contour plots of horizontal velocity, temperature and turbulent viscosity shows that boundary layer predicted by the present program is thinner with respect to the previous program. This is mainly, because of the viscosity predicted by the present program is lower.

Run number 8 is carried out with the computer code of the previous study, while the run number 4 is done with the code of the present study.

Table 8.1 List of Runs for Comparison of Present and Previous Studies

RUN NUMBER	DESCRIPTION
4	Turbulent case, computer code of the present study, for comparison with the previous program 21x61 mesh size, $u_\infty = 100 m/s$, $\mathrm{Re} = 1.67x10^5$, $\dot{r} = 0.015 m/s$, $T_s = 600K$, $\Delta t = 1.0x10^{-7} s$, input run parameters given in Table 7.3
8	Turbulent case, computer code of the previous study, for comparison with the present program 21x61 mesh size, $u_\infty = 100 m/s$, $\mathrm{Re} = 1.67x10^5$, $\dot{r} = 0.015 m/s$, $T_s = 600K$, $\Delta t = 1.0x10^{-7} s$ input run parameters given in Table 7.3

8.1.1 Horizontal Velocity Profiles

In this section, velocity profiles of the present and previous program is plotted at three different horizontal distances.

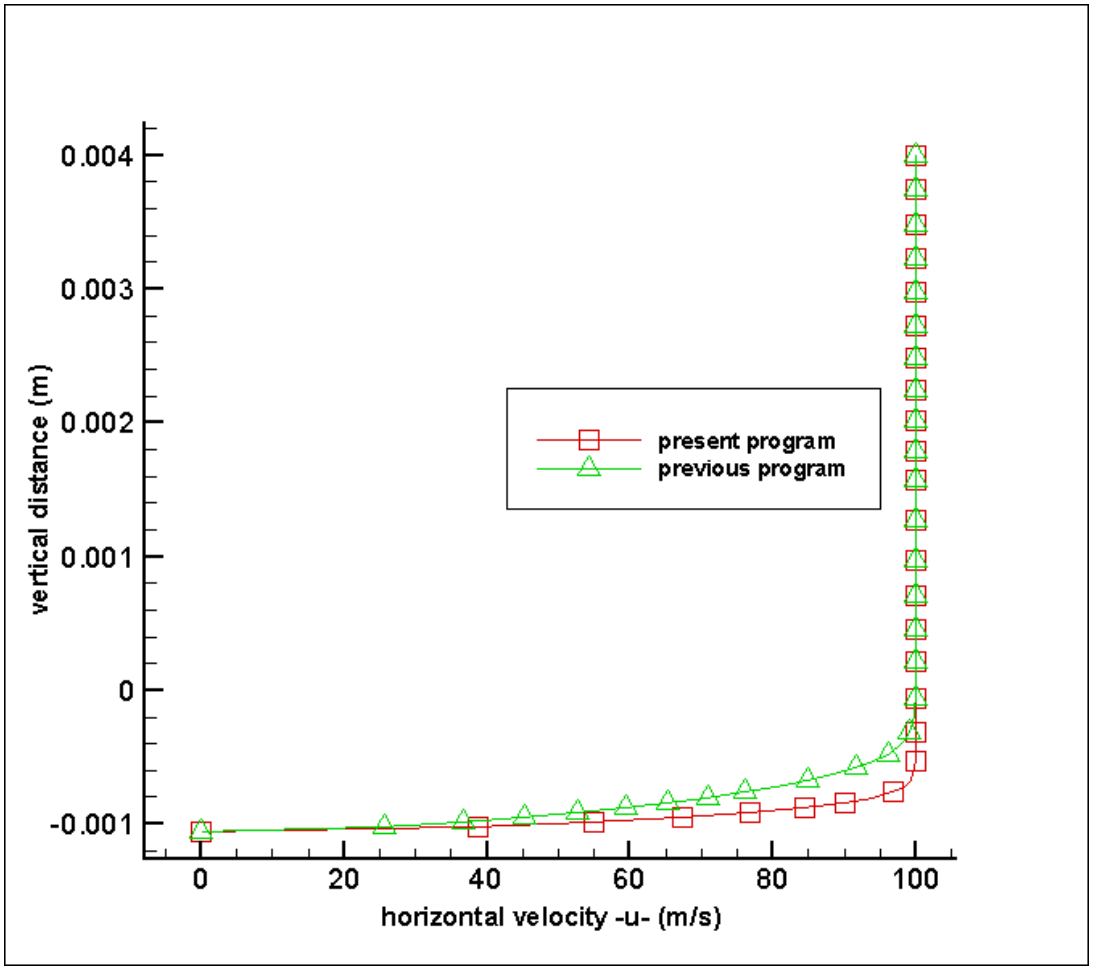

Figure 8.1 Velocity Profiles of the Previous and Present Programs at $x = 3.81x10^{-3} m$ ($u_\infty = 100 m/s$, $\mathrm{Re} = 3.34x10^{4}$, $t = 0.08 s$, $\dot{r} = 0.015 m/s$, $T_s = 600 K$)

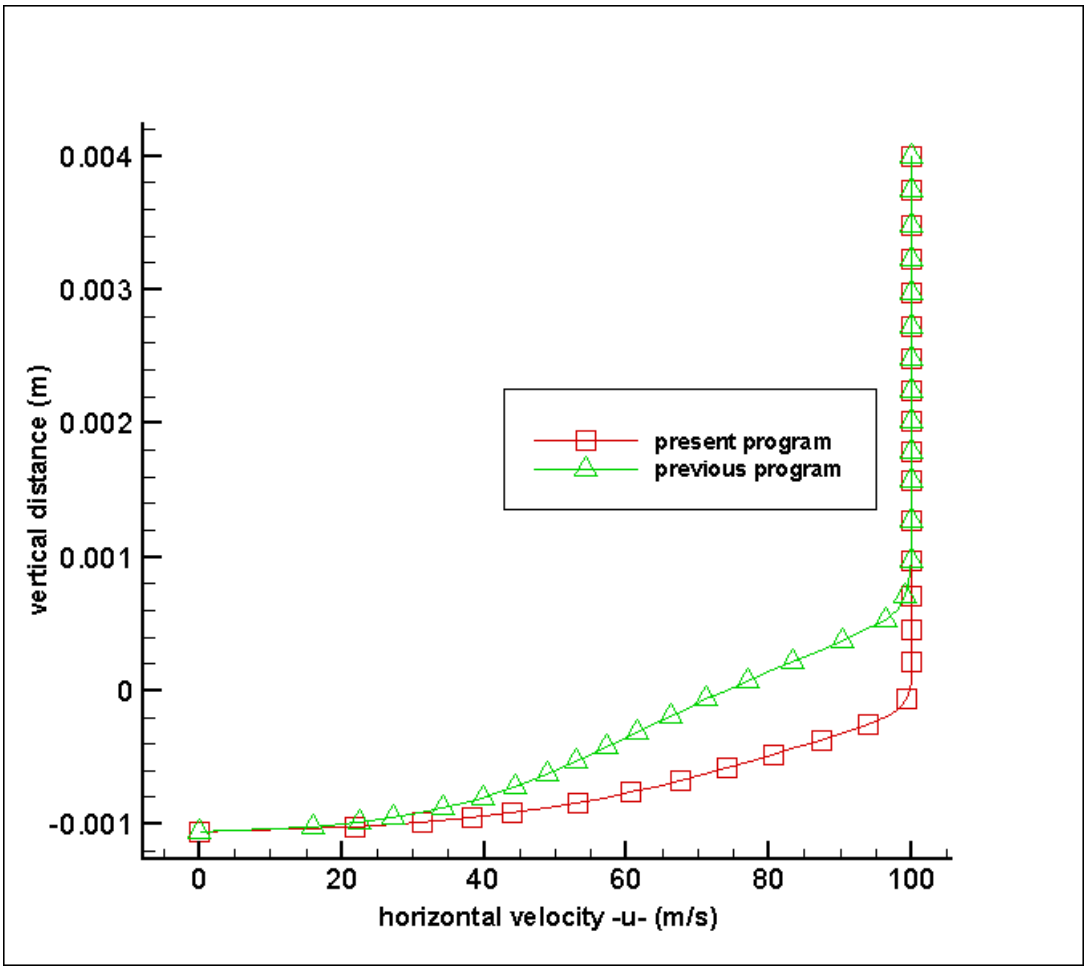

Figure 8.2 Velocity Profiles of the Previous and Present Programs at $x = 1.905x10^{-2}\,m$ ($u_\infty = 100m/s$, $\mathrm{Re} = 1.67x10^5$, $t = 0.08s$, $\dot{r} = 0.015m/s$, $T_s = 600K$)

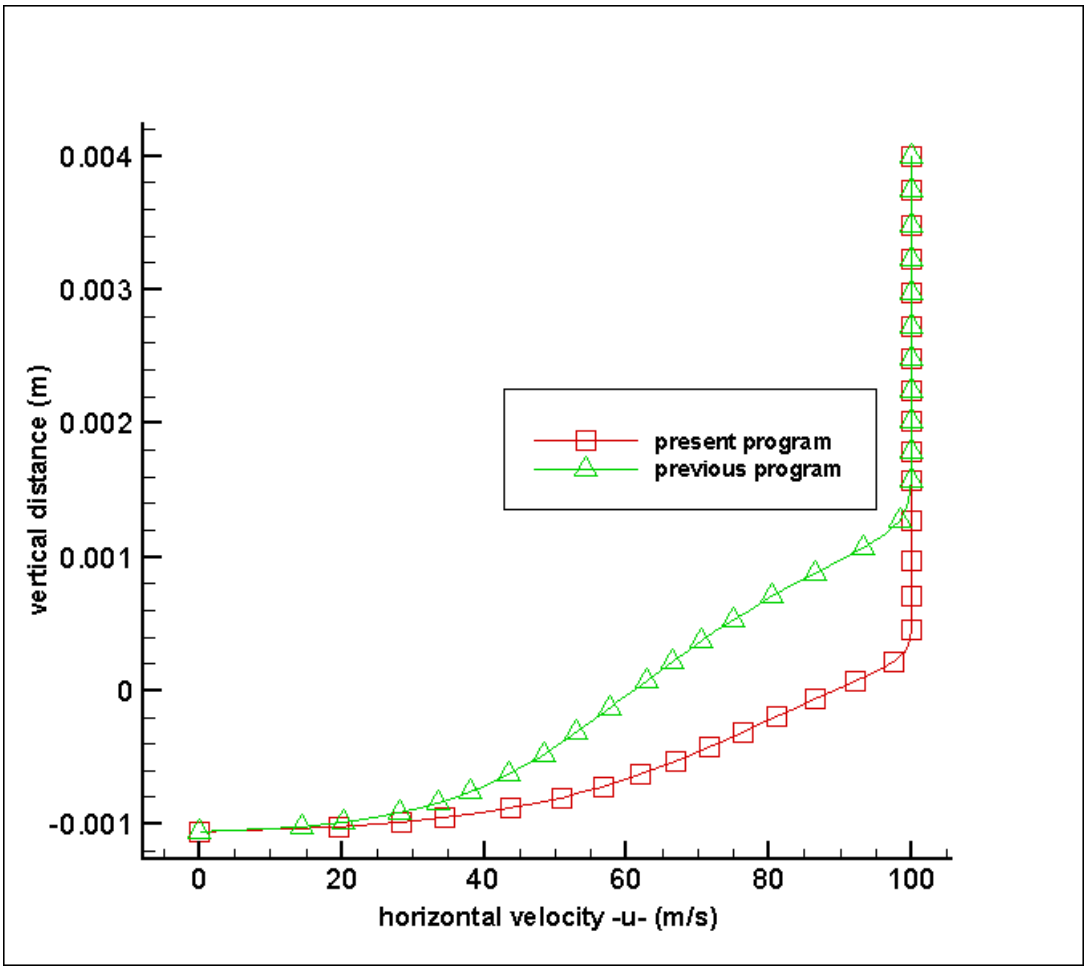

Figure 8.3 Velocity Profiles of the Previous and Present Programs at $x = 3.24x10^{-2}\,m$ ($u_\infty = 100m/s$, $\mathrm{Re} = 2.84x10^5$, $t = 0.08s$, $\dot{r} = 0.015m/s$, $T_s = 600K$)

8.1.2 Velocity Vectors and Contours

Velocity vectors for both the previous and present programs can be found in the following figures. In data files information of the whole domain is written, however to illustrate more clearly vectors at some of the horizontal distances are shown.

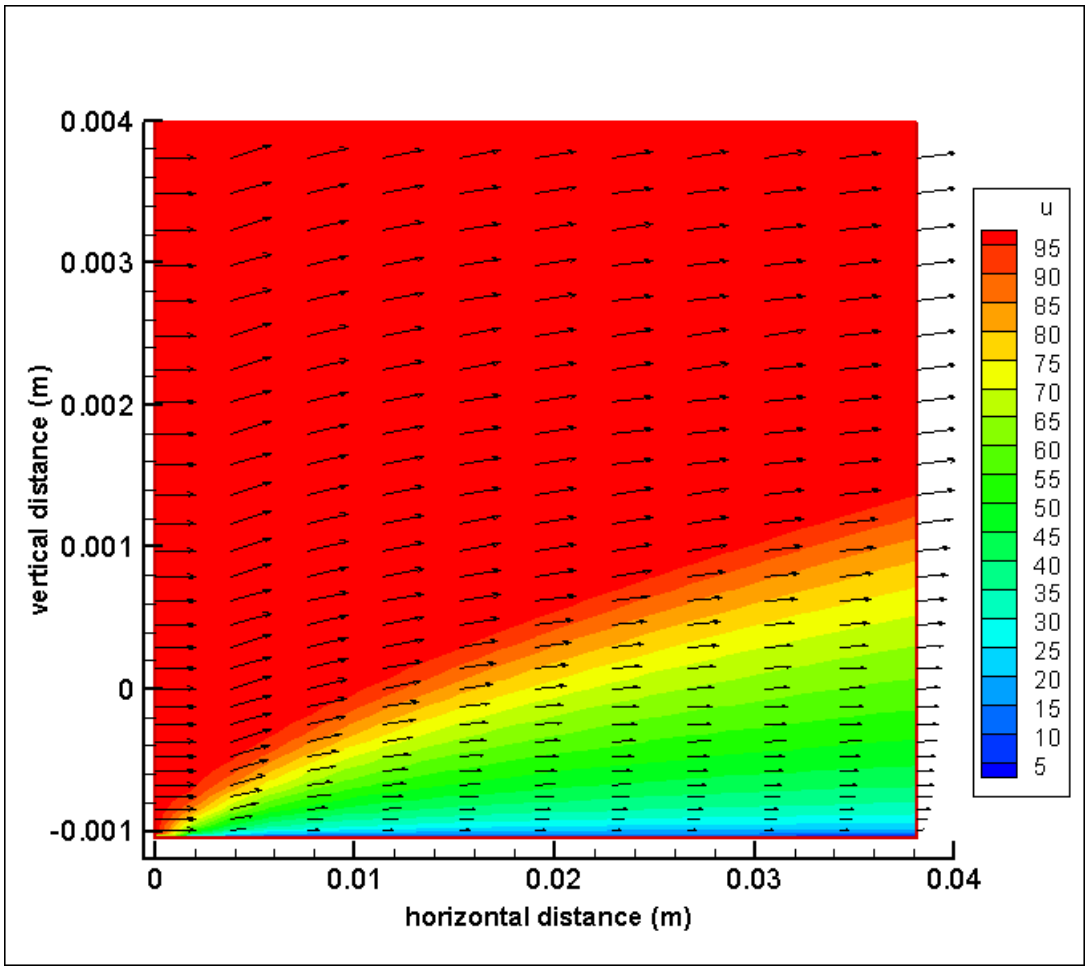

Figure 8.4 Velocity Vectors of Previous Program ($t = 0.08s$, $\dot{r} = 0.015m/s$, $u_\infty = 100m/s$, $T_s = 600K$)

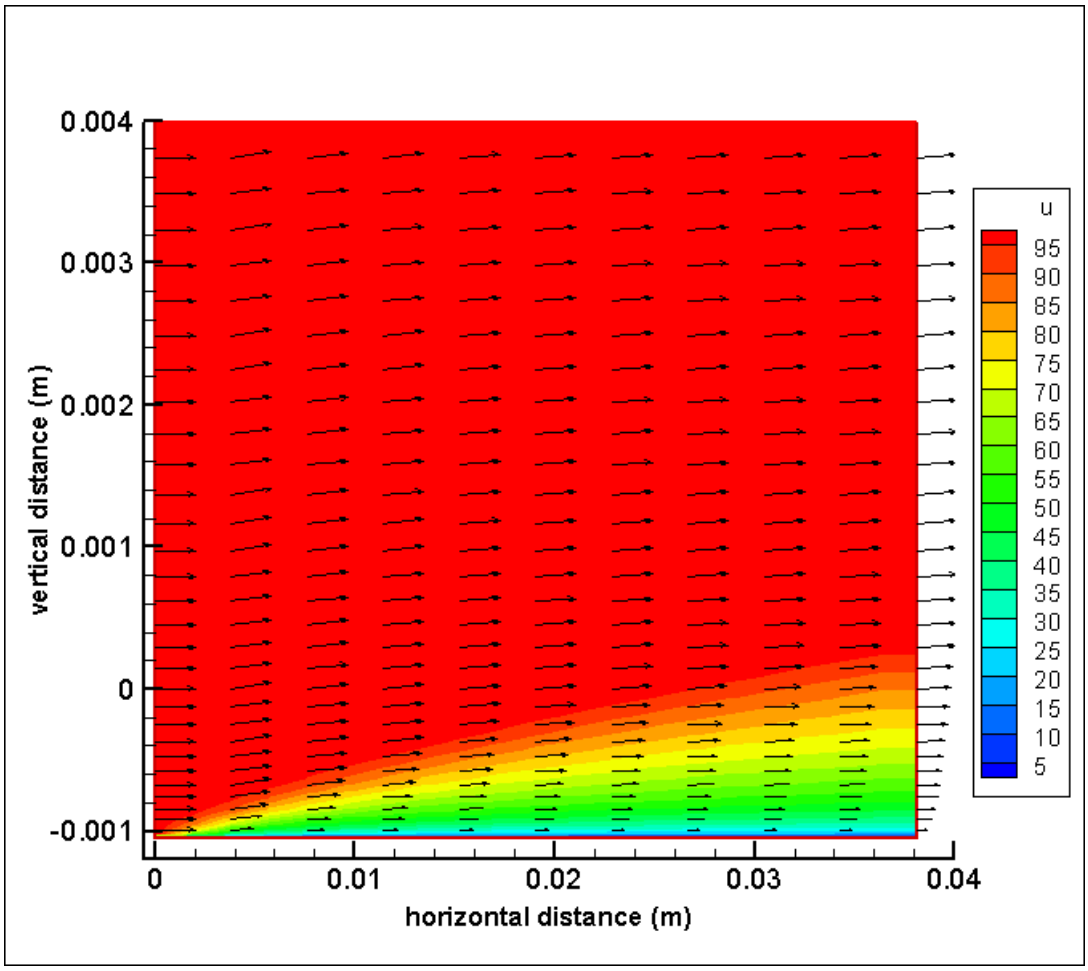

Figure 8.5 Velocity Vectors of Present Program ($t = 0.08s$, $\dot{r} = 0.015m/s$, $u_\infty = 100m/s$, $T_s = 600K$)

8.1.3 Temperature Contours

The temperature contours at the end of analysis, at time 0.08s, are given in Figure 8.8 for the previous program and in Figure 8.9 for the present program.

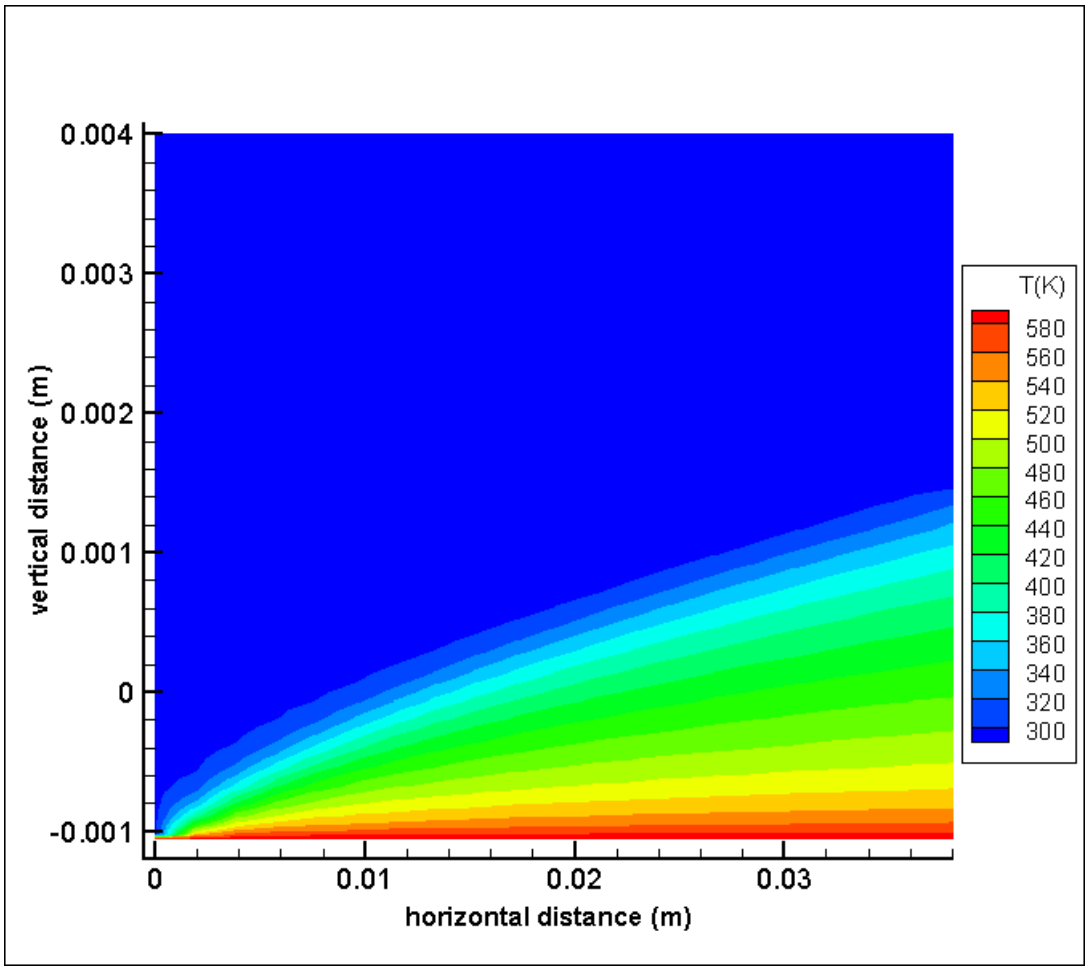

Figure 8.6 Temperature Contours of Previous Program ($t = 0.08s$, $\dot{r} = 0.015m/s$, $u_\infty = 100m/s$, $T_s = 600K$)

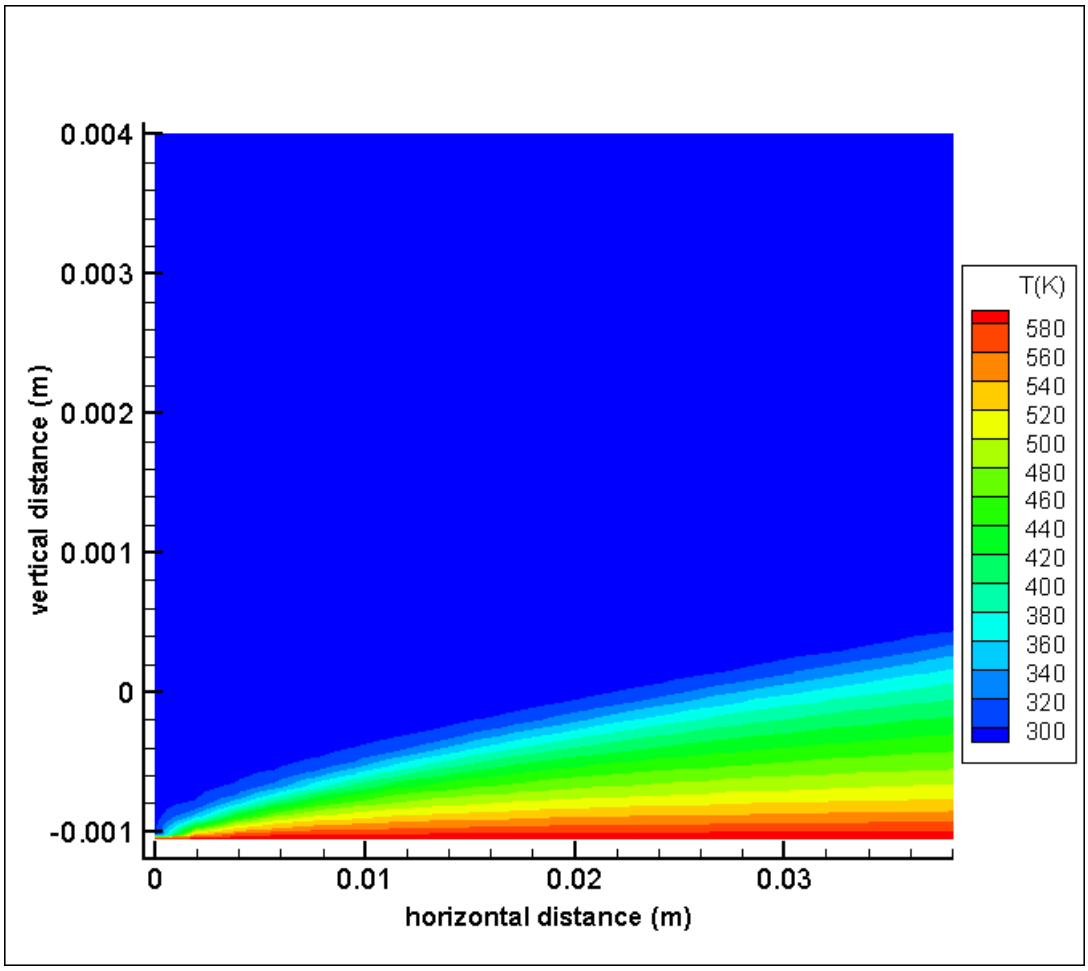

Figure 8.7 Temperature Contours of Present Program ($t = 0.08s$, $\dot{r} = 0.015m/s$, $u_\infty = 100m/s$, $T_s = 600K$)

8.1.4 Turbulent Viscosity Contours

The turbulent viscosity contours at the end of analysis, at time 0.08s, are given in Figure 8.10 for the previous program and in Figure 8.11 for the present program.

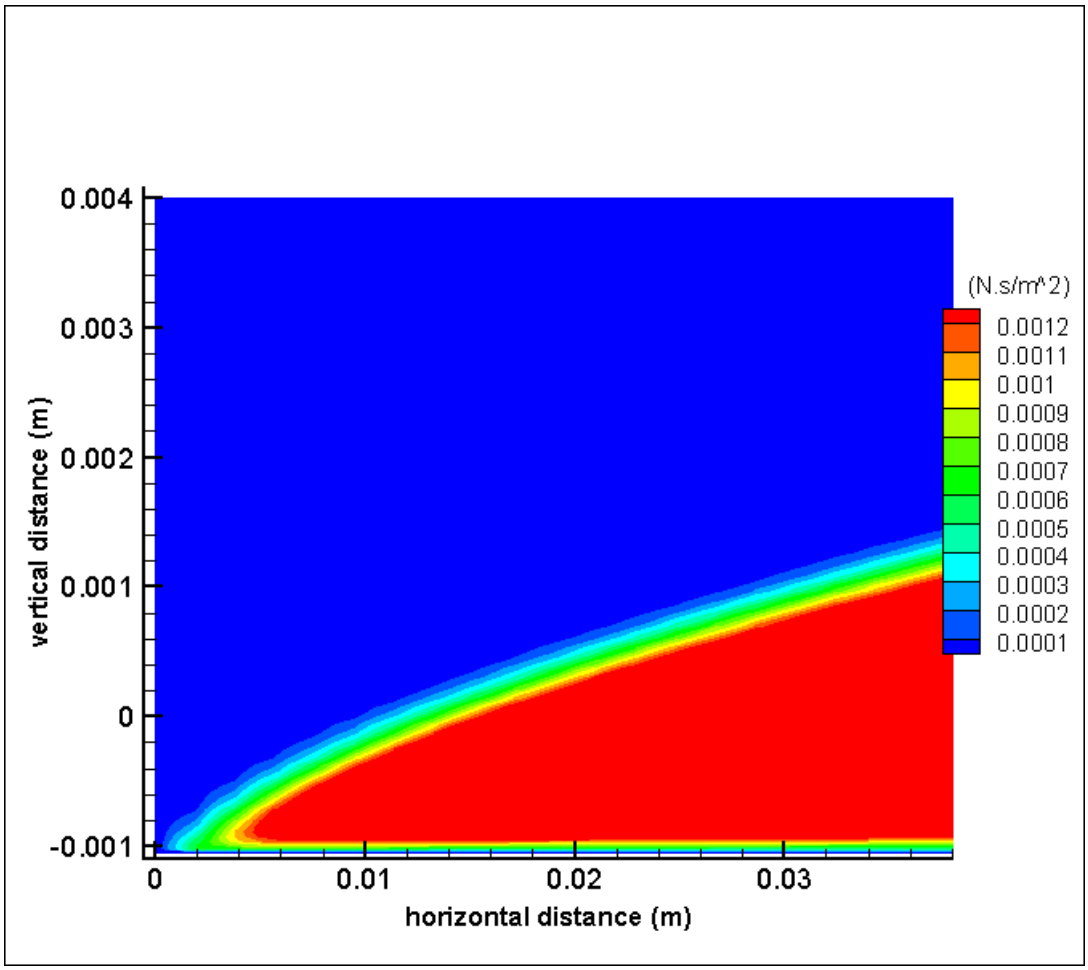

Figure 8.8 Turbulent Viscosity Contours of Previous Program ($t = 0.08s$, $u_\infty = 100m/s$, $\dot{r} = 0.015m/s$, $T_s = 600K$)

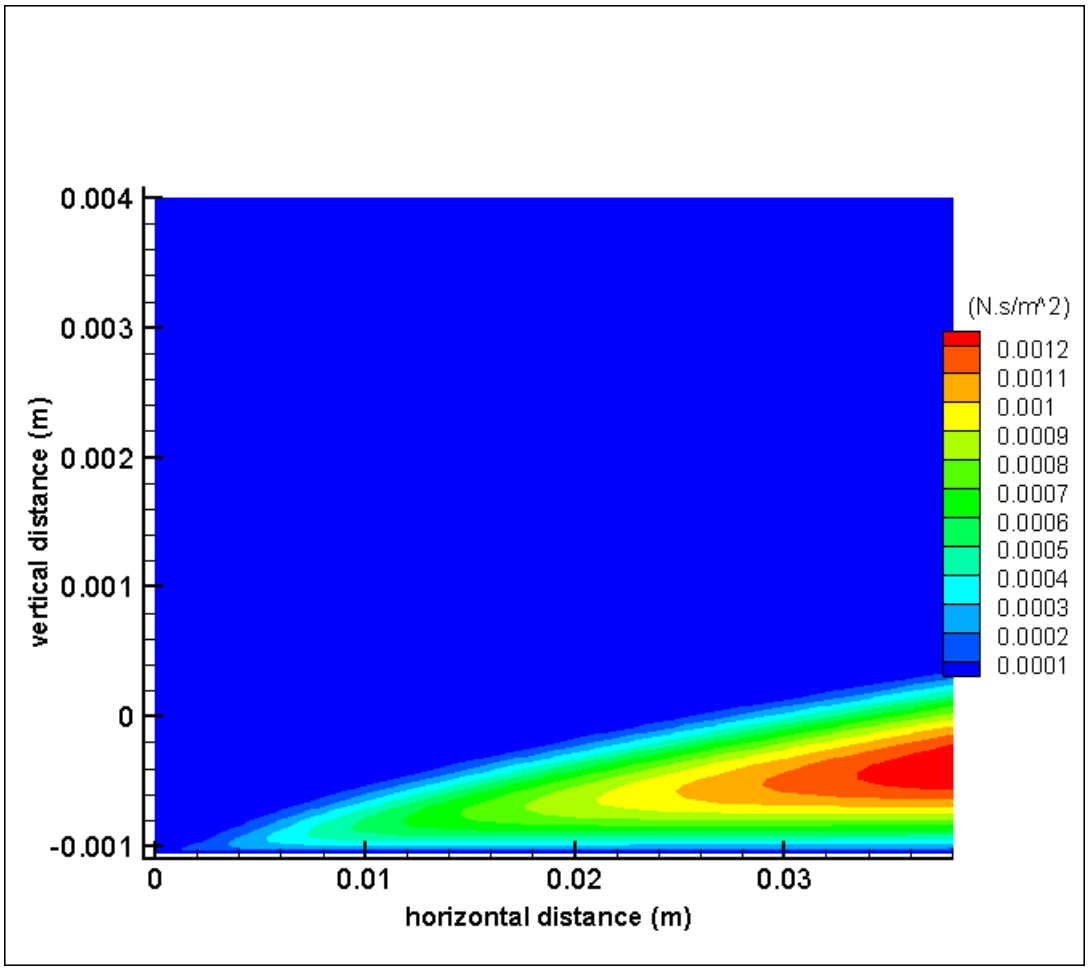

Figure 8.9 Turbulent Viscosity Contours of Present Program ($t = 0.08s$, $u_\infty = 100m/s$, $\dot{r} = 0.015m/s$, $T_s = 600K$)

8.1.5 Histogram Plots of Selected Variables

The values of horizontal velocities and temperatures are plotted for run numbers 4 and 8. There is a slight difference between two programs for the predicted value of temperature, less than 1%. For the horizontal velocity, this difference is as high as 28%.

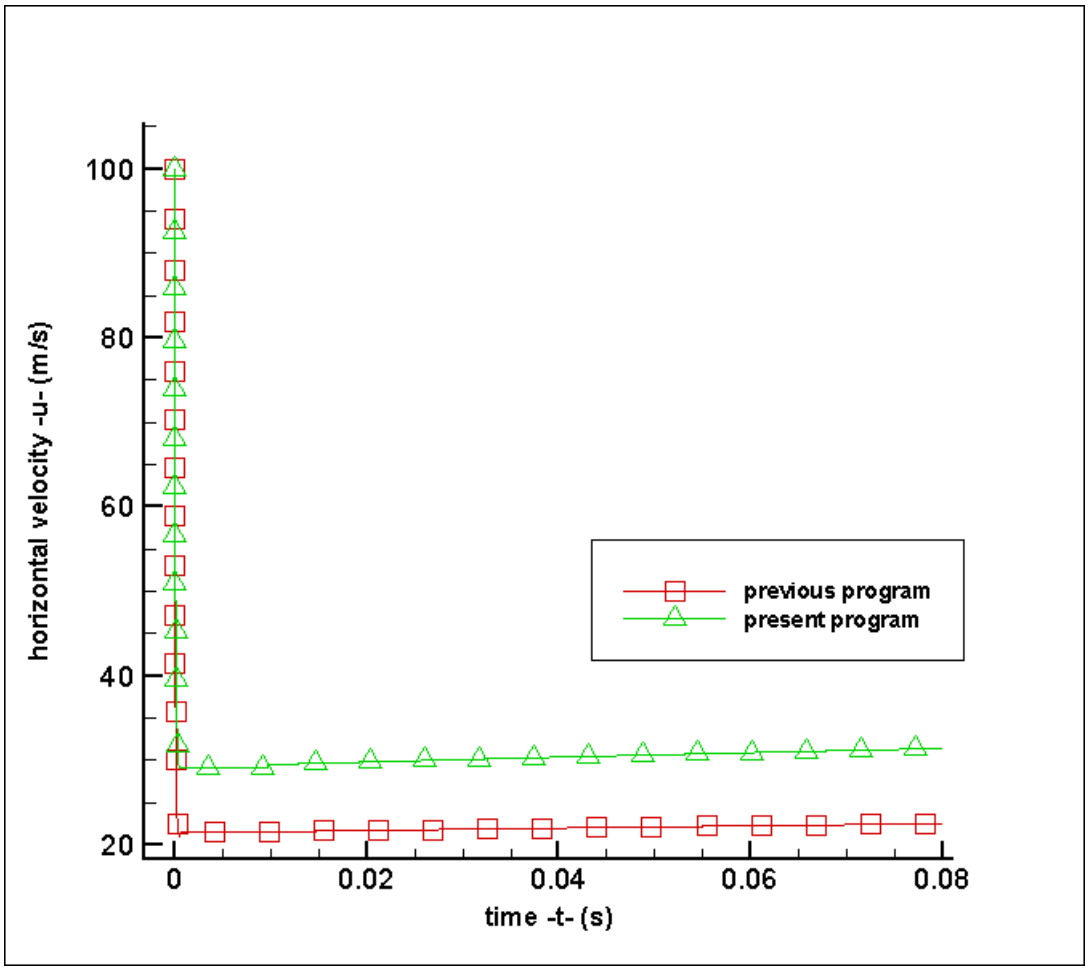

Figure 8.10 Variation of the Horizontal Velocities with Time at Node (11,59) which is Initially at $x = 1.905x10^{-2} m$, $y = 3.95x10^{-3} m$ ($t = 0.08s$, $u_\infty = 100m/s$, $\dot{r} = 0.015m/s$, $T_s = 600K$)

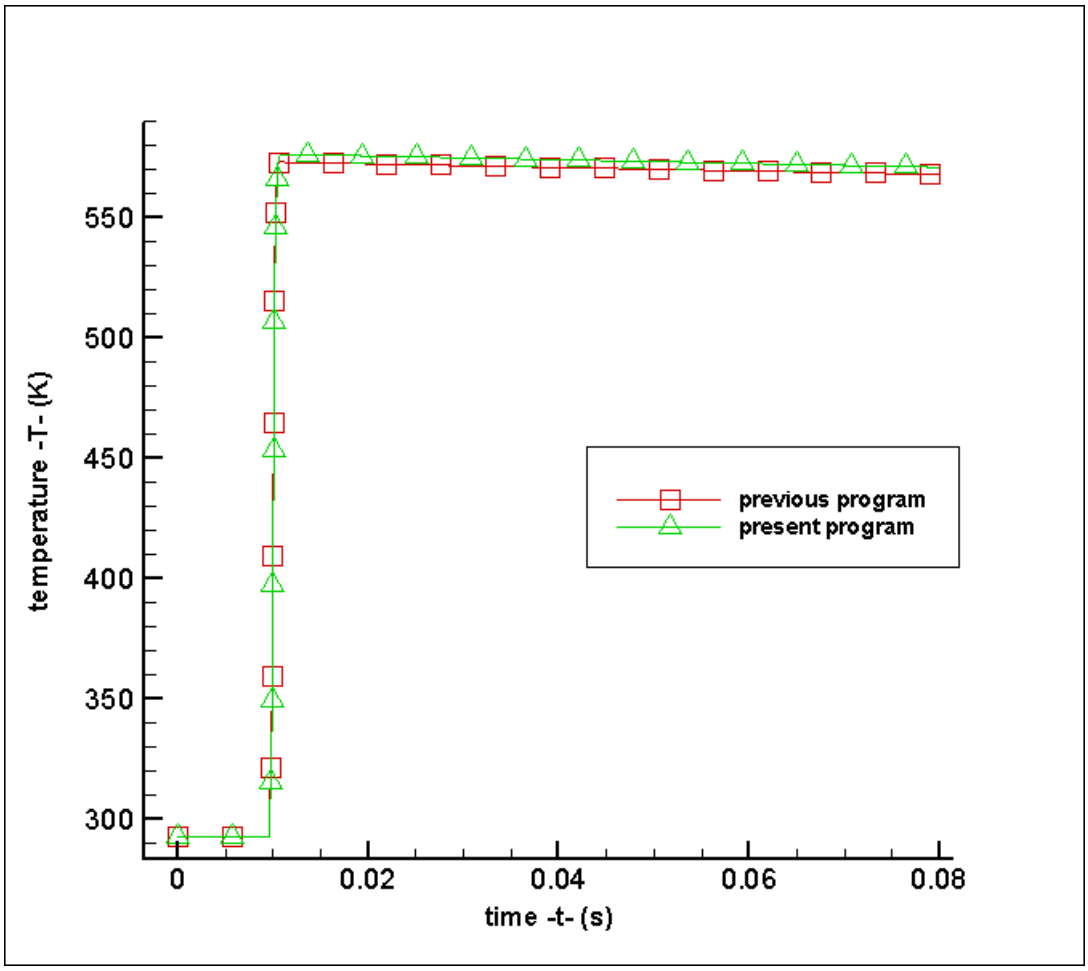

Figure 8.11 Variation of the Temperatures with Time at Node (11,59) which is Iinitially at $x = 1.905x10^{-2}\,m$, $y = 3.95x10^{-3}\,m$ ($t = 0.08s$, $u_\infty = 100m/s$, $\dot{r} = 0.015m/s$, $T_s = 600K$)

CHAPTER 9

PARAMETRIC STUDY

9.1 Study with Different Regression Rates

Present program is run with three different regression rates and results are presented in the following pages. It is observed that program worked successfully and no degeneration of the results near the boundary is found.

Table 9.1 List of Runs for Different Regression Rate Study

RUN NUMBER	DESCRIPTION	REGRESSION RATE
4	Turbulent flow, computer code of the present study, Re= $5.33x10^4$, $\dot{r} = 0.015m/s$, run parameters given in Table 7.3	$\dot{r} = 0.015m/s$
9	Turbulent flow, computer code of the present study, Re= $5.33x10^4$, $\dot{r} = 0.012m/s$ run parameters given in Table 7.3	$\dot{r} = 0.012m/s$
10	Turbulent flow, computer code of the present study, Re= $5.33x10^4$, $\dot{r} = 0.018m/s$ run parameters given in Table 7.3	$\dot{r} = 0.018m/s$

9.1.1 Horizontal Velocity Profiles

Horizontal velocity profiles at $x = 1.905x10^{-2}m$ is given in the following figure at the end of simulation, $t = 0.08s$. Regression caused the bounds of the physical domain to change, therefore plots start from different points in vertical direction.

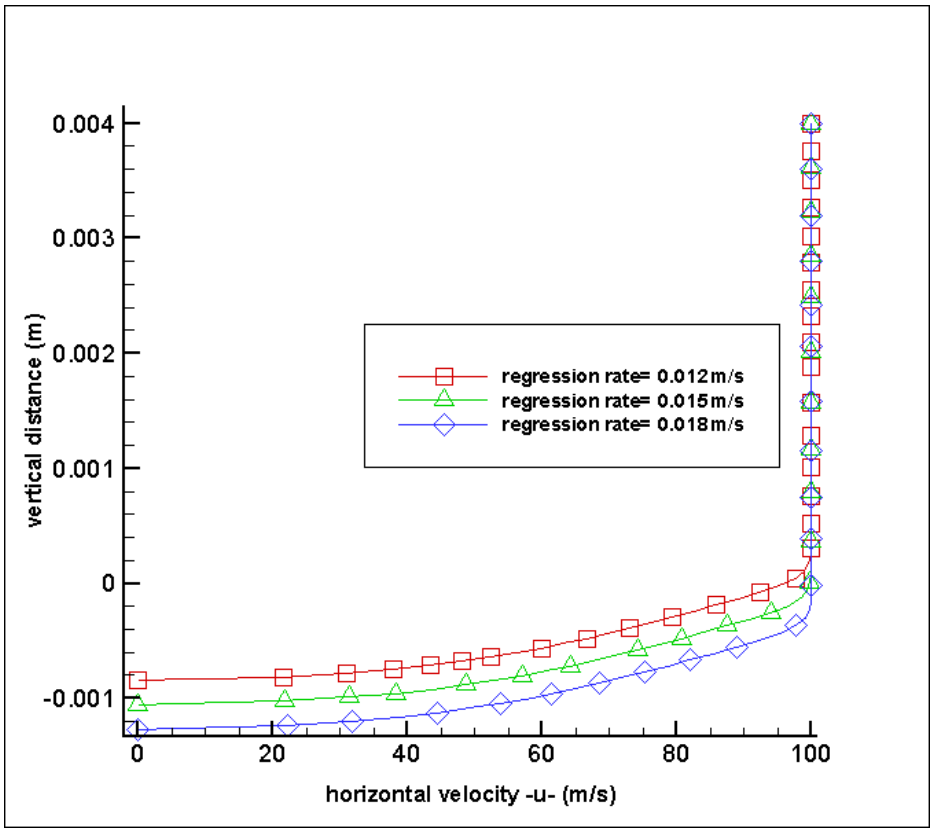

Figure 9.1 Horizontal Velocity Profiles at $x = 1.905x10^{-2} m$, for 3 Different Regression Rates ($u_\infty = 100 m/s$, $\mathrm{Re} = 1.67x10^5$, $t = 0.08s$)

9.1.2 Temperature Contours

In the following figures, temperature contours at the end of simulation for regression rates $\dot{r} = 0.012 m/s$ and $\dot{r} = 0.015 m/s$ are given. In Figure 9.4, for $\dot{r} = 0.018 m/s$ instantaneous temperature contours are given for various times. The regression of the boundary between gas and solid surface can be observed.

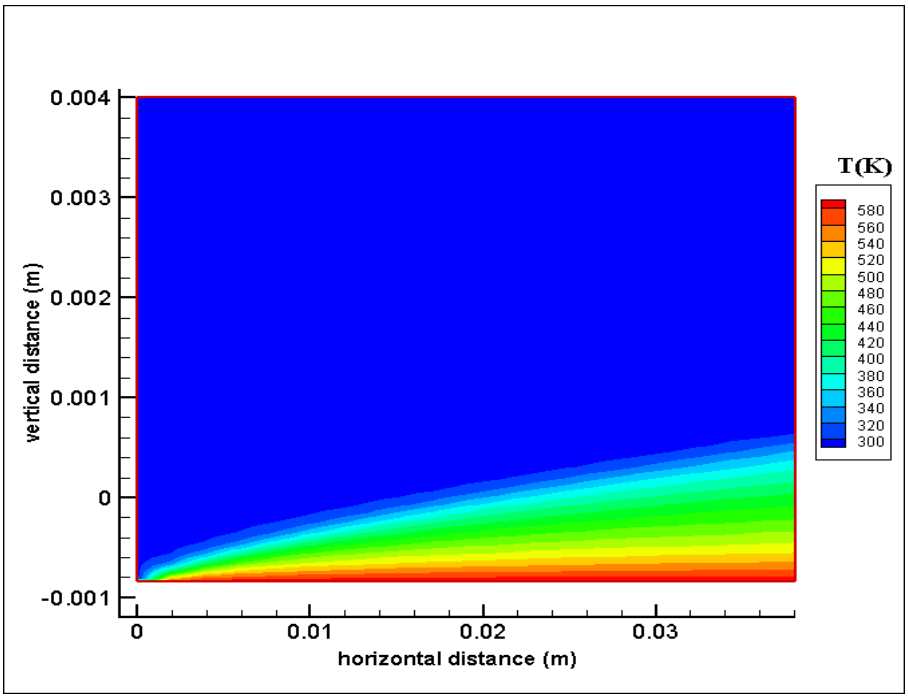

Figure 9.2 Temperature Contours of Present Study ($\dot{r} = 0.012m/s$, $u_\infty = 100m/s$, $\mathrm{Re} = 3.34x10^5$, $t = 0.08s$)

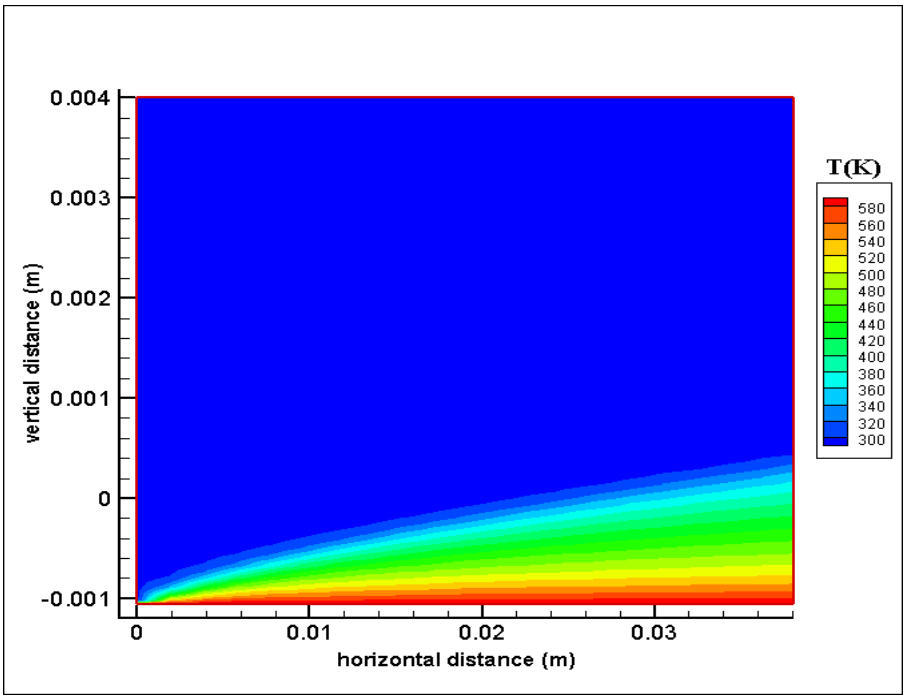

Figure 9.3 Temperature Contours of Present Study ($\dot{r} = 0.015m/s$, $u_\infty = 100m/s$, $\mathrm{Re} = 3.34x10^5$, $t = 0.08s$)

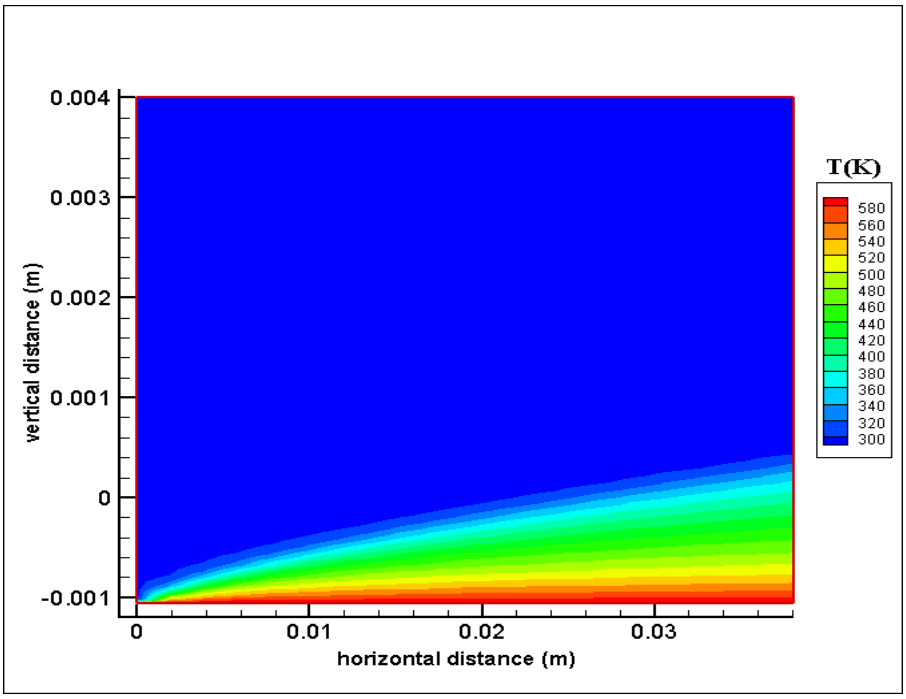

Figure 9.4 Temperature Contours of Present Study ($\dot{r} = 0.018m/s$, $u_\infty = 100m/s$, $\mathrm{Re} = 3.34x10^5$, $t = 0.08s$)

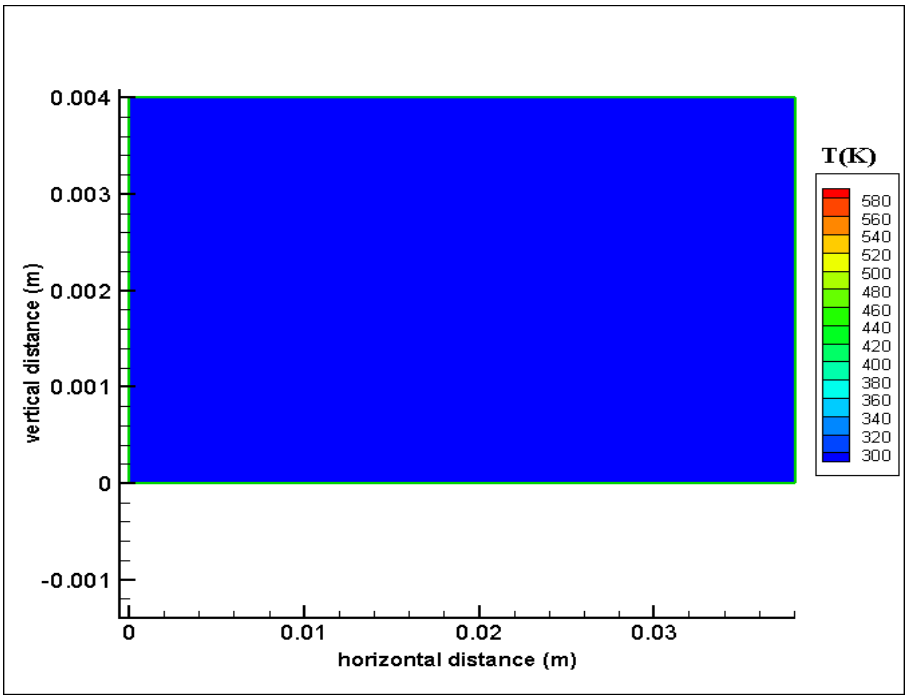

Figure 9.5a Temperature Contours of Present Study ($\dot{r} = 0.018m/s$, $u_\infty = 100m/s$, $\mathrm{Re} = 3.34x10^5$, $t = 0s$)

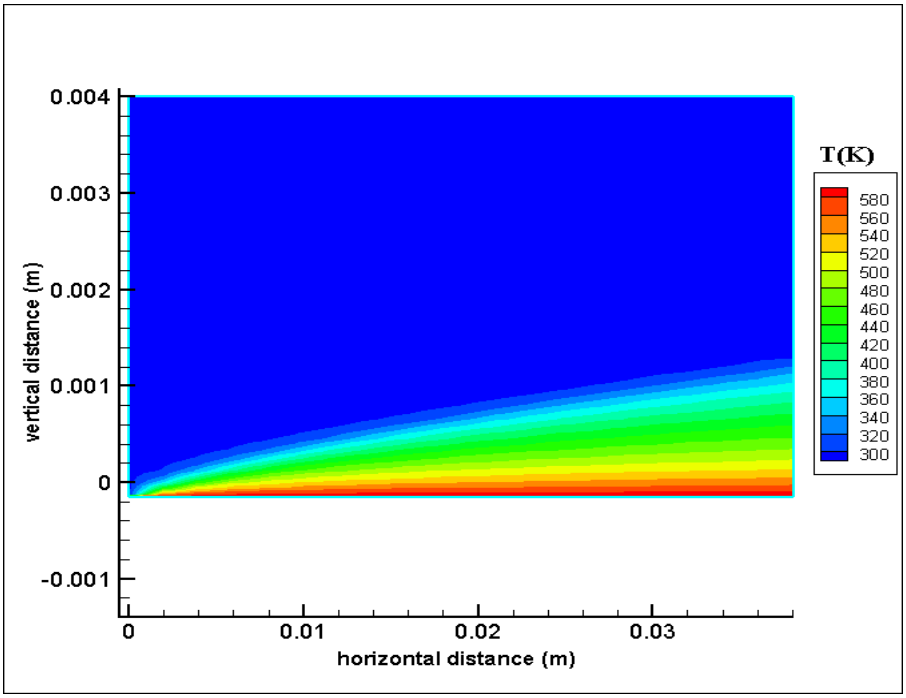

Figure 9.5b Temperature Contours of Present Study ($\dot{r} = 0.018m/s$, $u_\infty = 100m/s$, $\mathrm{Re} = 3.34x10^5$, $t = 0.02s$)

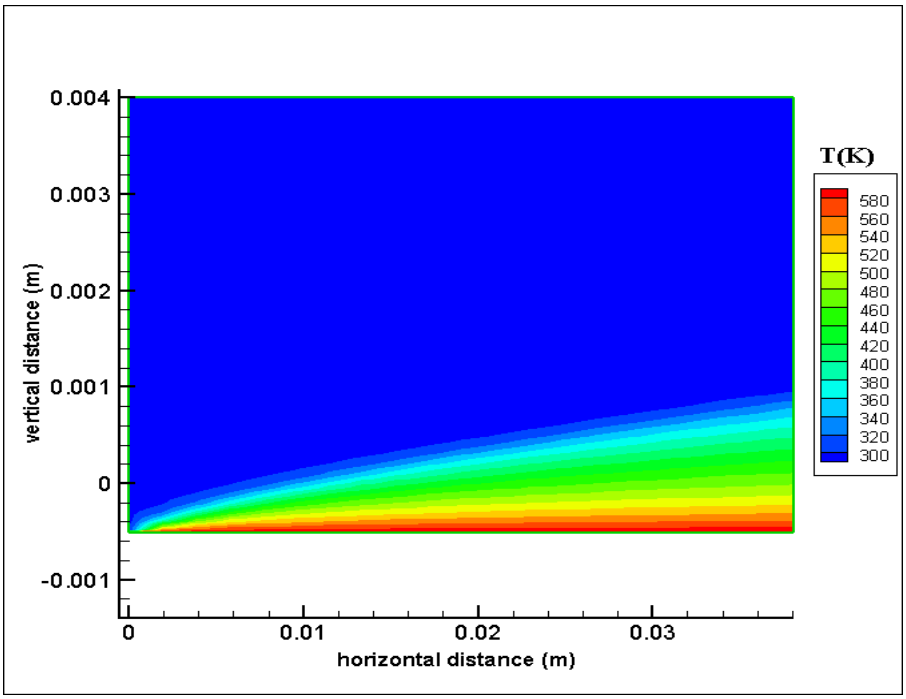

Figure 9.5c Temperature Contours of Present Study ($\dot{r} = 0.018m/s$, $u_\infty = 100m/s$, $\mathrm{Re} = 3.34x10^5$, $t = 0.04s$)

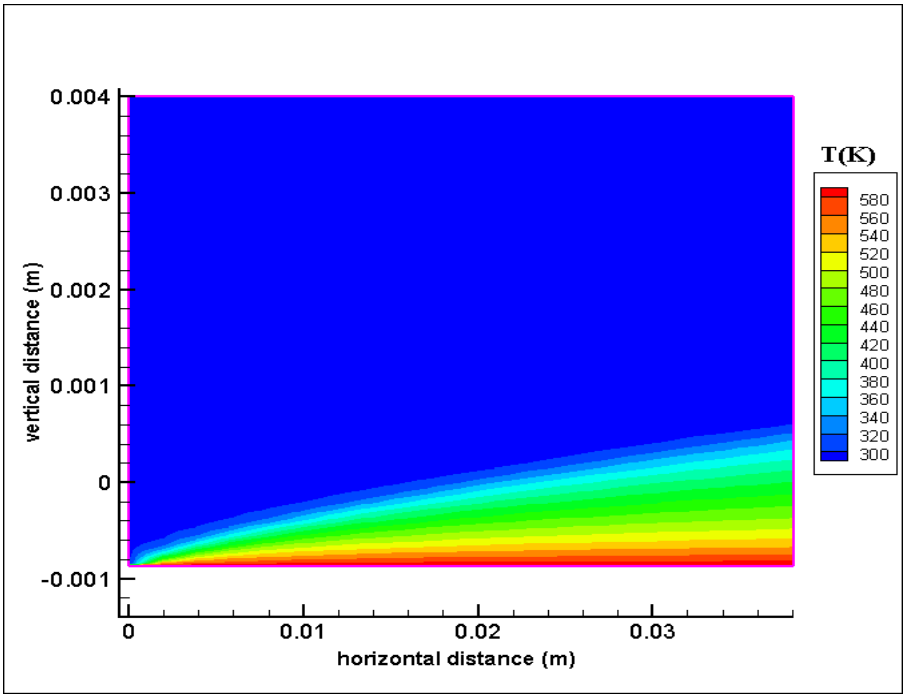

Figure 9.5d Temperature Contours of Present Study ($\dot{r} = 0.018m/s$, $u_\infty = 100m/s$, $\mathrm{Re} = 3.34x10^5$, $t = 0.06s$)

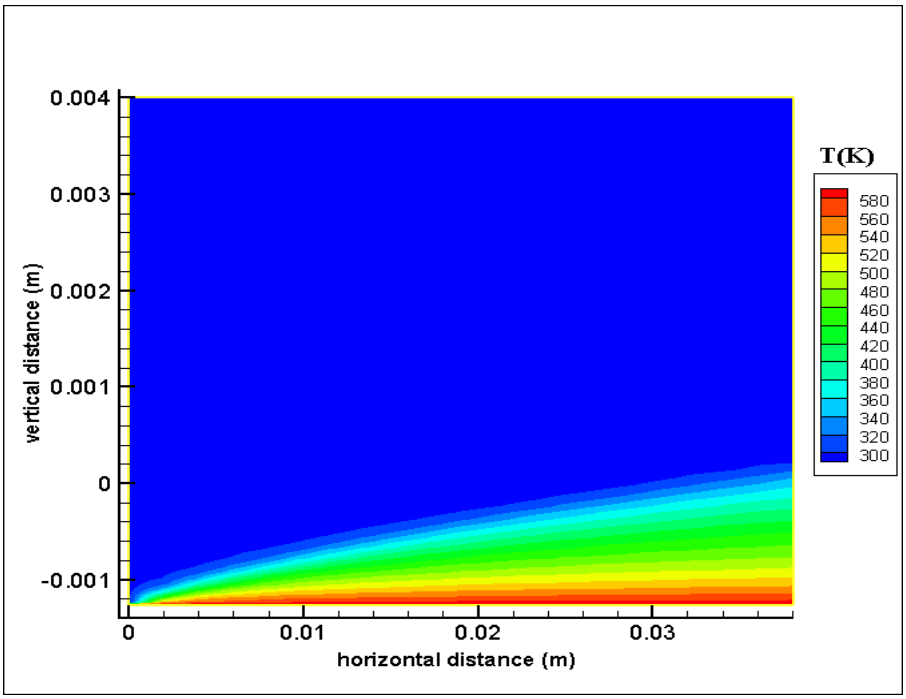

Figure 9.5e Temperature Contours of Present Study ($\dot{r} = 0.018m/s$, $u_\infty = 100m/s$, $\mathrm{Re} = 3.34x10^5$, $t = 0.08s$)

9.2 Study with Different Reynolds Numbers

Present program is run with three different Reynolds numbers and results are presented in the following pages. The boundary layer became thinner as the horizontal velocity increased.

Table 9.2 List of Runs for Different Reynolds Number Study

RUN NUMBER	DESCRIPTION	REYNOLDS NUMBER
4	Turbulent flow, computer code of the present study, $u_\infty = 100 m/s$, $\mathrm{Re} = 3.34x10^5$, $\dot{r} = 0.015 m/s$, run parameters given in Table 7.3	$\mathrm{Re} = 3.34x10^5$
11	Turbulent flow, computer code of the present study, $u_\infty = 150 m/s$, $\mathrm{Re} = 5.01x10^5$, $\dot{r} = 0.015 m/s$ run parameters given in Table 7.3	$\mathrm{Re} = 5.01x10^5$
12	Turbulent flow, computer code of the present study, $u_\infty = 150 m/s$, $\mathrm{Re} = 6.01x10^5$, $\dot{r} = 0.015 m/s$ run parameters given in Table 7.3	$\mathrm{Re} = 6.01x10^5$

9.2.1 Horizontal Velocity Profiles and Contours

Horizontal velocity profiles at $x = 1.905x10^{-2} m$ is given in the following figure at the end of simulation, $t = 0.08s$ are plotted in Figure 9.5. Horizontal velocity contours can be seen in figures 9.6, 9.7 and 9.8 for different free stream velocities.

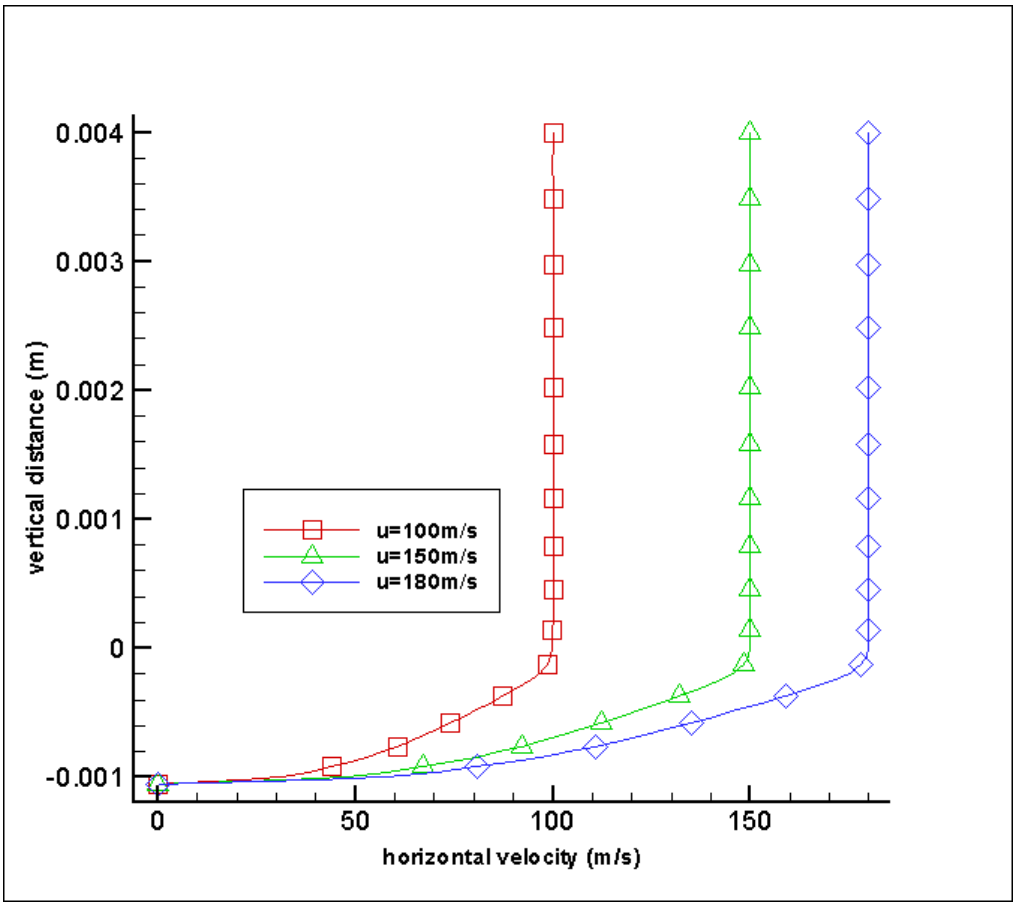

Figure 9.6 Horizontal Velocity Profiles at $x = 1.905x10^{-2} m$, for 3 Different Reynolds Numbers ($\dot{r} = 0.015m/s$, $t = 0.08s$)

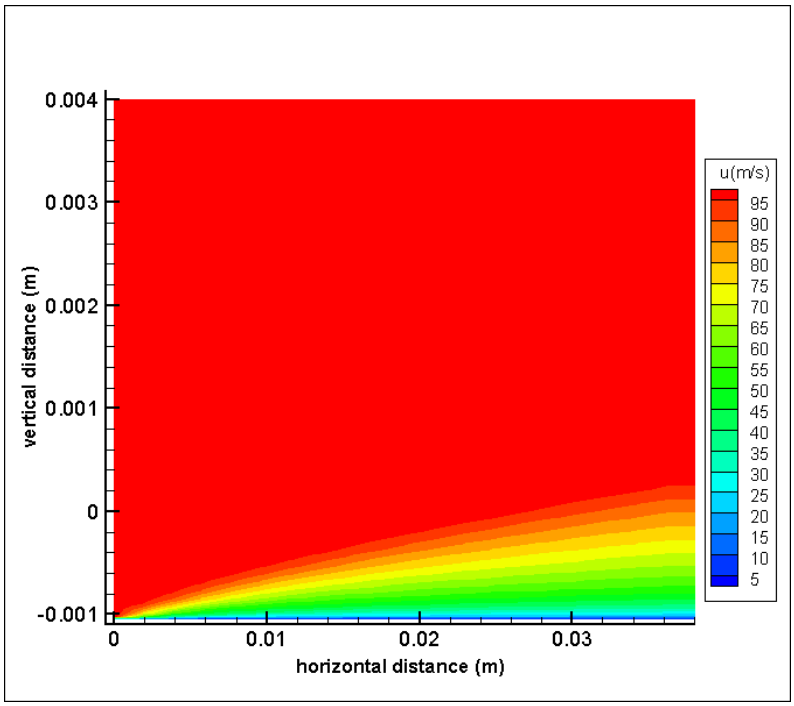

Figure 9.7 Horizontal Velocity Contours of Present Study ($\dot{r} = 0.015m/s$, $u_\infty = 100m/s$, $\mathrm{Re} = 3.34x10^5$, $t = 0.08s$)

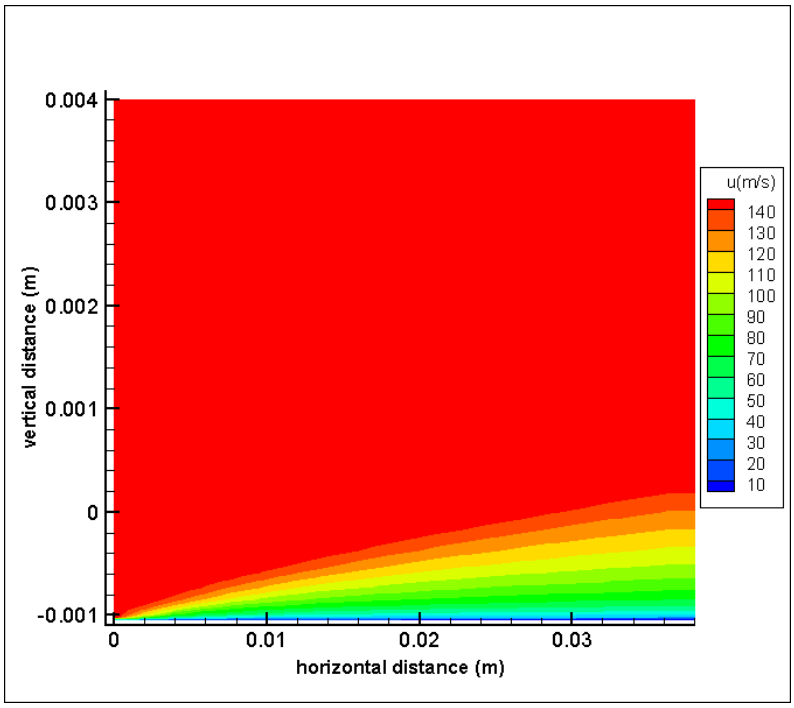

Figure 9.8 Horizontal Velocity Contours of Present Study ($\dot{r} = 0.015m/s$, $u_\infty = 150m/s$, $\mathrm{Re} = 5.01x10^5$, $t = 0.08s$)

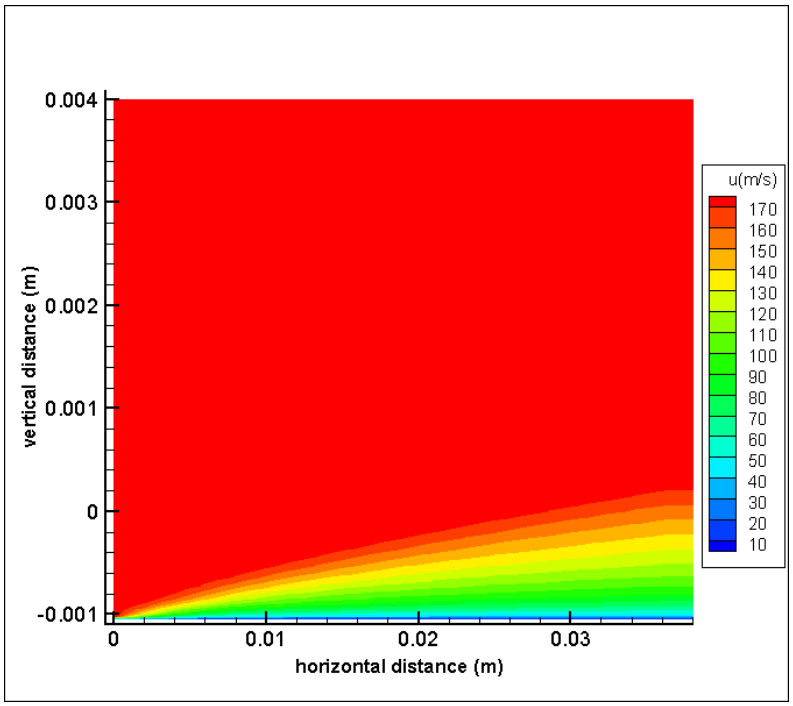

Figure 9.9 Horizontal Velocity Contours of Present Study ($\dot{r} = 0.015m/s$, $u_\infty = 180m/s$, $\mathrm{Re} = 6.01x10^5$, $t = 0.08s$)

9.2.2 Temperature Contours

Temperature contours can be seen in figures 9.9, 9.10 and 9.11 for different free stream velocities. The temperature field is slightly affected by the free stream horizontal velocity. Variation of T between $\mathrm{Re} = 3.34x10^5$ and $\mathrm{Re} = 6.01x10^5$ is less than 3%.

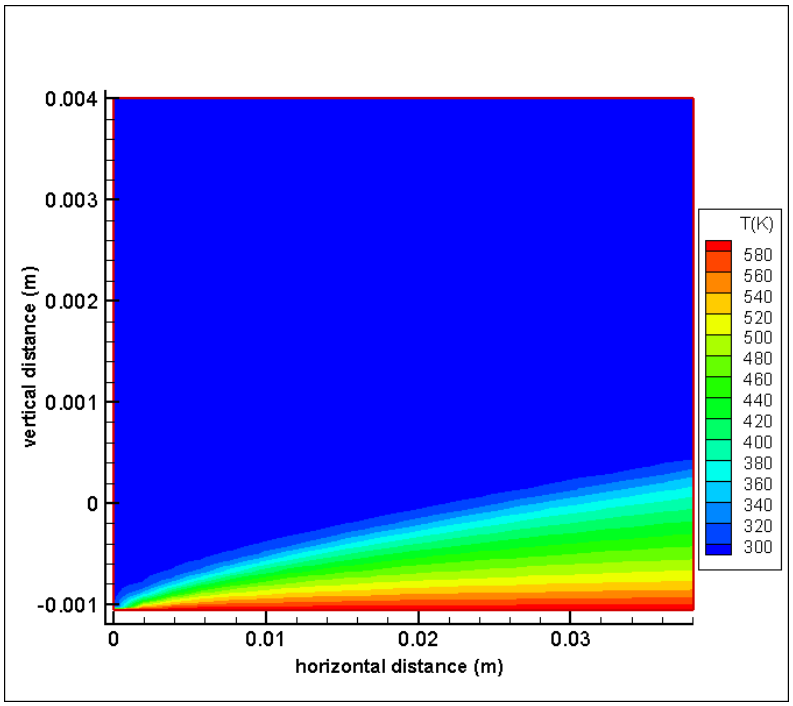

Figure 9.10 Temperature Contours of Present Study ($\dot{r} = 0.015m/s$, $u_\infty = 100m/s$, $\mathrm{Re} = 3.34x10^5$, $t = 0.08s$)

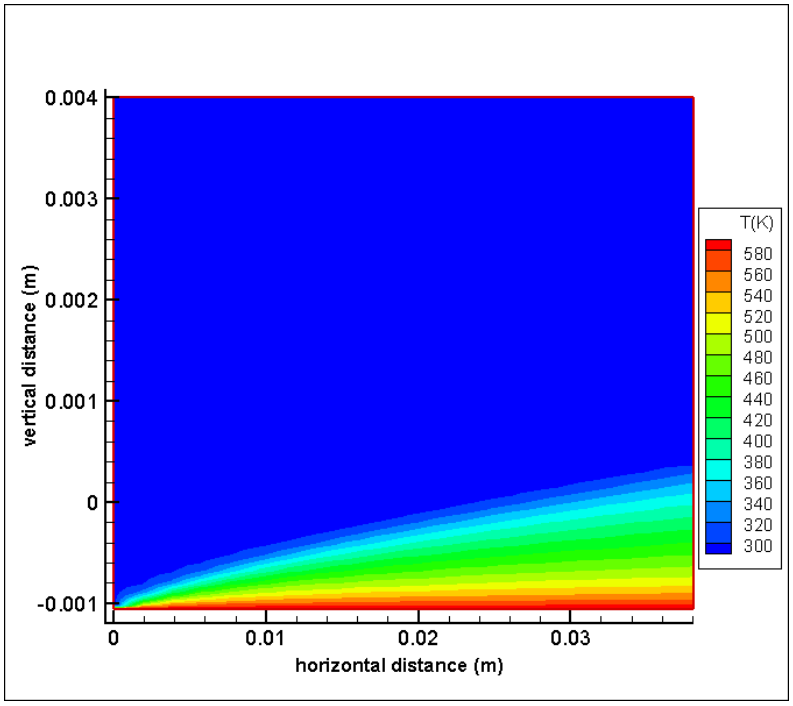

Figure 9.11 Temperature Contours of Present Study ($\dot{r} = 0.015m/s$, $u_\infty = 150m/s$, $\mathrm{Re} = 5.01x10^5$, $t = 0.08s$)

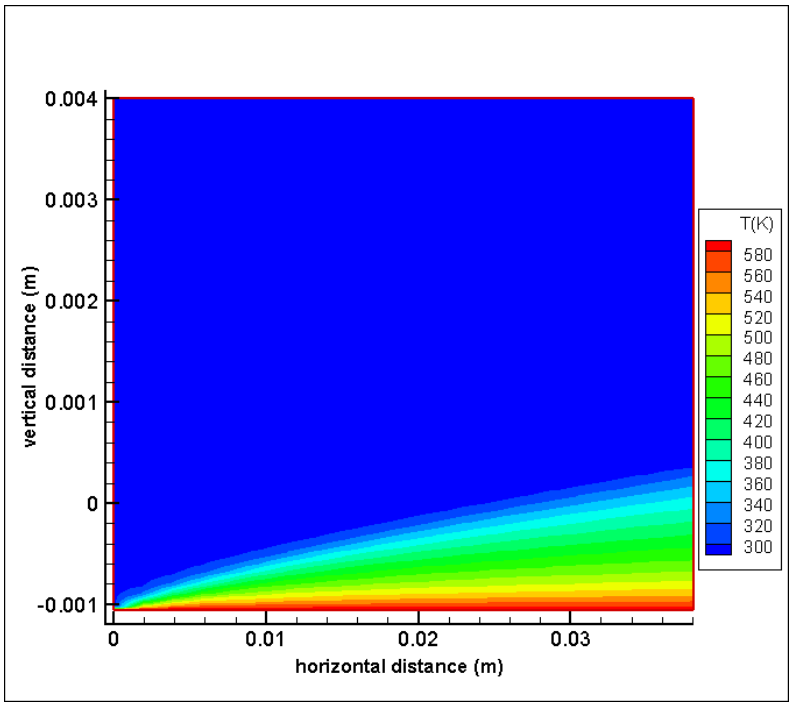

Figure 9.12 Temperature Contours of Present Study ($\dot{r} = 0.015m/s$, $u_\infty = 180m/s$, $\mathrm{Re} = 6.01x10^5$, $t = 0.08s$)

9.3 Study with Different Surface Temperatures

The present program is run with two different surface temperatures and results are plotted in this section. The list of runs are given in Table 9.3. The thermal boundary layer is found to be slightly thicker for $T_s = 700K$.

Table 9.3 List of Runs for Different Surface Temperatures

RUN NUMBER	DESCRIPTION	SURFACE TEMPERATURE
4	Turbulent flow, computer code of the present study, $u_\infty = 100m/s$, $\mathrm{Re} = 3.34x10^5$, $\dot{r} = 0.015m/s$, run parameters given in Table 7.3	$T_s = 600K$
13	Turbulent flow, computer code of the present study, $u_\infty = 100m/s$, $\mathrm{Re} = 3.34x10^5$, $\dot{r} = 0.015m/s$ run parameters given in Table 7.3	$T_s = 700K$

9.3.1 Temperature Contours

Temperature contours for different surface temperatures are as follows:

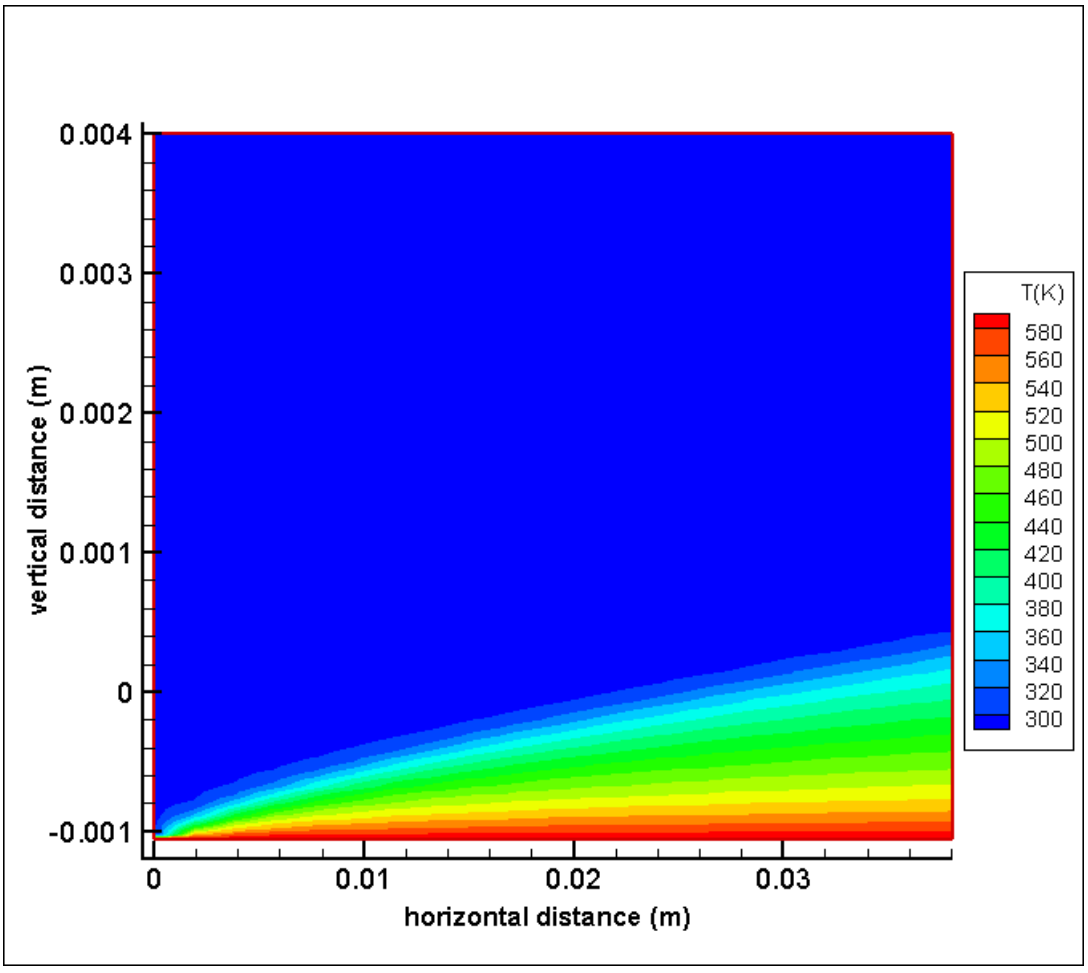

Figure 9.13 Temperature Contours of Present Study ($\dot{r} = 0.015m/s$, $u_\infty = 100m/s$, $\mathrm{Re} = 3.34x10^5$, $t = 0.08s$, $T_s = 600K$)

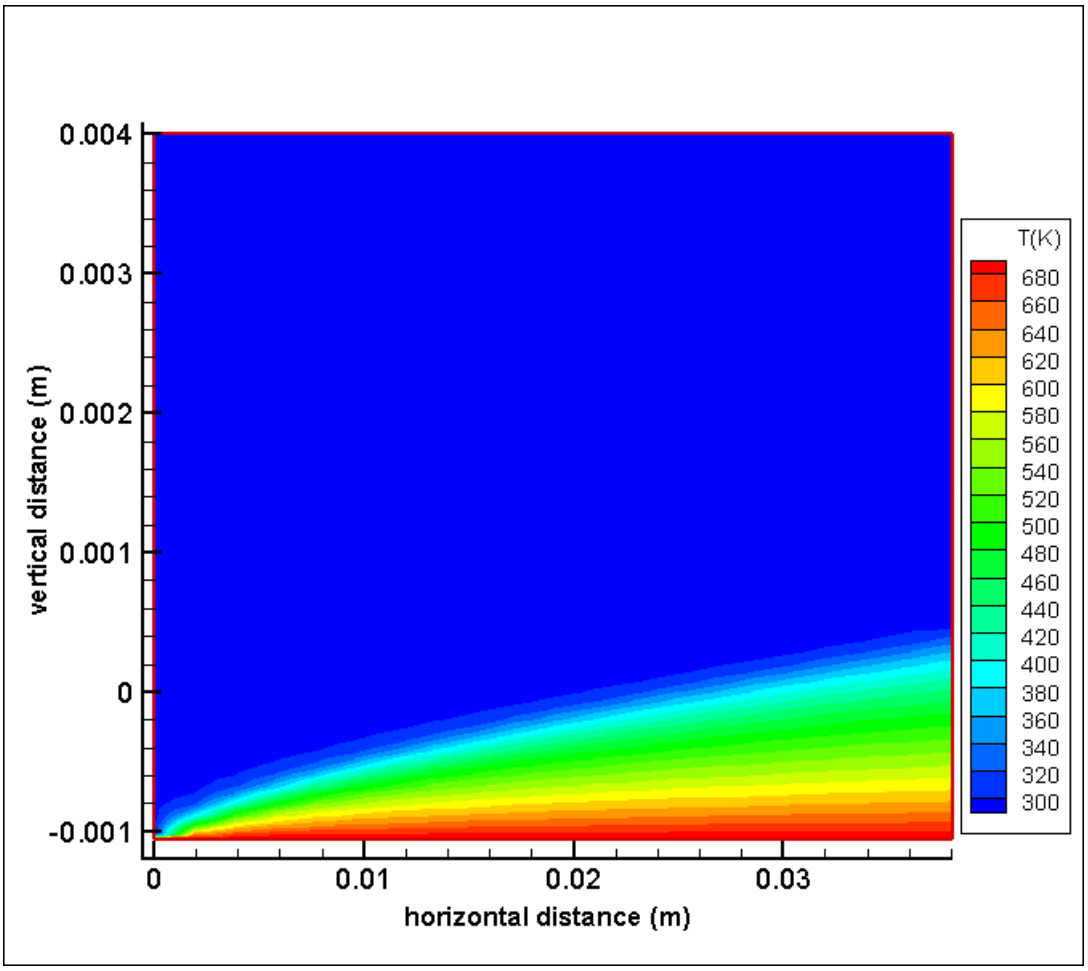

Figure 9.14 Temperature Contours of Present Study ($\dot{r} = 0.015 m/s$, $u_\infty = 100 m/s$, $\mathrm{Re} = 3.34 x 10^5$, $t = 0.08 s$, $T_s = 700 K$)

CHAPTER 10

CONCLUSIONS

In this study, an attempt was made to obtain stable and accurate solutions of the standard K-ε turbulence model equations for non-reacting turbulent flows over an isothermal solid surface in regression. The accomplishments of this effort and the conclusions drawn from the results of the numerical study can be summarized as follows:

1. A time-dependent coordinate transformation has been successfully used in handling the moving boundary condition (due to the uniform regression of the isothermal solid surface.)
2. Previously proposed two-step time averaging (which is a second order accurate numerical scheme) has been successfully adopted to discretize the temporal terms in the governing equations of the mathematical model.
3. The unsteady and parabolic form of the two-equation (standard K-ε) turbulence model can be considered modestly successful in predicting the turbulent behavior of the flow inside the boundary layer. (It should be noted that the velocities are underestimated by this model as one moves close to the wall.)
4. The results of the parametric study indicate that the solution algorithm adopted for the proposed numerical model results in solutions of the

unsteady turbulent flow and temperature fields which are rapidly converging and stable for the Reynolds number and temperature ranges studied.

5. Numerical solutions are shown to be stable for uniform regressions rates between 0.001 and 0.02 m/sec. As expected, no detachment of the viscous or thermal boundary layers has been observed for the regression rates studied.

CHAPTER 11

RECOMMENDATIONS

As noted in the previous chapters of this thesis, the mathematical model adopted for this study is based on various assumptions (such as incompressible flow and boundary layer approximations.) These assumptions result in a parabolized form of the governing equations. The two-equation turbulence model equations used in this study is also of the parabolized type. This form of the turbulence equations is known to underestimate the velocities very near to the moving surface. Furthermore, the discretization schemes used for the first order spatial derivates (the one for the convective terms in the horizontal direction) are first order accurate. Therefore, following recommendations are suggested to improve the numerical accuracy of the study:

1. The hyperbolic-parabolic version of the Navier-Stokes equations should be used to define the flow field.
2. Hyperbolic form of the turbulence model should be adopted for the study.
3. A modified version of the standard K-ε model (the one that gives better results near to the wall) should be used in the study.
4. To improve the accuracy of the numerical scheme, an alternating direction (backward then forward) finite difference scheme should be used in discretizing the convective terms in the horizontal direction.

5. The stretching and transformation coefficients should be updated for the prediction at the second time step.
6. The stability and convergence of the solutions obtained by the proposed numerical solution algorithm should be checked for high regression rates of the solid surface.)
7. Finally, the solution algorithm should be used to obtain solutions of the governing equations when the regression rate is non-uniform, that is, it changes as one moves along the surface.

REFERENCES

[1] Antoniou, A. and Akyuzlu, K. M., 2005, "A Physics Based Comprehensive Mathematical Model to Predict Motor Performance in Hybrid Rocket Propulsion Systems," 41st AIAA/ASME Joint Propulsion Conference and Exhibit, Paper No. 2005-3541, Tucson, Arizona.

[2] Akyuzlu, K.M., Antoniou, A., and Martin, M., 2002, "Determination of Regression Rate in Hybrid Rocket Solid Fuel Using a Physics Based Comprehensive Mathematical Model," 38th AIAA/ASME Joint Propulsion Conference, Paper No. 3577, Indianapolis, Indiana.

[3] Akyuzlu, K. M., Kagoo, R., and Antoniou, A., 2001, " A Physics Based Mathematical Model to Predict The regression Rate in Ablating Hybrid Rocket Solid Fuel," 37th AIAA/ASME Joint Propulsion Conference, Paper No. 2001-3242, Salt Lake City, Utah.

[4] Arpaci, V. and Larsen, P., 1984. Convective Heat Transfer. Prentice Hall, Inc., Englewoods Cliffs, New Jersey.

[5] Ozisik, N., 1973, " Radiative Transfer and Interactions with Conduction and Convection," John Wiley and Sons, Inc., New York, New York.

[6] Akyuzlu, K., Antoniou, A., and Kagoo, R., " The Effect of Radiation on Turbulent Convective Heat Transfer Over an Ablating Solid", Proceedings of the 36th AIAA/ASME/ SAE/ASEE Joint propulsion Conference and Exhibit, Orlando, FL, 2000.

[7] Syed, H., " An Experimental and Theoretical Study of Combustion of Solid Fuels for Hybrid Rockets Using a Two-Dimensional Sub-Scale Hybrid Rocket Motors," MS Thesis, Department of Mechanical Engineering, U of New Orleans, New Orleans, LA, 2004.

[8] Jones, W. and Launder, B., " The Calculation of Low-Reynolds-Number Phenomena with a Two –Equation Model of Turbulence", International Journal of heat and Mass Transfer, Vol. 16, 1973, pp. 1119-1130.

[9] Antoniou, A., " A Physics Based Two Dimensional Comprehensive Mathematical Model to Predict Non Uniform Regression Rate in Solid Fuels For Hybrid Rocket Motors," PhD thesis, Department of Mechanical engineering, University of New Orleans, New Orleans, LA, 2005

[10] Zedan, M. and Schneider, G.E., " A Coupled Strongly Implicit Procedure for Velocity and Pressure Computation in Fluid Flow Problems," Numerical Heat transfer, 8, 1985, pp. 537-557.

[11] Chen, K. and Pletcher, R., " Primitive Variable, Strongly Implicit Calculation Procedure for Viscous Flows at All Speeds", AIAA Journal, Vol. 29, No. 8, !991, pp. 1241-1248.

[12] Morihara, H. and Cheng, R.T., "Numerical Solution of the Viscous Flow in the Entrance Region of Parallel Plates", Journal of Computational Physics, Vol.11, 1973, pp. 550, 572.

[13] Chapra Steven C. and Canale Raymond P., "Numerical Methods for Engineers", McGrow Hill 2002.

[14] Schlichting Hermann and Gersten Klaus, "Boundary-Layer Theory", 8th Edition, Springer-Verlag Berlin Heidelberg 2000

[15] Anderson Dale A., Tannehill John C. and Pletcher Richard H., "Computational Fluid Mechanics and Heat Transfer", Hemisphere 1984

[16] Bruce R. Munson, Donald F. Young and Theodore H. Okiishi, "Fundamentals of Fluid Mechanics", 4th Edition, John Wiley & Sons 2002

[17] Roshko,A., "Structure of Turbulent Shear Flows-A New Look", AIAA Journal, Vol. 141349-1357

[18] Cantwell B.J., “Organized Motion in Turbulent Flow” Annu. Rev. Fluid Mech., Vol. 13, 457-515 1981

[19] Fiedler H.E , “Coherent Structures in Turbulent Flows” Prog. Aerospace Sci., Vol. 25, 235-269, 1988

[20] Cebeci T. and Smith, A.M.O. “Analysis of Turbulent Boundary Layers”, Academic Press, New York 1974

[21] Michel R., Quémard C. and Durant R., “Hypotheses on the Mixing Length and Application to the Calculation of the Turbulent Boundary Layers”, Proceedings Computation of Turbulent Boundary Layers, AFOSR-IFP-Stanford Conference, Vol. I, 195-207 1968

[22] Escudier M.P. “The Distribution of Mixing Length in Turbulent Flows Near Walls”, Imperial College, Heat Transfer Section, Rep. TWF/TN/1 1966

[23] Bradshaw P. and Ferriss D.H., “Calculation of Boundary Layer Development Using the Turbulent Energy Equation”, J. Fluid Mech. Vol. 28, 593-616 1971

[24] Rubesin M.W., “ A One-Equation Model of Turbulence for Use with the Compressible Navier-Stokes Equations” NASA-TM-X-73128 1976

[25] Goldberg U.C, “Derivation and Testing of a One-Equation Model Based on Two Time Scales”, AIAA Journal, Vol. 29, 1337-1340

[26] Baldwin B.S and Barth T.J., “A One-Equation Turbulence Transport Model for High Reynolds Number Wall-Bounded Flows” NASA-TM-102847

[27] Reynolds W.C., “Computation of Turbulent Flows”, Annu. Rev. Fluid Mech., Vol. 8, 183-208 1976

[28] Speziale C.G., Abid R. and Anderson E.C. , “A Critical Evaluation of Two-Equation Models for Near-Wall Turbulence”, AIAA Paper 90-1481 1990

[29] MacCormack R.W., “A Numerical Method for Solving the Equations of Compressible Viscous Flow”, AIAA Paper 81-0110 Louis, Missouri 1981

[30] MacCormack R.W and Paullay A.J., “Computational Efficiency Achieved by Time-Splitting of Finite Difference Operators”AIAA Paper 72-154, San Diego, California 1972

[31] Akyuzlu M. Kazim, “Modeling of Instabilities Due to Coupling of Acoustic and Hydrodynamic Oscillations in Hybrid Rocket Motors”, 43rd AIAA/ASME/SAE/ASEE Joint Propulsion Conference and Exhibit, Cincinnati, OH, July 8-11, 2007

[32] Schetz, Joseph A., “Boundary Layer Analysis”, Prentice-Hall Inc. Englewood Cliffs, New Jersey

APPENDIX A

TRANSFORMATION, STRETCHING AND LINEARIZATION OF PARABOLIC TURBULENT KINETIC ENERGY EQUATION

A.1 TRANSFORMATION OF TURBULENT KINETIC ENERGY EQUATION

The parabolic turbulent kinetic energy equation as given in (4.11) is:

$$\frac{\partial K}{\partial t}+u\frac{\partial K}{\partial x}+v\frac{\partial K}{\partial y}=\left(\frac{\mu}{\rho}+\frac{\mu_t}{\rho\,\mathrm{Pr}_K}\right)\frac{\partial^2 K}{\partial y^2}+\frac{\mu_t}{\rho}\left(\frac{\partial u}{\partial y}\right)^2-\varepsilon \tag{A.1}$$

Each term in the above equation is transformed according to (5.3), (5.5) and (5.7) to $x-\sigma$ coordinate axis as follows:

$$\frac{\partial K}{\partial t}=\frac{\partial K}{\partial t}-\frac{\sigma}{H}r_t\frac{\partial K}{\partial \sigma} \tag{A.2}$$

$$u\frac{\partial K}{\partial x}=u\frac{\partial K}{\partial x}-\frac{\sigma}{H}r_x u\frac{\partial K}{\partial \sigma} \tag{A.3}$$

$$v\frac{\partial K}{\partial y}=\frac{1}{H}v\frac{\partial K}{\partial \sigma} \tag{A.4}$$

$$\left(\frac{\mu}{\rho}+\frac{\mu_t}{\rho\,\mathrm{Pr}_K}\right)\frac{\partial^2 K}{\partial y^2}=\frac{1}{H^2}\left(\frac{\mu}{\rho}+\frac{\mu_t}{\rho\,\mathrm{Pr}_K}\right)\frac{\partial^2 K}{\partial \sigma^2} \tag{A.5}$$

$$\frac{\mu_t}{\rho}\left(\frac{\partial u}{\partial y}\right)^2=\frac{\mu_t}{\rho}\frac{1}{H^2}\left(\frac{\partial u}{\partial \sigma}\right)^2 \tag{A.6}$$

$-\varepsilon$ *(remains the same)* (A.7)

The final form of the transformed turbulent kinetic energy equation is:

$$\frac{\partial K}{\partial t}-\frac{\sigma}{H}r_t\frac{\partial K}{\partial \sigma}+u\frac{\partial K}{\partial x}-\frac{\sigma}{H}r_x u\frac{\partial K}{\partial \sigma}+\frac{1}{H}v\frac{\partial K}{\partial \sigma}= \frac{1}{H^2}\left(\frac{\mu}{\rho}+\frac{\mu_t}{\rho \mathrm{Pr}_K}\right)\frac{\partial^2 K}{\partial \sigma^2}+\frac{\mu_t}{\rho}\frac{1}{H^2}\left(\frac{\partial u}{\partial \sigma}\right)^2-\varepsilon \quad \text{(A.8)}$$

A.2 STRETCHING OF TURBULENT KINETIC ENERGY EQUATION

Each term in equation (A.8) is stretched in the vertical direction using equation (5.13) as follows:

$$\frac{\partial K}{\partial t} - \frac{\sigma}{H} r_t \frac{\partial K}{\partial \sigma} = \frac{\partial K}{\partial t} - \frac{\sigma}{H} r_t \eta_\sigma \frac{\partial K}{\partial \eta} \tag{A.9}$$

$$u\frac{\partial K}{\partial x} - \frac{\sigma}{H} r_x u \frac{\partial K}{\partial \sigma} = u\frac{\partial K}{\partial x} - \frac{\sigma}{H} r_x u \eta_\sigma \frac{\partial K}{\partial \eta} \tag{A.10}$$

$$\frac{1}{H} v \frac{\partial K}{\partial \sigma} = \frac{1}{H} v \eta_\sigma \frac{\partial K}{\partial \eta} \tag{A.11}$$

$$\frac{1}{H^2}\left(\frac{\mu}{\rho} + \frac{\mu_t}{\rho \mathrm{Pr}_K}\right)\frac{\partial^2 K}{\partial \sigma^2} = \frac{1}{H^2}\left(\frac{\mu}{\rho} + \frac{\mu_t}{\rho \mathrm{Pr}_K}\right)\eta_\sigma{}^2 \frac{\partial^2 K}{\partial \eta^2} \tag{A.12}$$

$$\frac{\mu_t}{\rho}\frac{1}{H^2}\left(\frac{\partial u}{\partial \sigma}\right)^2 = \frac{\mu_t}{\rho}\frac{1}{H^2}\eta_\sigma{}^2\left(\frac{\partial u}{\partial \eta}\right)^2 \tag{A.13}$$

$-\varepsilon$ (remains the same) (A.14)

The final form of the stretched turbulent kinetic energy equation is:

$$\begin{aligned}&\frac{\partial K}{\partial t} - \frac{\sigma}{H} r_t \eta_\sigma \frac{\partial K}{\partial \eta} + u\frac{\partial K}{\partial x} - \frac{\sigma}{H} r_x u \eta_\sigma \frac{\partial K}{\partial \eta} + \frac{1}{H} v \eta_\sigma \frac{\partial K}{\partial \eta} = \\ &\frac{1}{H^2}\left(\frac{\mu}{\rho} + \frac{\mu_t}{\rho \mathrm{Pr}_K}\right)\eta_\sigma{}^2 \frac{\partial^2 K}{\partial \eta^2} + \frac{\mu_t}{\rho}\frac{1}{H^2}\eta_\sigma{}^2\left(\frac{\partial u}{\partial \eta}\right)^2 - \varepsilon\end{aligned} \tag{A.15}$$

A.3 LINEARIZATION OF TURBULENT KINETIC ENERGY EQUATION

Linearization procedure is discussed in detail and can be found in Chapter 6. Each term of the transformed and stretched turbulent kinetic energy equation (A.15) is as follows:

FISRT TIME STEP

$$\frac{\partial K}{\partial t} = \frac{\overline{K_{i,j}^{n+1}} - K_{i,j}^{n}}{\Delta t} \tag{A.16}$$

$$-\frac{\sigma}{H} r_t \eta_\sigma \frac{\partial K}{\partial \eta} = -\left(\frac{\sigma}{H} r_t \eta_\sigma\right)_{i,j}^{n} \frac{K_{i,j+1}^{n} - K_{i,j-1}^{n}}{2\Delta\eta} \tag{A.17}$$

$$u \frac{\partial K}{\partial x} = u_{i,j}^{n} \frac{K_{i,j}^{n} - K_{i-1,j}^{n}}{\Delta x} \tag{A.18}$$

$$-\frac{\sigma}{H} r_x u \eta_\sigma \frac{\partial K}{\partial \eta} = -\left(\frac{\sigma}{H} r_x \eta_\sigma u\right)_{i,j}^{n} \frac{K_{i,j+1}^{n} - K_{i,j-1}^{n}}{2\Delta\eta} \tag{A.19}$$

$$\frac{1}{H} v \eta_\sigma \frac{\partial K}{\partial \eta} = \left(\frac{1}{H} v \eta_\sigma\right)_{i,j}^{n} \frac{K_{i,j+1}^{n} - K_{i,j-1}^{n}}{2\Delta\eta} \tag{A.20}$$

$$\frac{1}{H^2}\left(\frac{\mu}{\rho} + \frac{\mu_t}{\rho \mathrm{Pr}_K}\right)\eta_\sigma{}^2 \frac{\partial^2 K}{\partial \eta^2} = \left[\frac{1}{H^2}\left(\frac{\mu}{\rho} + \frac{\mu_t}{\rho \mathrm{Pr}_K}\right)\eta_\sigma{}^2\right]_{i,j}^{n} \frac{\left(K_{i,j+1}^{n} - 2K_{i,j}^{n} + K_{i,j-1}^{n}\right)}{(\Delta\eta)^2} \tag{A.21}$$

$$\frac{\mu_t}{\rho}\frac{1}{H^2}{\eta_\sigma}^2\left(\frac{\partial u}{\partial \eta}\right)^2 = \left(\frac{\mu_t}{\rho}\frac{1}{H^2}{\eta_\sigma}^2\right)_{i,j}^{n}\left(\frac{u_{i,j+1}^{n}-u_{i,j-1}^{n}}{2\Delta\eta}\right)^2 \tag{A.22}$$

$$-\varepsilon = -\varepsilon_{i,j}^{n} \tag{A.23}$$

Predicted value of turbulent K, at time n+1:

$$K_{i,j}^{\overline{n+1}} = K_{i,j}^{n} + \Delta t\left(\begin{array}{l} -(\frac{\sigma}{H}r_t\eta_\sigma)_{i,j}^{n}\frac{K_{i,j+1}^{n}-K_{i,j-1}^{n}}{2\Delta\eta} + u_{i,j}^{n}\frac{K_{i,j}^{n}-K_{i-1,j}^{n}}{\Delta x} \\ -(\frac{\sigma}{H}r_x\eta_\sigma u)_{i,j}^{n}\frac{K_{i,j+1}^{n}-K_{i,j-1}^{n}}{2\Delta\eta} + (\frac{1}{H}v\eta_\sigma)_{i,j}^{n}\frac{K_{i,j+1}^{n}-K_{i,j-1}^{n}}{2\Delta\eta} \\ -\left[\frac{1}{H^2}\left(\frac{\mu}{\rho}+\frac{\mu_t}{\rho\,\mathrm{Pr}_K}\right){\eta_\sigma}^2\right]_{i,j}^{n}\frac{\left(K_{i,j+1}^{n}-2K_{i,j}^{n}+K_{i,j-1}^{n}\right)}{(\Delta\eta)^2} \\ -\left(\frac{\mu_t}{\rho}\frac{1}{H^2}{\eta_\sigma}^2\right)_{i,j}^{n}\left(\frac{u_{i,j+1}^{n}-u_{i,j-1}^{n}}{2\Delta\eta}\right)^2 + \varepsilon_{i,j}^{n} \end{array}\right) \tag{A.24}$$

SECOND TIME STEP

Same differencing scheme used for the second time step, and the predicted value of turbulent K at time n+2 is:

$$K_{i,j}^{\overline{n+2}} = K_{i,j}^{\overline{n+1}} + \Delta t\left(\begin{array}{l} -(\frac{\sigma}{H}r_t\eta_\sigma)_{i,j}^{n}\frac{K_{i,j+1}^{\overline{n+1}}-K_{i,j-1}^{\overline{n+1}}}{2\Delta\eta} + u_{i,j}^{\overline{n+1}}\frac{K_{i,j}^{\overline{n+1}}-K_{i-1,j}^{\overline{n+1}}}{\Delta x} \\ -(\frac{\sigma}{H}r_x\eta_\sigma)_{i,j}^{n}u_{i,j}^{\overline{n+1}}\frac{K_{i,j+1}^{\overline{n+1}}-K_{i,j-1}^{\overline{n+1}}}{2\Delta\eta} + (\frac{1}{H}\eta_\sigma)_{i,j}^{n}v_{i,j}^{\overline{n+1}}\frac{K_{i,j+1}^{\overline{n+1}}-K_{i,j-1}^{\overline{n+1}}}{2\Delta\eta} \\ -\left[\frac{1}{H^2}\left(\frac{\mu}{\rho}+\frac{\mu_t}{\rho\,\mathrm{Pr}_K}\right){\eta_\sigma}^2\right]_{i,j}^{n}\frac{\left(K_{i,j+1}^{\overline{n+1}}-2K_{i,j}^{\overline{n+1}}+K_{i,j-1}^{\overline{n+1}}\right)}{(\Delta\eta)^2} \\ -\left(\frac{1}{\rho H^2}{\eta_\sigma}^2\right)_{i,j}^{n}\mu_{ti,j}^{\overline{n+1}}\left(\frac{u_{i,j+1}^{\overline{n+1}}-u_{i,j-1}^{\overline{n+1}}}{2\Delta\eta}\right)^2 + \varepsilon_{i,j}^{\overline{n+1}} \end{array}\right) \tag{A.25}$$

Time averaging to find the final value of turbulent K, at time n+1:

$$K_{i,j}^{n+1} = \frac{K_{i,j}^{n} + \overline{K_{i,j}^{n+2}}}{2} \tag{A.26}$$

APPENDIX B

FLOWCHART OF THE COMPUTER CODE

Figure B.1 Flowchart of the Computer Code (new added subroutines are marked in red)

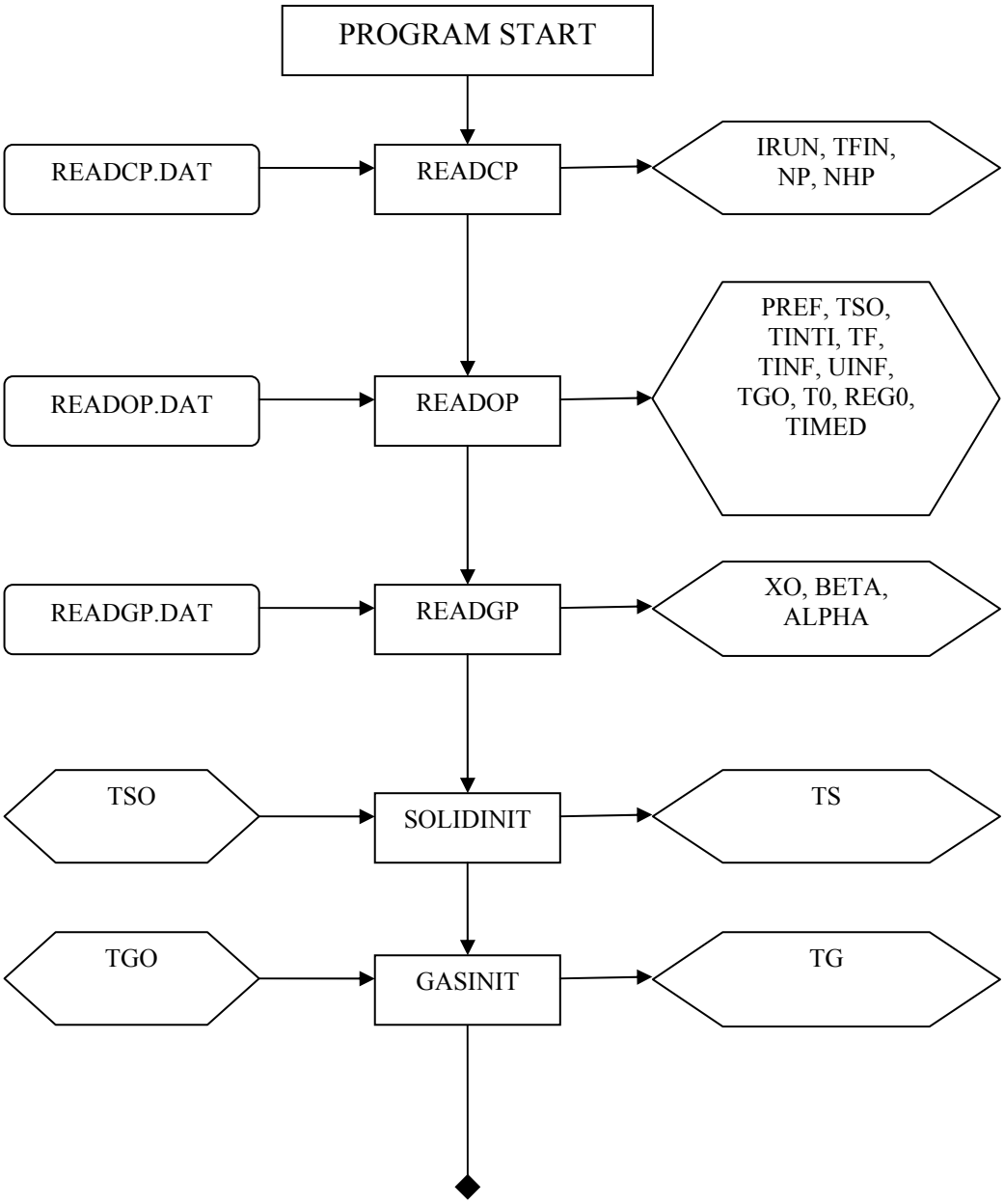

Figure B.1 cont'd

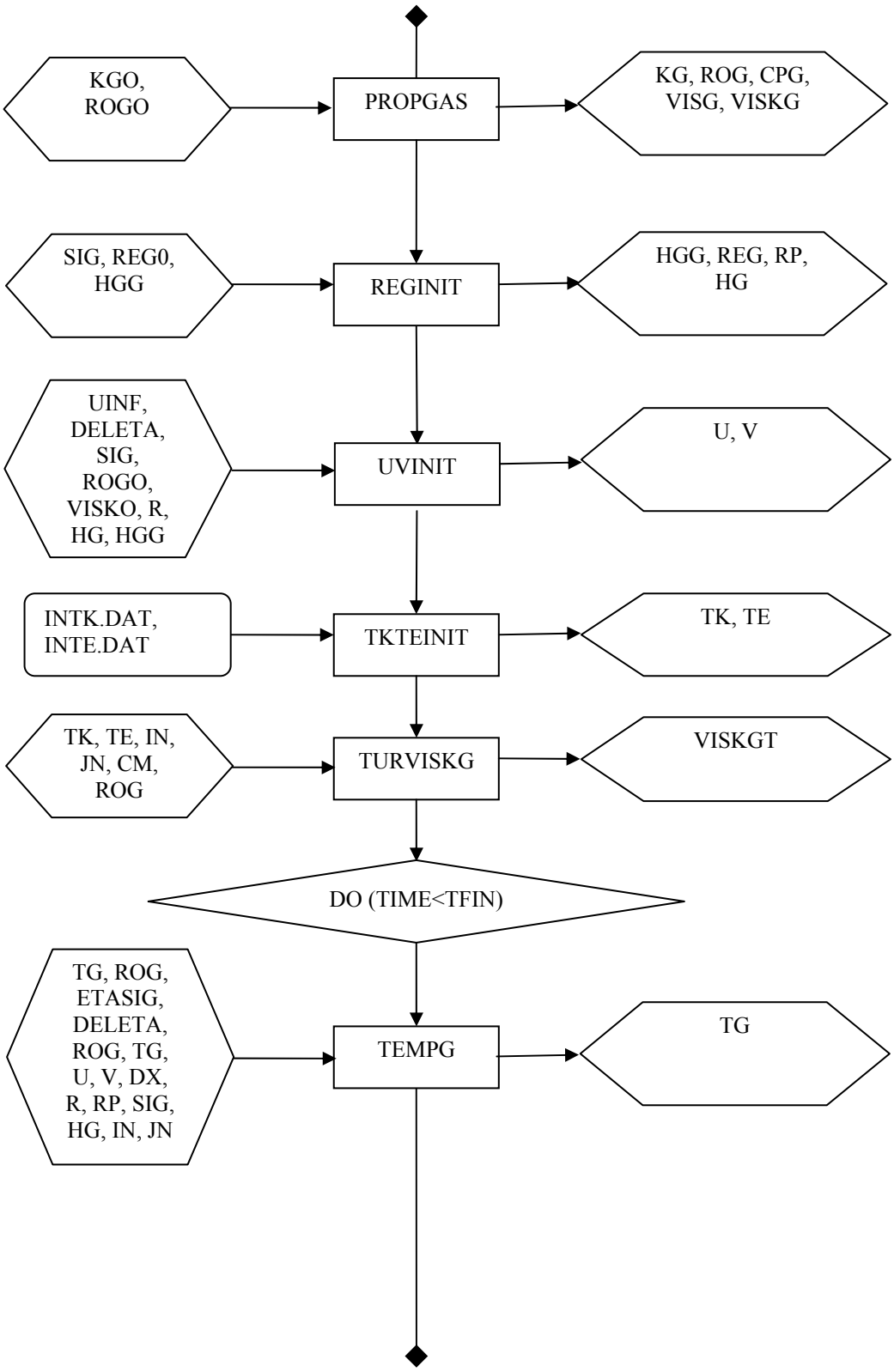

Figure B.1 cont'd

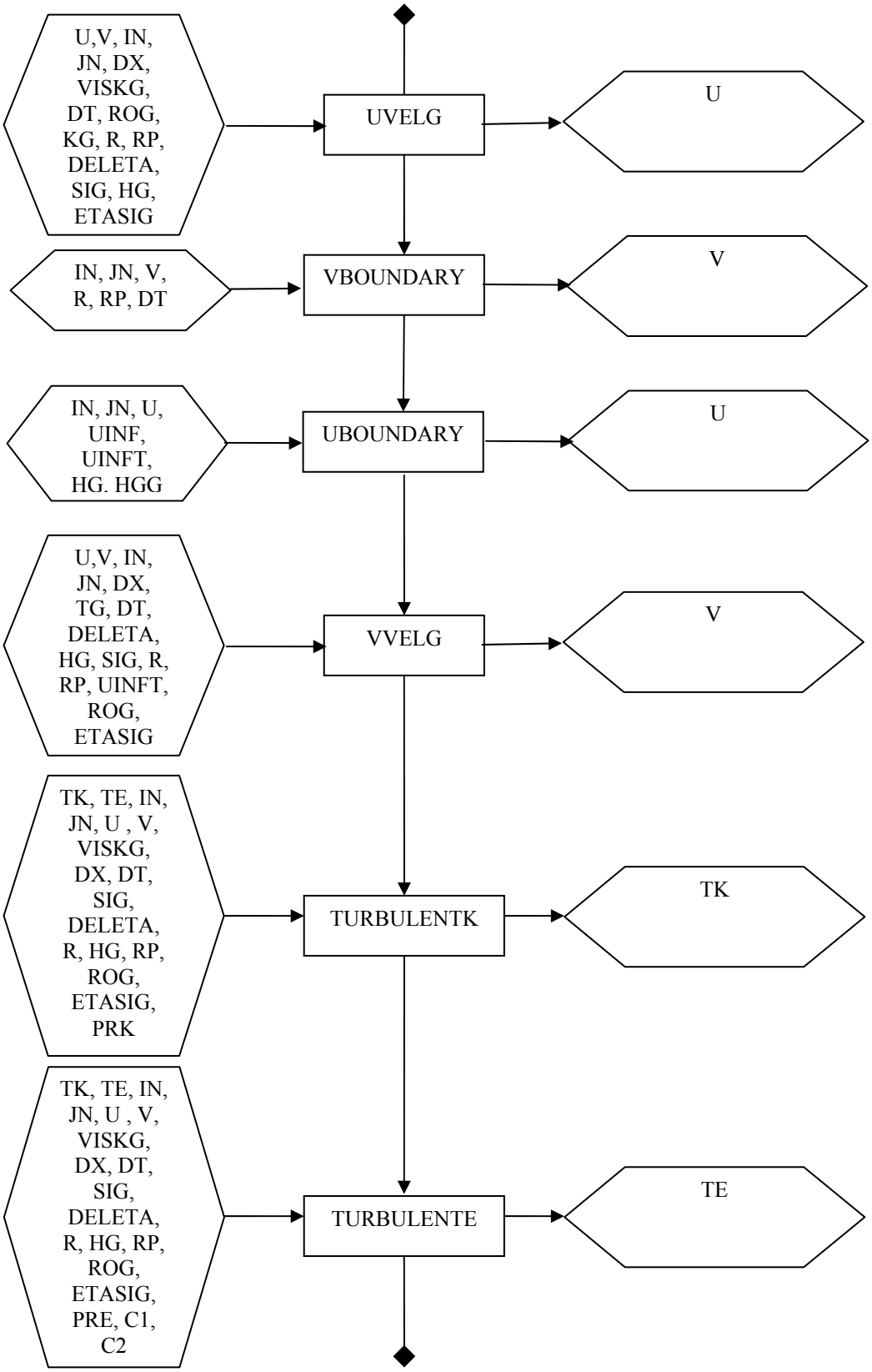

Figure B.1 cont'd

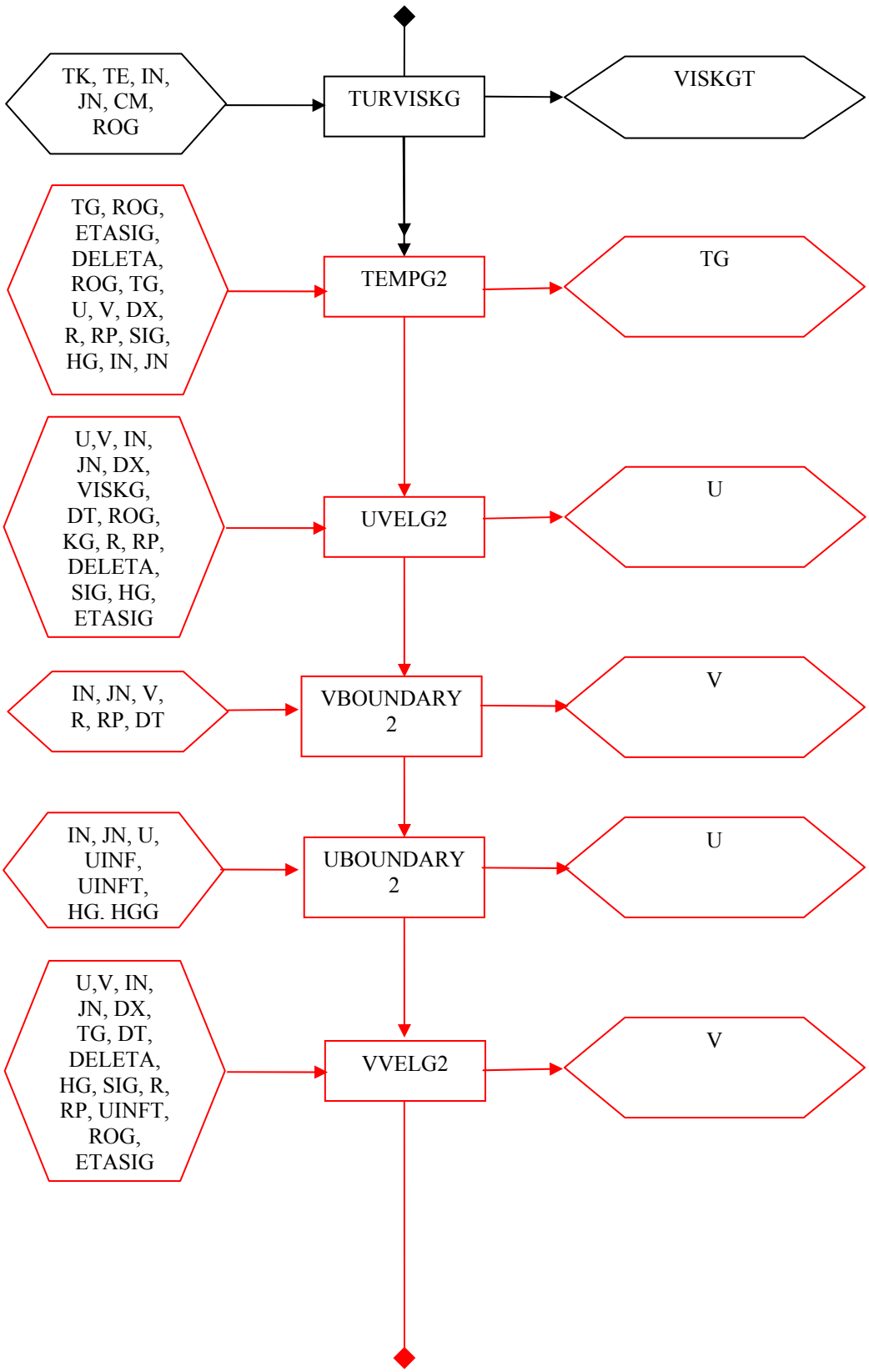

Figure B.1 cont'd

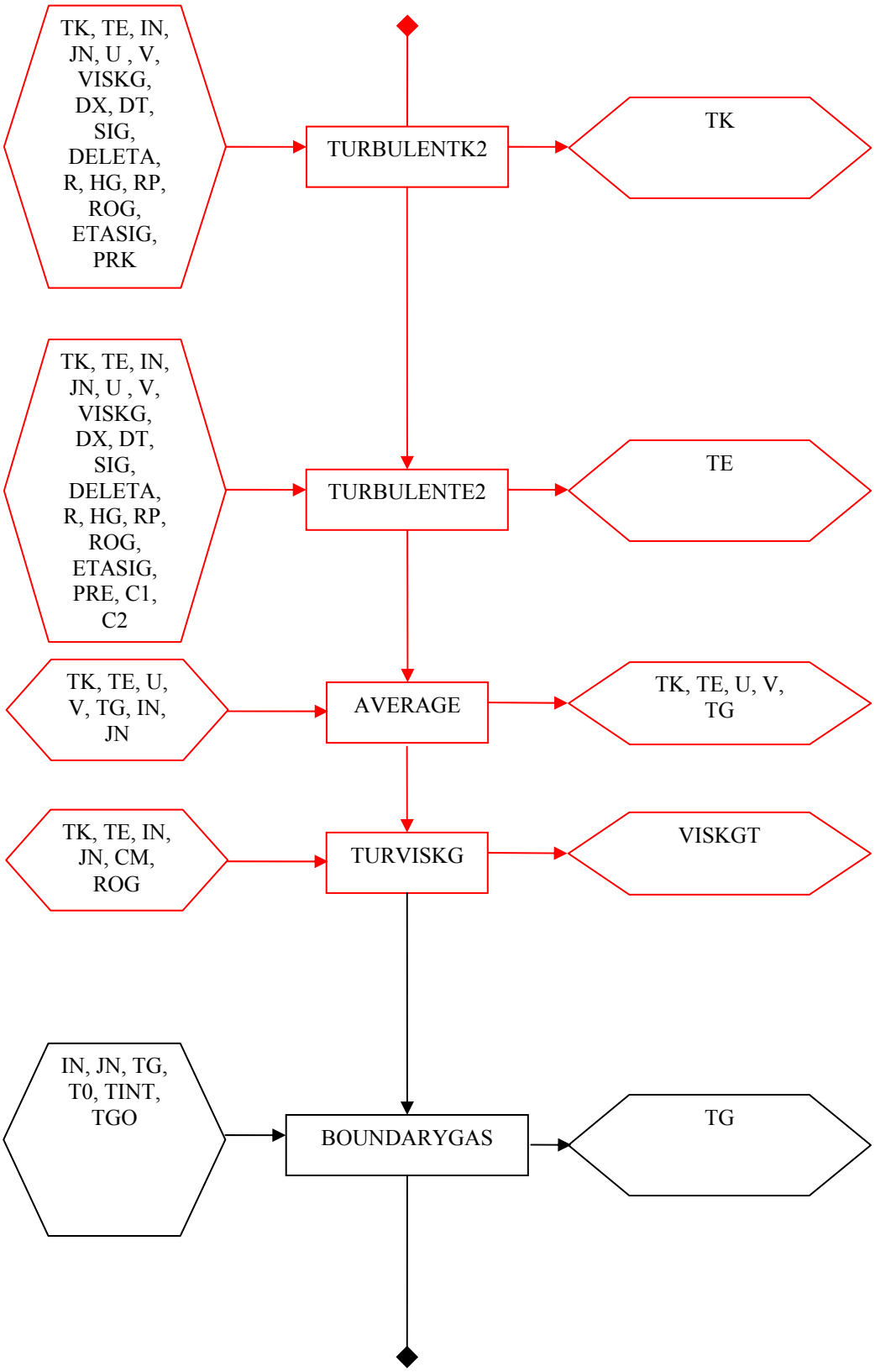

Figure B.1 cont'd

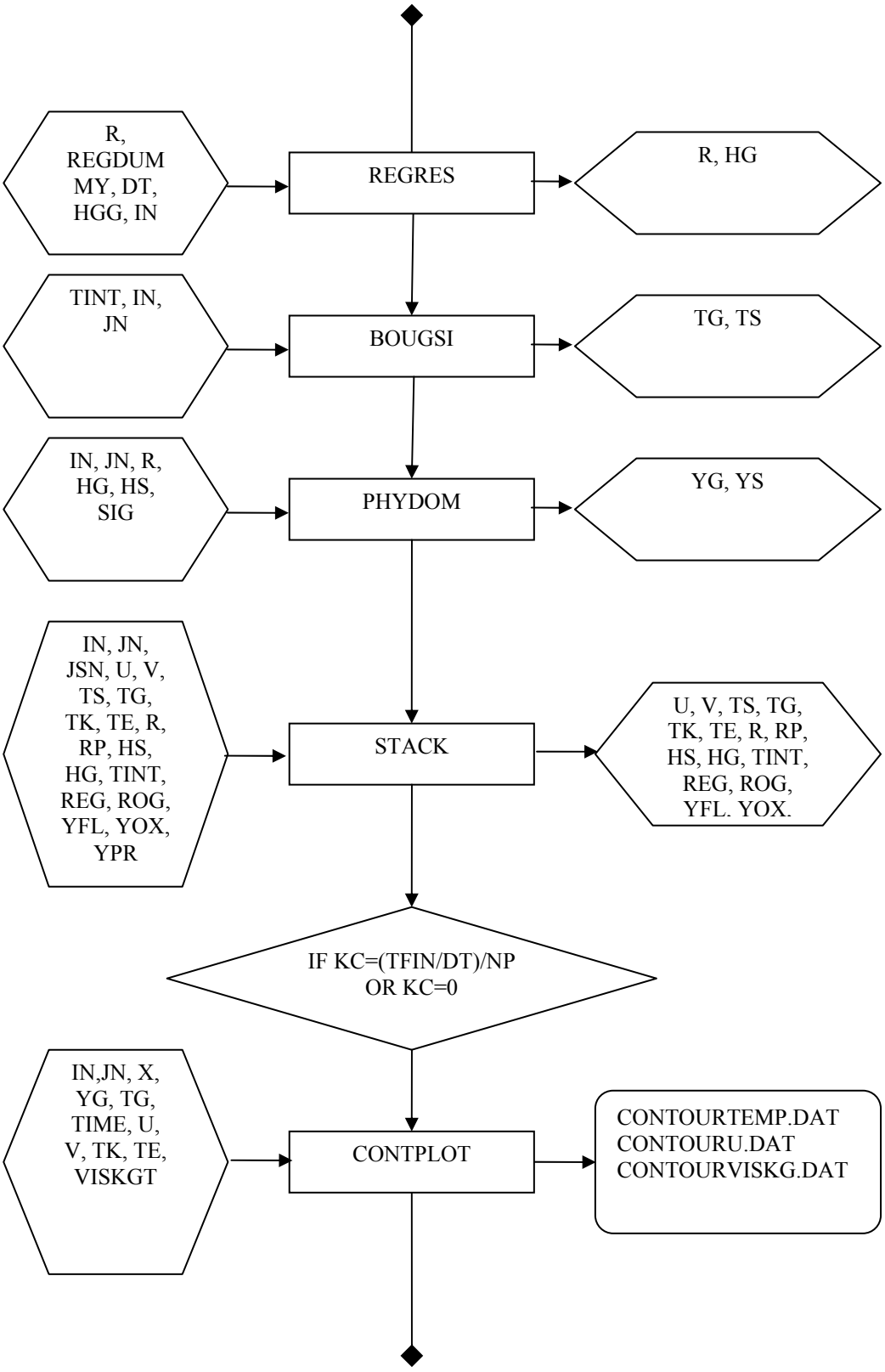

Figure B.1 cont'd

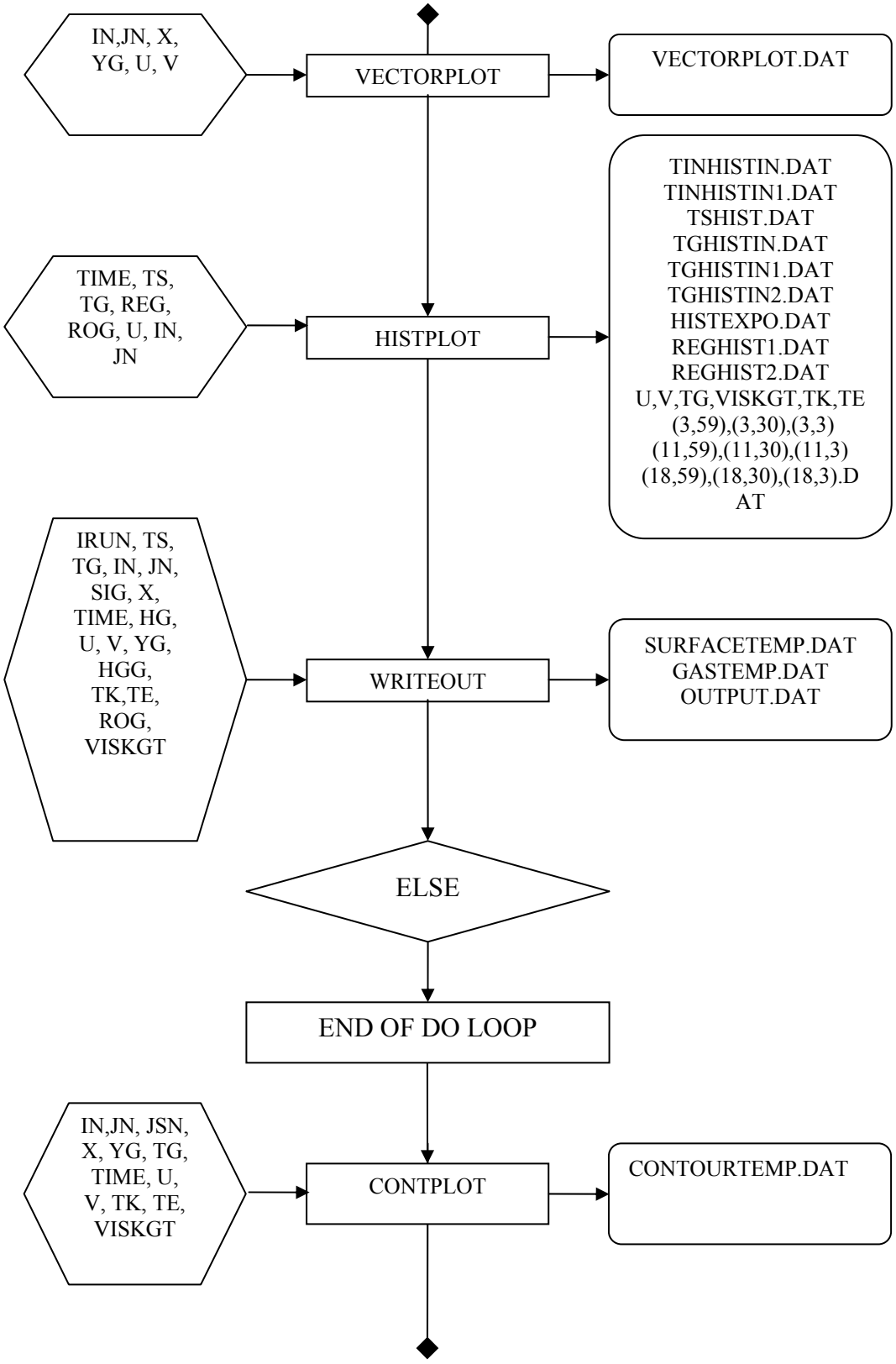

Figure B.1 cont'd

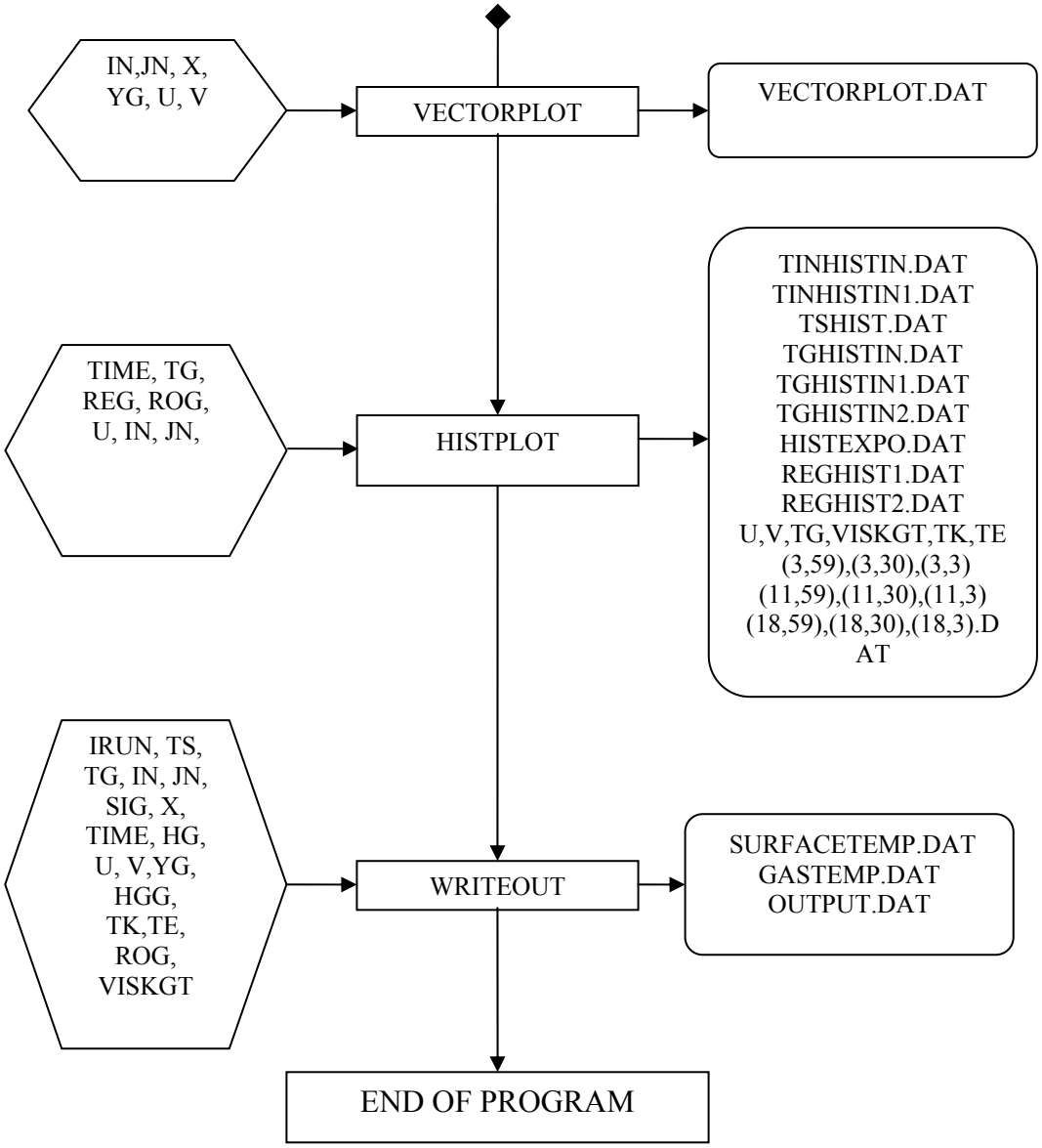

Table B.1 List of Subroutines Used in the Computer Code

NAME OF THE SUBROUTINE	DESCRIPTION	OUTPUT PARAMETERS
READCP	*read input computational parameters*	IRUN, TFIN, NP, NPH
READOP	*read input operational parameters*	IRUN, PREF, TSO, TINF, UINF, REGO, TIMED
READGP	*read input geometrical parameters and calculate stretching parameters*	IRUN, XO, HSS, ETASIG, ETASIGS, VLAX, X, SIG
SOLIDINIT	*set the initial temperature of the solid surface*	TS
GASINIT	*set the initial temperature of the gas*	TG
PROPGAS	*define and calculate properties of gas*	KG, CPG, ROGO, CPGO, VISG, VISGO, ROG
REGINIT	*set initial regression rate values*	HGG, R0
UVINIT	*set initial values of horizontal and vertical velocities*	U, V, UB, VB
TKTEINIT	*set the initial values of K-ε*	TK, TE
TURVISKG	*calculate the turbulent eddy viscosity*	VISGT
PHYDOM	*update the height of the gas domain every time step*	YG
WRITEOUT	*write the values of various variables in output files*	-
CONTPLOT	*create file to enable plotting of temperature contours in TecPlot*	-
VECTORPLOT	*create file to enable plotting of velocity vectors contours in TecPlot*	-
HISTPLOT	*create the histograms of various variables*	-
TEMPG	*calculate the temperature of the gas*	TG

Table B.1 cont'd

UVELG	*calculate the horizontal velocity*	U
UBOUNDARYG	*calculate or set the horizontal velocities at boundaries*	U
VVELG	*calculate the vertical velocity*	V
VBOUNDARYG	*calculate or set the vertical velocities at boundaries*	V
TURBULENTK	*predict the turbulent kinetic energy*	TK
TURBULENTE	*predict the rate of dissipation of the turbulent kinetic energy*	TE
BOUNDARYGAS	*update the temperatures of the gas at the boundaries*	TG
BOUNDARYSOLID	*update the temperatures of the solid surface*	TS
STACK	*update the values of variables every time step*	TG, HG, TK, TE, ROG
TURVISKG	*calculate the turbulent eddy viscosity*	VISKGT

Table B.2 List of Variables Used in the Computer Code

BETA	y-direction stretching factor for gas
CE1	coefficient 1 for turbulence
CE2	coefficient 2 for turbulence
CM	coefficient for turbulent viscosity for turbulence
CPG	specific heat for constant pressure for gas
CPGO	initial specific heat for constant pressure for gas
DELETA	non-dimensional space increment in y-direction
DT	time increment
DX	space increment in x-direction for gas
ETASIG	y-direction stretching coefficient for gas
HG	height of the gas at any time
HGG	total height of the gas
IN	number of nodes in x-direction
IRUN	run number
JN	number of nodes in y-direction
KEFF	effective thermal conductivity of gas
KG	absolute thermal conductivity of gas
KGO	initial absolute thermal conductivity of gas
KGTURB	turbulent thermal conductivity of gas
NP	number of zones created in plots
NPH	number of points in histogram
NPH	number of points in histogram
PRANDTGT	turbulent Prandtl number
PRE	turbulent Prandtl number for dissipation energy
PRK	turbulent Prandtl number for kinetic energy
R	regression at any time
REG	regression rate at any time
REGDUMMY	dummy regression rate
REGO	initial regression rate

Table B.2 cont'd

RG	gas constant
ROG	density of gas at any time
ROGO	initial density of gas
RP	regression at previous time
RU	universal gas constant
SIG	stretching variable for gas domain
TE	turbulent dissipation energy
TFIN	final time
TG	temperature of gas at any time
TGO	initial temperature of gas
TIME	time
TINF	reference temperature of gas
TK	turbulent kinetic energy
U	horizontal velocity component of gas at any time
UB	boundary value of horizontal velocity component
UINF	reference horizontal velocity
V	vertical velocity component of gas
VB	boundary value of vertical velocity component of gas
VISKEF	effective viscosity
VISKGT	turbulent viscosity
VISG	absolute viscosity
VISGO	initial absolute viscosity
X	horizontal distance for gas

APPENDIX C

LAMINAR BOUNDARY LAYER

Table C.1 Comparison of the Results of the Present Solution and Blasius Solution for the Laminar Case $x = 3.24x10^{-2}\,m$

-vertical distance- (m)	horizontal velocity predicted by present study (m/s)	horizontal velocity predicted by previous study (m/s)	horizontal velocity given by Blasius solution (m/s)	percentage deviation between present and previous studies	percentage deviation between present study and Blasius solution
0.0000000	0.0000000	0.0000000	0.0000000	0.0000000	0.0000000
0.0000254	1.0599740	1.0599740	0.7645720	0.0000000	38.6362516
0.0000517	2.1614569	2.1614569	1.5588560	0.0000000	38.6566104
0.0000791	3.3043873	3.3043873	2.3835400	0.0000000	38.6336011
0.0001076	4.4872150	4.4872150	3.2383200	0.0000000	38.5661400
0.0001371	5.7064038	5.7064038	4.1241400	0.0000000	38.3659096
0.0001678	6.9558906	6.9558906	5.0389400	0.0000000	38.0427344
0.0001996	8.2265642	8.2265642	5.9809000	0.0000000	37.5472628
0.0002326	9.5058757	9.5058757	6.9492400	0.0000000	36.7901481
0.0002668	10.7777339	10.7777339	7.9411600	0.0000000	35.7198942
0.0003023	12.0228697	12.0228697	8.9469400	0.0000000	34.3796844
0.0003390	13.2198126	13.2198126	9.9616200	0.0000000	32.7074576
0.0003771	14.3465090	14.3465090	10.9793000	0.0000000	30.6687039
0.0004166	15.3824117	15.3824117	11.9902400	0.0000000	28.2911079
0.0004574	16.3106729	16.3106729	12.9830600	0.0000000	25.6304208
0.0004996	17.1199700	17.1199700	13.9451800	0.0000000	22.7662172
0.0005433	17.8055612	17.8055612	14.8629000	0.0000000	19.7987017
0.0005885	18.3693763	18.3693763	15.7230000	0.0000000	16.8312428

Table C.1 cont'd

0.0006352	18.8192008	18.8192008	16.5133200	0.0000000	13.9637627
0.0006834	19.1672153	19.1672153	17.2236600	0.0000000	11.2842176
0.0007332	19.4282368	19.4282368	17.8471400	0.0000000	8.8591048
0.0007846	19.6179970	19.6179970	18.3800600	0.0000000	6.7352174
0.0008376	19.7517020	19.7517020	18.8229400	0.0000000	4.9342026
0.0008923	19.6179970	19.8430096	19.1657000	1.1339641	2.3599294
0.0009486	19.7517020	19.9034497	19.4317200	0.7624192	1.6466993
0.0010066	19.8430096	19.9422369	19.6312800	0.4975737	1.0785318
0.0010663	19.9034497	19.9663762	19.7700200	0.3151623	0.6749094
0.0011277	19.9422369	19.9809511	19.8624400	0.1937556	0.4017478
0.0011908	19.9663762	19.9894928	19.9235800	0.1156439	0.2148018